Dissertation
submitted to the
Combined Faculty for the Natural Sciences and Mathematics
of the Ruperto Carola University Heidelberg, Germany
for the degree of
Doctor of Natural Sciences

Presented by
M. Sc. Ann Kathrin Heilig
born in: Tettnang
Oral examination: 23.04.2021

Molecular and cellular mechanisms of myotome dorsalization in the medaka embryo

Referees: Prof. Dr. Joachim Wittbrodt
Prof. Dr. Hiroyuki Takeda

魚たちは 夜
自分たちが 地球のそとに
流れでるのを感じる
水が少なくなるので
尾ひれをしきりにふりながら
夜が あまり静かなので
自分たちの水をはねる音が 気になる
誰かにきこえやしないかと思って
夜をすかして見る
すると
もう何年も前にまよい出た
一匹の水すましが
帰り道にまよって 思案もわすれたように
ぐるぐる廻っているのに出会う

From “Time within a Fish”, Toshio Nakae, 1952

At night fish have a sense
that they are flowing out of the earth
busily flapping their tailfins
as water becomes scarce
the night is so serene
they are self-conscious about their noisy splashing
lest they be heard by someone
they peer through the night
and come upon a single water-strider
who drifted out many years ago, and
lost his way home
he, is circling about
as if he has no worries

Translation: Takako Lento

Abstract

Axial muscles in the trunk and tail are important for stabilization and locomotion of the body. In jawed vertebrates, these muscles are further divided into the epaxial (dorsal) and the hypaxial (ventral) muscles. The epaxial muscles eventually cover the neural tube to form the muscles of the back. While it is well described how these muscles differentiate from the somites during early development, it is only poorly understood how the epaxial myotome further develops to form the muscles of the back.

The spontaneous medaka (*Oryzias latipes*) mutant *Double anal fin* (*Da*) exhibits an unique axial muscle phenotype where the epaxial muscles fail to cover the neural tube during embryonic development. Recent studies showed that the mutant has a mutation in the somite enhancer region of *zic1/zic4*, suggesting a role of the transcription factors Zic1/Zic4 as dorsalization factors during late somite development.

In this thesis, I elucidated the regulation and the developmental process underlying dorsal somite extension, which ultimately gives rise to epaxial myotome covering the neural tube. Firstly, I addressed the regulation of *zic1/zic4* expression by the canonical Wnt signaling pathway during late somite development. I examining the expression of *zic1/zic4* after manipulation of the Wnt signaling pathway and performed a ChIP-seq against β-catenin. I could show that *zic1/zic4* are direct downstream targets of the canonical Wnt signaling pathway.

Next, I found that after the onset *zic1/zic4* expression in Wt dorsal somites the proliferative activity of dorsal dermomyotome cells is reduced. Additionally, during somite extension these dermomyotome cells form numerous, large protrusions extending dorsally. This process probably guides the myotome towards the top of the neural tube. In the *Da* mutant, however, both reduction of cell proliferation and extensive protrusive behavior of dorsal dermomyotome cells was not observed. Furthermore, I identified a direct downstream target of *zic1*, *wnt11r*, as additional dorsalization factor. Knockdown of Wnt11r in Wt embryos recapitulated the ventralized somite phenotype of the *Da* mutant, whereas injection of Wnt11 protein could partially rescue the *Da* mutant phenotype. By inhibiting the Wnt/Ca^{2+} signaling pathway, I found that Wnt11r probably acts through this non-canonical Wnt signaling pathway during somite extension.

In summary, my results propose that the regulation of *wnt11r* by *zic1/zic4* during late somite development is essential for dorsal somite extension which is key for the morphology of epaxial trunk muscles.

Zusammenfassung

Die axiale Muskulatur des Rumpfes und des Schwanzes sind wichtig für die Stabilität und Fortbewegungsfähigkeit des Körpers. In Kiefermäulern sind diese Muskeln weiter in epaxiale (dorsal) und hypaxiale (ventral) Muskeln unterteilt. Letztendlich werden die epaxialen Muskeln das Neuralrohr bedecken und die Muskeln des Rückens bilden. Während es gut untersucht ist wie sich diese Muskeln von den Somiten, während der frühen Embryonalentwicklung, differenzieren, ist es jedoch kaum verstanden wie sich das epaxiale Myotom weiterentwickelt, um die Rückenmuskulatur zu bilden.

Die spontane Medaka (*Oryzias latipes*) Mutante *Double anal fin* (*Da*) weist einen einzigartigen axialen Muskelphänotyp auf. Hierbei scheitern die epaxialen Muskel während der Embryonalentwicklung das Neuralrohr zu bedecken. Aktuelle Studien konnten zeigen, dass die Mutante eine Mutation in dem Somitenenhancer von *zic1/zic4* hat, dies lässt vermuten, dass die Transkriptionsfaktoren Zic1/Zic4 eine Rolle als Dorsalisierungsfaktoren während der späten Somitenentwicklung spielen.

In dieser Doktorarbeit befasse ich mich mit der Regulation und dem Prozess, welcher der Somitenextension zu Grunde liegt. Die Somitenextension führt dazu, dass die epaxiale Muskulatur das Neuralrohr bedeckt.

Zuerst habe ich die Regulation von *zic1/zic4* während der späten Somitenentwicklung durch den kanonischen Wnt Signalweg adressiert. Ich untersuchte die Expression von *zic1/zic4* nachdem ich den Wnt Signalweg manipuliert habe, und führte eine ChIP-Seq gegen β-Catenin durch. Damit konnte ich zeigen, dass *zic1/zic4* direkte Zielgene des kanonischen Wnt Signalwegs sind.

Des Weiteren fand ich heraus, dass sich die Teilungsaktivität von dorsalen Dermomyotomzellen reduziert, nachdem die dorsalen Somiten anfingen *zic1/zic4* zu exprimieren. Zusätzlich konnte ich beobachten, dass die Dermomyotomzellen, während der Somitenextension, zahlreiche lange Fortsätze bilden, welche sich nach dorsal, ausstreckten. Mutmaßlich wird bei diesem Vorgang das Myotom zur Oberseite des Neuralrohrs geleitet. In der *Da* Mutante jedoch, konnten weder eine reduzierte Teilungsaktivität, noch das ausgiebiges Bilden von Fortsätzen von den dorsalen Dermomyotomzellen beobacht werden. Zudem konnte ich ein direktes Zielgen von *zic1*, *wnt11r*, als weiteren Dorsalisierungsfaktor identifizieren. Der Knockdown von Wnt11r in Medakaembryonen konnte den ventralisierten Somitenphänotyp der *Da* Mutante rekapitulieren, während die Injektion von Wnt11 Proteinen den Phänotyp der *Da* Mutante teilweise reversieren konnte. Durch die Inhibition des Wnt/Ca^{2+} Signalwegs fand ich heraus, dass während der Somitenextension Wnt11r wahrscheinlich durch diesen nicht-kanonischen Wnt Signalweg agiert.

Zusammengefasst zeigen meine Ergebnisse, dass während der späten Somitenentwicklung die Regulierung von *wnt11r* durch *zic1/zic4* essenziell für die Somitenextension ist, welche wiederum entscheidend für die Morphologie der epaxialen Rumpfmuskeln ist.

Contents

Abbreviations

3D	three-dimensional
ABC	anterior border cell
AC-GFP	Actin-Chromobody-GFP
APC	adenomatous polyposis coli
ATAC-seq	assay for transposase-accessible chromatin using sequencing
Az	1-Azakenpaullone
BMP	bone morphogenic protein
bp	base pairs
CaMKII	calcium/calmodulin-dependent protein kinase type II
Cas	CRISPR-associated system
Cdc42	cell division control protein 42
cDNA	complementary DNA
ChIP	chromatin immunoprecipitation
CK1	casein kinase 1
CRISPR	clustered regularly interspaced short palindromic
Da	*Double anal fin*
DAPI	4',6-diamidino-2-phenylindole
dpi	days past induction
DM	dermomyotome
DML	dorsomedial lip
DNA	deoxyribonucleic acid
Dvl	dishevelled
E. coli	*Escherichia coli*
ECM	extracellular matrix
EMT	epithelial-mesenchymal transition
ERM	embryonic rearing medium
F/FW	forward
FGF	fibroblast growth factor
FMP	fast muscle progenitor
Fz	frizzled
g	gram
g	gravity

Gas1	growth-arrest specific gene 1
gDNA	genomic DNA
GFP	green fluorescent protein
Gli	glioma-associated oncogene
Glis	gli-similar
GSK3	glycogen synthase kinase 3
h	hour
Hh	hedgehog
Hi-C	high-throughput sequencing chromosome conformation capture
HM	horizontal myoseptum
hrWnt11	human recombinant Wnt11
HSE	heat shock element
Hyb	hybridization
INDELs	insertion and deletion
k	kilo
l	liter
LB	lysogeny broth
Lef	lymphoid enhancer factor
LMA	low melting agarose
LMF	lateral muscle fiber
LRP6	low-density lipoprotein receptor related protein 6
M	myotome
M	molar (mol/l)
MFF	medial fast fiber
min	minute
ml	milliliter
mmCherry	membrane mCherry
mmp14	*metalloproteinase Matrix metalloproteinase 14*
MO	morpholino
MRF	myogenic regulatory factors
mRNA	messenger RNA
myf5	*myogenic factor 5*
MyHC	myosin heavy chain
myoD	*myoblast determination protein 1*
n	nano

NC	notochord
NT	neural tube
OCA	oculo-cutaneous albinism
OPT	ocean pout terminator
PAM	protospacer adjacent motif
pax	*paired box gene*
PBS	phosphate buffered saline
PCR	polymerase chain reaction
pH3	phospho-histone H3
pH	negative common logarithm of proton concentration
PIP3	phosphatidylinositol 3,4,5-trisphosphate
PhotoMO	Photo-morpholino
PTW	phosphate buffered saline plus tween 20
qPCR	quantitative *PCR*
R/RV	reverse
Rac1	ras-related c3 botulinum toxin substrate 1
RNA	ribonucleic acid
rpm	revolutions per minute
RT	room temperature
RT-PCR	reverse transcription PCR
S	somite
Scl45a2	solute carrier family 45 member 2
sec	second
Seq	sequencing
Sfrp2	secreted frizzled-related protein 2
Sim1	single-minded 1
sgRNA	single guide RNA
Shh	sonic hedgehog
SMF	slow muscle fiber
sp5	*trans-acting transcription factor 5*
SSC	saline sodium citrate
SSCT	saline sodium citrate plus tween 20
st.	developmental stage
TAE	Tris-acetate-EDTA-buffer
Tcf	T-cell factor

TEM	transmission electron microscopy
Tris	Tris-(hydroxymethyl-) amino methane
U	unit
UV	ultraviolet radiation
VLL	ventrolateral lip
Wt	wildtype
x	times
YRS	Yamamoto Ringer Solution
Zic	zinc finger of cerebellum
µ	micro
°C	degree Celsius

1 Introduction

Movement, feeding, communication and respiration are tremendously important processes which are powered by skeletal muscles in vertebrates. The skeletal muscles are subdivided into axial muscles (the muscles of the head, trunk and tail) and appendicular muscles (the muscles of the limbs) (Clifton, 2002).

Axial muscles first arose in chordates to stabilize and enable flexing of the notochord. With the evolution of jawed vertebrates the axial muscles became subdivided into the epaxial (dorsal) and hypaxial (ventral) muscles which led to an increased range of motion (Fetcho, 1987; Glass and Goodrich, 1960; Sefton and Kardon, 2019). The differentiation of the axial myotome form the somites and its initial patterning during early development is well described. However, the developmental process underlying myotome patterning into epaxial and hypaxial muscles, as well as how the epaxial muscles adopt the muscle morphology found in adults during late developmental stages is only poorly understood. Approximately half of the body mass of teleost consist of axial muscles (Keenan and Currie, 2019), which makes teleosts the perfect model to study epaxial muscle development. In this thesis, I used the Japanese rice fish (*Oryzias latipes*), commonly known as medaka, which belongs to the teleost infraclass. Due to its exuterine development, high egg laying capacity, relatively small genome (in comparison to zebrafish) and easy maintenance, it is a widely used model organism in developmental genetics and molecular biology. Key advances in genetics have been made in medaka, including the first vertebrate proof for Mendelian segregation of alleles (Toyama, 1916) and the discovery of the first active transposon (Tol1) in vertebrates (Koga et al., 1995). This discovery led to the development of the Tol2-mediated transgenesis systems (Urasaki et al., 2006)). A big milestone in the establishment of medaka as a genomic model organism, was the assembly of its genome in 2007, one of the first vertebrate genomes to be assembled (Kasahara et al., 2007).

To date, a large variety of genetic tools are available in medaka, including the Cre/LoxP recombination system (Centanin et al., 2014), meganuclease transgenesis (Grabher and Wittbrodt, 2007) and the CRISPR/Cas9 gene editing system (Ansai and Kinoshita, 2014; Stemmer et al., 2015). Molecular methods including ChIP-seq to analyze DNA-protein interactions (Nakamura et al., 2014) and ATAC-seq to investigate chromatin accessibility (Fernández-Miñán et al., 2016) are also established.

Due to its fast development and transparent embryos, medaka is a valuable model to study developmental processes *in vivo*. In this thesis, I will make use of several molecular methods in combination with *in vivo* imaging techniques and utilize a spontaneous medaka mutant, *Double anal fin* (*Da*), with a ventralized trunk to investigate myotome dorsalization from its induction to the morphogenesis of the epaxial muscle.

1.1 Development of the somites and myogenesis in vertebrates

Somites are transient structures which are derived from the presomitic or unsegmented paraxial mesoderm and are located on both sides of the neural tube (Gilbert and Barresi, 2017). Somitogenesis is highly conserved among vertebrates, most cellular and molecular processes are similar in amniotes, amphibia and fish. Particular differences can, however, be observed in the timing of somitic cell differentiation and their spatial organization (Rossi and Messina, 2014). Since most of our knowledge is derived from studying somite differentiation in amniotes, I will briefly introduce this developmental process in amniotes before discussing differences in fish.

During somitogenesis, the presomitic mesoderm undergoes segmentation, forming the somites. Somites are segmented from the anterior to the posterior end of the presomitic mesoderm. After somitogenesis the somites are patterned into distinct compartments, namely the sclerotome and the dermomyotome (Figure 1.1 A) (Buckingham, 2001; Gilbert and Barresi, 2017). Cells giving rise to the sclerotome delaminate from the ventral part of the somites. These cells will eventually give rise to cartilage cells of the vertebrae and ribs (Carlson, 2015).

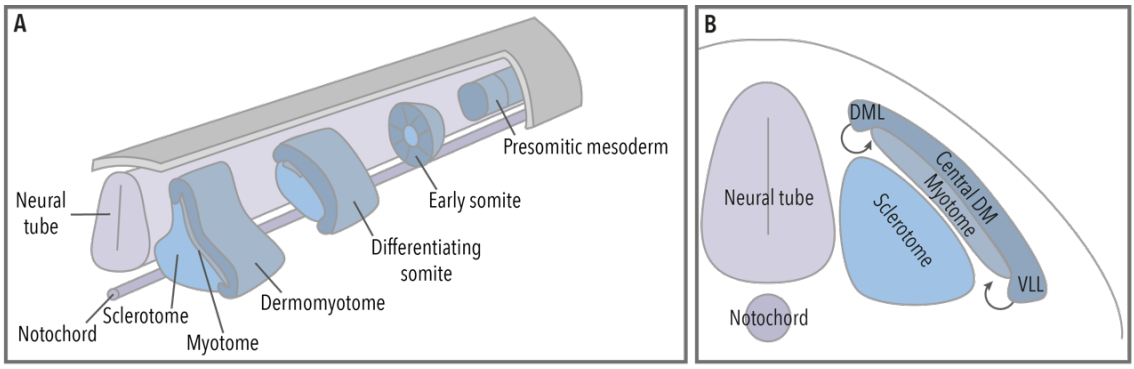

Figure 1.1: Somite differentiation showcased in chicken.

(A) Somites are segmented from the presomitic mesoderm and can be found on the right and left side of the neural tube. Somitogenesis proceeds from anterior to posterior. During somite differentiation, the sclerotome is formed from the ventral part and the dermomyotome is formed from the dorsal part of the somites. The dermomyotome gives rise to the myotome and dermal precursors. Adapted from (Buckingham, 2001) (B) The most dorsal part of the dermomyotome forms the dorsomedial lip (DML), whereas the ventrolateral lip (VLL) is formed from the ventral dermomyotome. The DML and the VLL are proliferation zones, contributing to the growth of the dermomyotome (DM) and myotome. Cells from the central dermomyotome give rise to the dermis of the back, muscle progenitors, satellite cells and brown adipose cells. Adapted from (Marcelle et al., 1997). DM = dermomyotome, DML = dorsomedial lip, VLL = ventrolateral lip.

Fate mapping experiments in the 90's using chicken-quail chimeras discovered that the dermomyotome is subdivided into three additional regions. The dorsal most end forms the dorsomedial lip (DML), its ventral counterpart the ventrolateral lip (VLL) and the central portion is the central dermomyotome (Figure 1.1B). The DML and the VLL are

epithelized proliferation zones, crucial for the mediolateral growth of the dermomyotome (Brand-Saberi et al., 1996; Geetha-Loganathan, 2006; Kato and Aoyama, 1998; Ordahl and Le Douarin, 1992). Ablation experiments in chicken showed that removal of the DML blocked further growth of myotome. Rescuing a somite following DML ablation by transplanting a new DML, led to the generation of new myocytes. These experiments indicated that the DML is necessary for myotome growth and morphogenesis (Ordahl et al., 2001).
Later, the DML and the VLL were identified as myotomes. Muscle precursor cells, the myoblasts, migrate out from the myotomes and beneath the dermomyotome. The central part of the dermomyotome gives rises to dorsal dermis and subcutaneous precursor cells. Additionally it had been discovered that the central dermomyotome also gives rise to muscle progenitor cells and satellite cells (Geetha-Loganathan, 2006; Gros et al., 2005). Aside, previous studies showed that the central dermomyotome also gives rise to brown adipose cells, which are sharing the same somitic precursor cells as skeletal muscles (Atit et al., 2006; Tseng et al., 2008).
The proliferating muscle precursor cell express *paired box gene 3* (*pax3)* and *paired box gene 7* (*pax7)*. For further commitment, the expression of myogenic regulatory factors (MRFs) need to be initiated in the precursor cells. The MRFs regulate genes crucial for muscle function (reviewed in (Gilbert and Barresi, 2017)). Myoblasts, the committed muscle precursor cells, are characterized by *myogenin* expression. Eventually, these committed myoblasts align and fuse their cell membranes to generate myofibers, large multinucleated cells. This establishes the basic muscle frame and completes the primary myogenesis. During secondary myogenesis fetal myoblast fuse with each other or with preexisting primary myofibers. (Konigsberg, 1963; Mintz and Baker, 1967; Richardson et al., 2008; Rossi and Messina, 2014). Generally, primary myogenesis will give rise to muscle fibers which mainly adopt a slow muscle fiber fate, whereas fast muscle fibers are mainly derived during the secondary myogenesis. Slow and fast muscle fibers can be distinguished by their expression of either slow myosin heavy chain (MyHC) or fast MyHC. (Biressi et al., 2007).

Fish unlike terrestrial vertebrates, do not require the robust skeleton. Instead, they need large muscles for the locomotion through aquatic environments. One of the striking differences between the somite differentiation of amniotes and fish is that in fish, somites mainly give rise to myotome and only a small ventral portion of somites will differentiate into sclerotome (Rossi and Messina, 2014). Differences on a cellular and molecular level will be outlined by showcasing previous works in zebrafish.
In amniotes, the dermomyotome initiates primary and secondary myogenesis and dissociates afterwards (Delfini et al., 2009; Kahane et al., 2013). In zebrafish, primary myogenesis happens just before and during somite segmentation, the dermomyotome is established once the somites are formed and will initiate secondary myogenesis. The

dermomyotome persists post embryonic development, enabling its post-embryonic growth. Similar to amniotes, satellite cells are scattered in the teleost's myotome for muscle regeneration (Amthor et al., 1999; Goulding et al., 1994).

The primary myotome gives rise to slow muscle fibers and develops independently of the dermomyotome (Barresi et al., 2001; Stellabotte and Devoto, 2007). During primary myogenesis, mesodermal cells next to the notochord start to express the MRFs *myoblast determination protein 1* (*myoD)* and *myogenic factor 5* (*myf5)*. Hedgehog (Hh) signaling from the notochord induces these cells to commit to the slow fiber fate. These called adaxial cells are the precursors of embryonic slow muscle fibers.

When somite segmentation is completed, the majority of adaxial cells differentiate into superficial slow fiber cells and a few will differentiate into muscle pioneer cells. The superficial slow fiber cells will migrate radially through the somite and form a monolayer below the dermomyotome at the end of primary myogenesis (Jackson and Ingham, 2013; Nguyen-Chi et al., 2012) (Figure 1.2A-A"). The muscle pioneer cells, which remain next to the notochord, start to express the transcription factor *engrailed* which is induced by Hh signals from the notochord (Maurya et al., 2011). It has been suggested that these cells give rise to the horizontal myoseptum, an anatomical structure dividing the myotome into a dorsal epaxial compartment and a ventral hypaxial compartment (Ahmed et al., 2017).

At the time when slow muscle fibers start to differentiate, fast muscle fiber precursor cells and anterior border cells (ABCs, also known as row-one cells) can be observed. The ABCs will later form the dermomyotome.

Fast muscle precursor cells, which are located in the posterior part of the somite, start to express MRFs. MRF expression is induced by retinoic acid (Groves et al., 2005; Hamade et al., 2006; Reifers et al., 1998). Like slow muscle fibers, fast muscle fibers also differentiate into two different cell types. The majority of fast muscle fibers will differentiate into lateral muscle fibers and the remaining fast muscle fibers will differentiate into medial fast fibers. The lateral muscle fibers will fuse to become multinucleated and will be the major contributor to the body mass of adult fish. The medial fast fibers are located dorsally and ventrally of the muscle pioneer cells and surround the notochord when embryonic development is completed (Figure 1.2A"). The differentiation of these fibers depends on signals derived from the notochord (Groves et al., 2005; Maurya et al., 2011; Wolff et al., 2003). Recent studies showed that differentiation and translocation of adaxial cells is closely coupled with the differentiation of fast muscle progenitors. The fast fiber muscle progenitor cells physically force the adaxial cells away from the notochord, and by this away from the source of Hh signaling, towards the lateral part of the somite (Yin et al., 2018).

In zebrafish, as in amniotes, the dermomyotome is established right after the somites are formed, readily expressing the myocyte markers Pax3 and Pax 7 and giving rise to muscle fibers (Feng et al., 2006; Hammond et al., 2007; Hollway et al., 2007). Interestingly, among teleost species the morphology of the dermomyotome varies. While the

dermomyotome of trout's and cichlid's is a thick epithelium containing a dorsal and ventral lips, the dermomyotome in zebrafish and tuna is a flat, non-polarized epithelial layer (Devoto et al., 2006; Steinbacher et al., 2007). In medaka, the dermomyotome is a one-cell thick epithelial layer covering the myotome (Figure 1.2 B-C")(Abe et al., 2019).
The dermomyotome is derived from the ABCs positioned on the anterior side of the somite. ABCs do not express MRF and their number seems to be regulated by Fibroblast Growth Factor (FGF) signal (Stellabotte et al., 2007). Linage tracing and live imaging revealed that the ABCs undergo a lateral rotation and end up at the lateral surface of the somite (Figure 1.2A-A") (Hollway et al., 2007; Stellabotte et al., 2007).

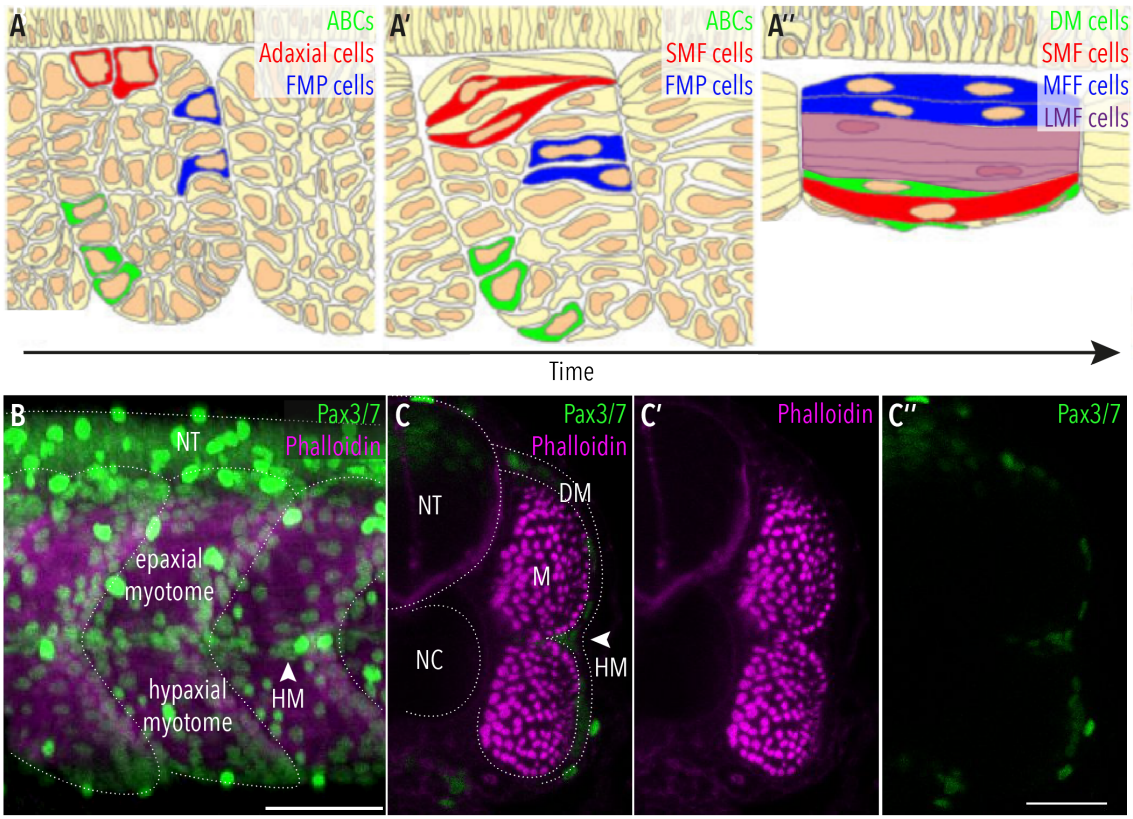

Figure 1.2: Myotome development in teleosts.
(A-A") Schematic representation of time series of myotome development in zebrafish. Dorsal view, anterior is to the left, notochord to the top. (A) Epithelial cells surround the mesenchymal core of nascent somites. Anterior border cells (ABCs, green), are the most anterior epithelial cells and lie next to the slow muscle precursor cells the adaxial cells (red). Fast muscle progenitor cells are positioned at the posterior side of the somite (blue). (A') Next to the notochord, adaxial cells differentiate into slow muscle fiber cells (red). Fast muscle progenitor cells (blue) start to elongate. The ABCs (green) move laterally. (A") Fast muscle cells differentiate into lateral muscle fibers (purple) and medial fast fibers (blue). Superficial slow muscle fibers (red) move laterally and form a monolayer beneath the elongated dermomyotome cells (green), which are derivatives of the ABCs. Adapted from (Stellabotte and Devoto, 2007). (B-C") Immunostaining of stage 30 medaka embryos. Pax3/7 (green) labels dermomyotome cells, Phalloidin (magenta) labels myofibers. (B) Lateral view, anterior is to the left. (C-C") Optical cross sections, dorsal is to the top. The dermomyotome is a one cell thick cell layer, marked by cells expressing *pax3* and *pax7*. The dermomyotome lays on the external surface of the myotome. Arrow heads indicate horizontal myoseptum, which separates the epaxial myotome form the hypaxial myotome. ABC = anterior border cell, DM = dermomyotome, FMP = fast muscle progenitor, HM = horizontal myoseptum, LMF = lateral muscle fiber, MFF = medial fast fiber, M = myotome, NC = notochord, NT = neural tube, SMF = slow muscle fiber, scale bar = 50 µm.

In summary, prior to secondary myogenesis, zebrafish somites undergo drastic spatial rearrangements (Figure 1.2A-A"). A reason why the primary myogenesis in teleosts occurs before the dermomyotome is set up might be due to the development of most teleost embryos in an external environment and the necessity of an early functioning myotome for swimming (Stellabotte and Devoto, 2007).
During secondary myogenesis in zebrafish and other vertebrates, muscle tissue is rapidly enlarged. To contribute to the zebrafish myotome, myoblasts derived from the dermomyotome have to migrate between the superficial slow muscle fibers to enter the primary myotome. In amniotes dermomyotome cells enter the myotome by migrating from the DML or VLL into the myotome, located directly beneath the dermomyotome. However, it had been also observed that some dermomyotome cells enter the myotome by "parachuting" form the central dermomyotome (Gros et al., 2005).
The axial muscles, derived from the dermomyotome in teleosts and the DML in amniotes, are subdivided into the dorsal epaxial and the ventral hypaxial muscles. These muscles are physically separated by a connective tissue called horizontal myoseptum in fish and septum laterale in amniotes (Figure 1.2 B-C) (Cheng et al., 2004; Glass and Goodrich, 1960). While the slow and fast muscle fibers in amniotes are intermixed in bundles, they are separated in teleost. The slow-twitch fibers are located in the superficial myotome whereas the fast-twitch muscle fibers are located in the deep myotome (Devoto et al., 1996; van Raamsdonk et al., 1982; Talbot and Maves, 2016). Teleost dermomyotome cells not only give rise to the secondary myotome but also give rise to the mesenchyme of the dorsal fin, fin muscles and potentially to the dermis. (Hollway et al., 2007; Stellabotte et al., 2007).
Somite differentiation and muscle development in vertebrates are complex processes which are orchestrated by an interplay of multiple signaling pathways. One of the central signaling pathway is the Wnt signaling cascade.

1.2 The canonical Wnt signaling pathway

Wnt proteins are highly conserved glycoproteins and found in all metazoan clades (reviewed in (Holstein, 2012)). The secreted Wnt proteins mediate cell-cell communication across short distances or in a contact dependent manner. Before they are secreted, Wnt proteins are lipid-modified by the addition of palmitoleic acids (Willert et al., 2003). This post translational modification causes the hydrophobic character of Wnt proteins limiting their diffusion rate in the aqueous extracellular environment to neighboring cells or cells in close proximity. The Wnt signaling cascade is involved in the regulation of multiple processes including proliferation, cell polarity, stem cell renewal, cell fate specification, tissue homeostasis and migration. Thus, Wnt signaling plays a crucial role during embryonic development and in cancer (reviewed in (Wiese et al., 2018)). Wnt proteins act through different signaling cascades. In the canonical Wnt signaling pathway cytosolic β-catenin is translocated to the nucleus where it acts as transcriptional co-activator. What

all non-canonical Wnt signaling pathways have in common is that the translocation of β-catenin into the nucleus is not involved in the signaling cascade.

In the canonical Wnt signaling pathway (Figure 1.3), the absence of Wnt ligands leads to the binding of cytosolic β-catenin by the "destruction complex". The destruction complex consists of Axin, adenomatous polyposis coli (APC), casein kinase 1 (CK1) and glycogen synthase kinase 3 (GSK3). β-catenin is bound by Axin and APC and phosphorylated by the kinases CK1 and GSK3 (Stamos and Weis, 2013). The phosphorylation creates a site for β-Trcp, a subunit of the E3 ubiquitin ligase, to ubiquitylate β-catenin, which ultimately leads to its proteasomal degradation.

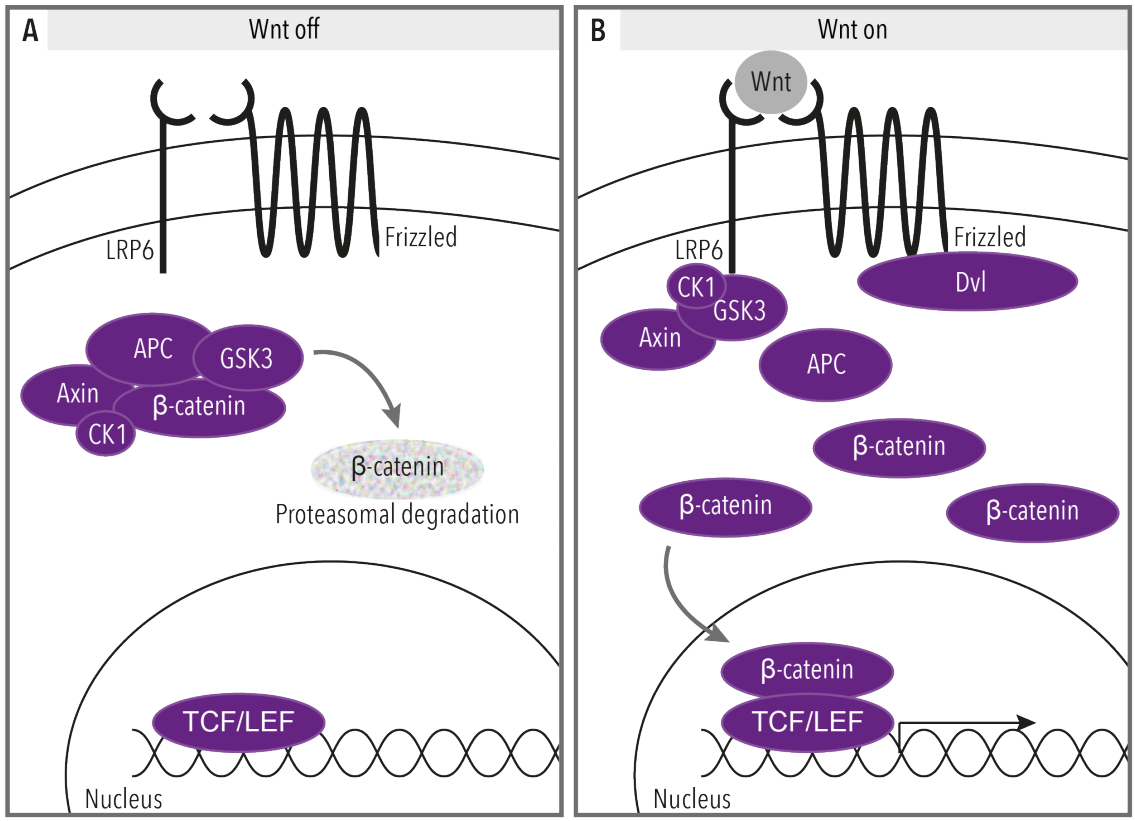

Figure 1.3: Simplified model of the canonical Wnt signaling pathway.

(A) In the absent of Wnt ligands, β-catenin is bound by proteins of the "destruction complex". In the destruction complex β-catenin is phosphorylated by the kinases GSK3 and CK1. This phosphorylation leads to further ubiquitylation by a subunit of an E3 ubiquitin ligase and the proteasomal degradation of β-catenin. (B) In the presence of Wnt ligands, Wnt binds the transmembrane receptor Fz and the co-receptor LRP6. This leads to the phosphorylation of the cytoplasmic tail of LRP6 by GSK3 and CK1 and additionally, the translocation of Axin to the cell membrane. Furthermore, Dvl is recruited to the cell membrane and binds the cytoplasmic tail of Fz. Altogether, a signalosome is formed at the cell membrane and the destruction complex is disrupted. β-catenin is now able to accumulate in the cytosol and translocate to the nucleus where it binds the transcription factors TCF and LEF. This initiates the transcription of target genes. APC = adenomatous polyposis coli, CK1 = casein kinase 1, Dvl = dishevelled, Fz = frizzled, GSK3 = glycogen synthase kinase 3; LRP6 = low-density lipoprotein receptor related protein 6, Tcf/Lef = T-cell factor/lymphoid enhancer factor. Adapted from (MacDonald et al., 2009).

If Wnt is present, it binds to the transmembrane receptor Frizzled (Fz) and its co-receptor low-density lipoprotein receptor related protein 6 (LRP6). Upon Wnt binding, GSK3 and CK1 phosphorylate the cytoplasmic tail of LRP6 which leads to the binding of Axin. Dishevelled (Dvl) is recruited to the cell-membrane and binds the cytoplasmic tail of Fz. Together these events lead to the formation of a "signalosome", resulting in the disruption of the destruction complex (Bilić et al., 2007; Gammons et al., 2016; Gerlach et al., 2018). Now, β-catenin can accumulate in the cytoplasm and is subsequently translocated into the nucleus. In the nucleus β-catenin binds to the T-cell factor (TCF) and Lymphoid enhancer-binding factor (LEF) to initiate target gene transcription (Behrens et al., 1996; Molenaar et al., 1996). It is proposed that the robustness of Wnt signaling is achieved by feedback loops since, multiple of Wnt signaling target genes, for example *axin2,* are also involved in the Wnt signaling cascade (Jho et al., 2002).

1.3 Wnt signaling during muscle development

Wnt proteins are involved in numerous developmental processes including somitogenesis, dermomyotome specification and muscle development. So far, this has been mainly studied in amniotes. In chicken it was shown that Bone morphogenic protein (BMP) signaling initiates the expression of *wnt1* and *wnt3a* in the dorsal part of the neural tube. Surgical ablations of parts of the neural tube and ectopically expression of *wnt1* revealed that Wnt1 and Wnt3a are necessary for dermomyotome induction. In somites, the *wnt11* expression pattern is known to serve as a proxy for dermomyotome induction. This non-canonical Wnt protein is a marker for the DML (Marcelle et al., 1997). Consistently, the dermomyotome in *wnt1/wnt3a* mutant mice is decreased in size. In these mice a reduction of the expression domain of *pax3* and *myf5* further indicated that the medial compartment of the dermomyotome is absent (Ikeya and Takada, 1998). A study in chicken revealed that to maintain the epithelial state of the dermomyotome, the expression of *wnt6* from the ectoderm overlaying the central part of the somite is essential. Blocking Wnt6 activity, by interfering with canonical Wnt signaling components, leads to the de-epithelialization of the dermomyotome. (Linker, 2005).
Groundbreaking works using chicken embryos helped to elucidate the relationship between Wnt proteins and the patterning of the dermomyotome. The injection of cells expressing *wnt1* or *wnt3a* into epithelial somites resulted in the inhibition of *wnt6* expression from the ectoderm. It turned out that in this context Wnt1 and Wnt3a act through the induction of Wnt11. Wnt11 from the DML inhibits *wnt6* expression and additionally restricts its expression to the part of the ectoderm overlaying the VLL. It was shown that Wnt11 and Wnt6 are crucial for the maintenance of the epithelialization of the DML and VLL of the dermomyotome (Figure 1.4). Overexpression of *wnt11* led to an excessive epithelialization of the somites and an overexpression of the epithelialization

marker *paraxis* (Geetha-Loganathan, 2006). Moreover, *wnt11* expression in the DML during myogenesis is essential for the correct orientation of elongating myocytes. The directional cues for the myocyte orientation are provided through the planar cell polarity pathway, a non-canonical Wnt signaling pathway (Gros et al., 2008).

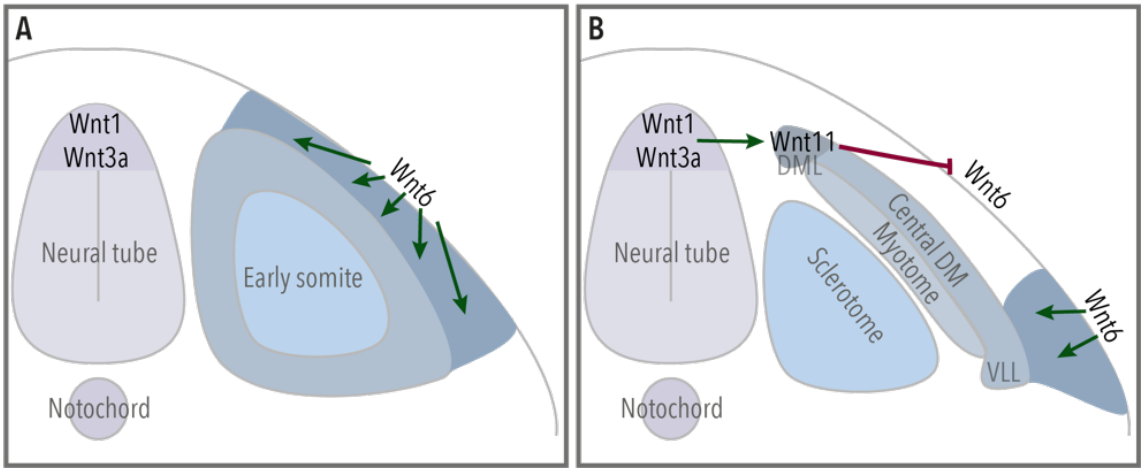

Figure 1.4: Wnt signaling during somite differentiation.
(A) While the somite is still in an epithelial state, *wnt6* is expressed in the ectoderm overlaying the somite. *Wnt1* and *wnt3a* are expressed in the dorsal neural tube. (B) During somite differentiation, Wnt1 and Wnt3a in the dorsal neural tube induce the expression of *wnt11* in the DML. Wnt11 in turn inhibits the expression of *wnt6* in the ectoderm overlaying the DML and the central DM restricting its expression to the ectoderm overlaying the VLL. Adapted from (Geetha-Loganathan, 2006; Marcelle et al., 1997) DM = dermomyotome, DML = dorsomedial lip, VLL = ventrolateral lip.

Another crucial role of Wnt signaling during dermomyotome specification is the regulation of the expression of *pax3*, *pax7* and MRFs (Galli et al., 2004; Otto et al., 2006; Schmidt et al., 2004). Inactivation of β-catenin in newly formed somites inhibited *myoD* and *myf5* expression as well as the formation of the myotome. It was shown in mouse that Pax3 acts as a mediator between canonical Wnt signaling and the induction of *myoD* and *myf5* in myoblasts (Hutcheson et al., 2009).
Wnt proteins play also an important role in muscle development. Myoblasts derived from the DML, are induced by a combination of Wnt1/Wnt3 signaling from the neural tube and low levels of Sonic hedgehog (Shh) signaling from the neural tube floor plate (Borycki and Emerson, 1999; Münsterberg et al., 1995). This leads to the induction of *myf5* and subsequently the activation of other muscle specific genes. Although induction of myoblasts derived from the VLL is a bit more complicated, Wnt proteins are involved, too. The combined presence of Wnt7 from the ectoderm and the absence of BMP signal from the lateral plate mesoderm, are necessary for the induction of myoblasts. Wnt7 induces *myoD* expression by a non-canonical Wnt cascade involving protein kinase C which in turn activates further MRFs (Brunelli et al., 2007; Gerhart et al., 2006, 2011; Reshef et al., 1998).
Until recently it was not known how Wnt1 and Wnt3a from the dorsal neural tube induce Wnt11 in the distant DML. Only lately it was observed that neural crest cells are

loaded with Wnt proteins, expressed in the dorsal the neural tube, and subsequently transported to cells of the DML (Serralbo and Marcelle, 2014). Neural crest cells are not just involved in the transportation of Wnt proteins from the neural tube, but also have been shown to initiate the translocation of β-catenin to the nucleus of DML cells in a Wnt-independent manner. Neural crest cells induce epithelial mesenchymal transition (EMT) of DML cells via the Notch signaling pathway. During the EMT, membrane bound β-catenin is released into the cytoplasm and translocated to the nucleus, where it acts as a co-activator to initiate *myf5* expression (Sieiro et al., 2016).
The expression of *wnt1* and *wnt3a* in the dorsal neural tube, as well as the expression of *wnt11* in the dorsal part of the somites are highly conserved among vertebrates. Nevertheless, in teleosts the role of Wnt signaling during somite differentiation is poorly understood.

1.4 Dorsoventral patterning of the somites and during muscle formation

One of the key questions in developmental biology is, how are newly formed tissues patterned. Grafting experiments in chicken, have shown that nascent somites are not restricted in their fate, yet (Aoyama and Asamoto, 1988; Dockter and Ordahl, 2000; Ordahl et al., 2001). External signaling cues from surrounding tissues initiate the formation of the mediolateral and the dorsoventral axis. Secreted Wnt ligands form the dorsal neural tube and Shh ligands from the notochord and the neural tube floor plate initially pattern the somites by forming a dorsalizing Wnt gradient and a ventralizing Shh gradient. It has been proposed that the long range effect of these signaling molecules is constrained by inhibitors. A potential Wnt antagonist is Secreted frizzled-related protein 2 (Sfrp2) which is expressed in sclerotome cells and upregulated by Shh signaling (Lee et al., 2000). Whereas the membrane glycoprotein growth-arrest specific gene 1 (Gas1), which is induced by Wnt signaling and expressed in the dorsal somites, was identified as a potential Shh inhibitor (Lee et al., 2001).
This initial patterning is crucial for the determination of the sclerotome and the dermomyotome (Dockter and Ordahl, 1998; Williams and Ordahl, 1997). The sclerotome is induced and maintained by Noggin and Shh which are secreted from the neural tube floor plate and the notochord. (Dietrich et al., 1997; Johnson et al., 1994; McMahon et al., 1998; Pourquié et al., 1993). As discussed previously, the induction of the dermomyotome is Wnt-dependent. Interestingly, myotome formation depends on ventrally-derived Shh and on dorsally-derived Wnt. It was shown that Shh induces the expression of the early MRFs *myoD* and *myf5* (Dietrich et al., 1997; Münsterberg et al., 1995), while Wnt ligands are required to maintain MRF expression (Cossu et al., 1996; Tajbakhsh et al., 1998).

Patterning of the dermomyotome which gives rise to dorsal epaxial and ventral hypaxial myocytes is well conserved among vertebrates. The part of the dermomyotome giving rise to epaxial myocytes expresses *wnt11* in chicken, mouse and zebrafish and its homologue *wnt11r* in medaka and *Xenopus* (Garriock and Krieg, 2007; Isabel Olivera-Martinez et al., 2002; Kawanishi et al., 2013). Additional markers for the dorsal dermomyotome and dorsal somites are Zic family member 1 (Zic1) and Zic family member 4 (Zic4) (Houtmeyers et al., 2013; Ohtsuka et al., 2004; Sun Rhodes and Merzdorf, 2006). Single-minded 1(Sim1) labels the part of the dermomyotome giving rise to hypaxial myocytes (Coumailleau et al., 2000; Kawanishi et al., 2013; Pourquié et al., 1996). While the markers for initial patterning are known, it is still not understood how this dorsoventral patterning is maintained and the developmental process which makes the epaxial and hypaxial myotome adopt their specific morphology.

1.5 Spontaneous medaka mutants are a valuable resource to identify novel genes and uncover developmental dynamics

Mutagenesis screens are a common method to identify unknown genes in embryonic development as well as genes causing diseases. The first large-scale mutagenesis screen in vertebrates was performed in zebrafish using the chemical N-ethyl-N-nitrosourea (ENU) (Driever et al., 1996). Similarly, ENU mutagenesis screens have been performed in medaka (Ishikawa et al., 1999; Furutani-Seiki et al., 2004). In addition, a natural resource consisting of spontaneous medaka mutants has long been used to identify novel genes.
The first description of spontaneous medaka mutants tracks back to a fish encyclopedia in 1838, where an orange-red and a white medaka mutant were described (pictured by Motohisa Mouri 1798-1851). Most of the spontaneous mutants studied today have been collected in Japan during the second half of the twentieth century. The spontaneous mutants were isolated from the wild and screened by extensive back crossing. This exhaustive work was done by Hideo Tomita, giving this collection of spontaneous mutants the name "Tomita collection". To date, this collection contains of more than 80 mutants and is maintained in stock centers at Nagoya University. (Naruse et al., 2011; Tomida, 1992; Wittbrodt et al., 2002). Most of the collected mutants are affected in their pigmentation. This led to the description of five genetic loci responsible for melanophore pigmentation (*b*, *dl*, *dl2*, *i-1* and *i-3*) by Tomita (reviewed in (Kelsh et al., 2004; Naruse et al., 2011)). The albino mutant *i-1* has an amelanotic skin and red eyes. It was shown that the tyrosinase gene is responsible for this mutant phenotype. On a side note, tyrosinase was the first mutant gene identified in medaka (Koga et al., 1995). Patients with oculocutaneous albinism type 1 (OCA1) have red eyes, white hair and skin. It was shown that the tyrosinase gene is mutated in patients with OCA1. Strikingly, three of the four OCA exist in

medaka (Fukamachi et al., 2001, 2004). Studying these mutants provided valuable insights into the conserved mechanism of vertebra melanin synthesis. Most of the early studies using the pigmentation mutants of the Tomita collection, focused on the adult phenotype. By describing the embryonic phenotypes, Kelsh and colleagues establish a valuable resource to study neural crest cell development, complementing studies performed in mouse and zebrafish (Kelsh et al., 2004).
The spontaneous mutants are often caused by the insertion of a transposons into the respective gene locus (Iida et al., 2004; Koga et al., 1995). In three of the four *i*-locus alleles (*il*, *i4* and *ib*), a transposon (Tol1/Tol2) insertion was identified (Koga and Hiroshi, 1997).
The Tomita collection does not just contain pigmentation mutants. Mutants with affected body morphology, eyes, fins and skeletal elements can be also found. In the *fused centrum* mutant, all invertebral ligaments are absent and the central parts of the vertebra, the centrum, are fused together causing an extremely shortened body axis (Inohaya et al., 2010). In the *eyeless* mutant, the complete absent of eyes can be observed (Loosli et al., 2001), and the *reduced scales* mutant has almost complete lost all of their scales (Kondo et al., 2001). What all these mutants have in common that the insertion of a transposon into either the promoter or an intronic region altered the regulation of the genes underlying the mutant phenotypes.
An invaluable mutant to study late somite patterning, is the *Double anal fin* (*Da*) mutant. In contrast to the mutants described above, the transposon causing the *Da* mutant phenotype is not inserted into the promoter or an intronic region but in an enhancer region. This leads to the restriction of the mutant phenotype to the trunk region and allows the investigation of the affected genes in a spatial restricted manner.

1.6 The *Da* mutant

In the 1960s, the *Da* mutant was collected in Toyokawa and kept as a separate medaka strain. The *Da* mutant obtained its name from the dorsal fin which is transformed into an anal fin. In addition to the transformed dorsal fin, the adult mutant phenotype contains multiple additional alterations from pigmentation to skeletal elements. Bright iridophores, which in wildtype (Wt) medaka are found on the belly, are distributed on the dorsal trunk region in the *Da* mutant. The caudal fin of the *Da* mutant has a rhombic shape whereas the caudal fin in Wt medaka is triangular in shaped. The body morphology of the *Da* mutant is teardrop like, resembling the streamlined body morphology of fast swimming fish in the middle layer, which contrasts the wedged shaped body morphology of slow swimming fish, living near the water surface like medaka. Alterations observed in the skeletal elements of the *Da* mutant include irregular shaped neural arches and the deformed shape and increased size of neural spines. In addition to the lateral and ventral line of neuromasts, a dorsal line of neuromasts can be observed in the *Da* mutant. Over

all, the mutant phenotype looks like the ventral half is mirrored at the lateral midline (Figure 1.5A, C)(Ishikawa, 1990; Ohtsuka et al., 2004).
Differences between Wt and *Da* mutant become apparent towards the end of embryonic development. Instead of the single line of melanophores formed at the dorsal midline above the neural tube, two parallel lines of melanophores are present at the dorsal midline in *Da* mutant embryos. A prominent trait of the *Da* phenotypes is the morphology of the dorsal myotome. The shape of the dorsal myotome resembles that of the ventral myotome. Furthermore, the ends of the dorsal myotome fail to extend sufficiently, which results in the incomplete coverage of the neural tube by the epaxial myotome at the end of embryonic development. It is postulated that the misshaped myotome causes the teardrop body shape observed in adult *Da* mutants (Ohtsuka et al., 2004; Tamiya et al., 1997). Nevertheless, the early embryonic development, behavior and reproduction are completely normal in the *Da* mutant. In summary, the *Da* mutant exhibits a ventralized trunk phenotype, and therefore, studying the *Da* mutant could provide insights into the dorsalization of somites and their derivatives such as the myotome.

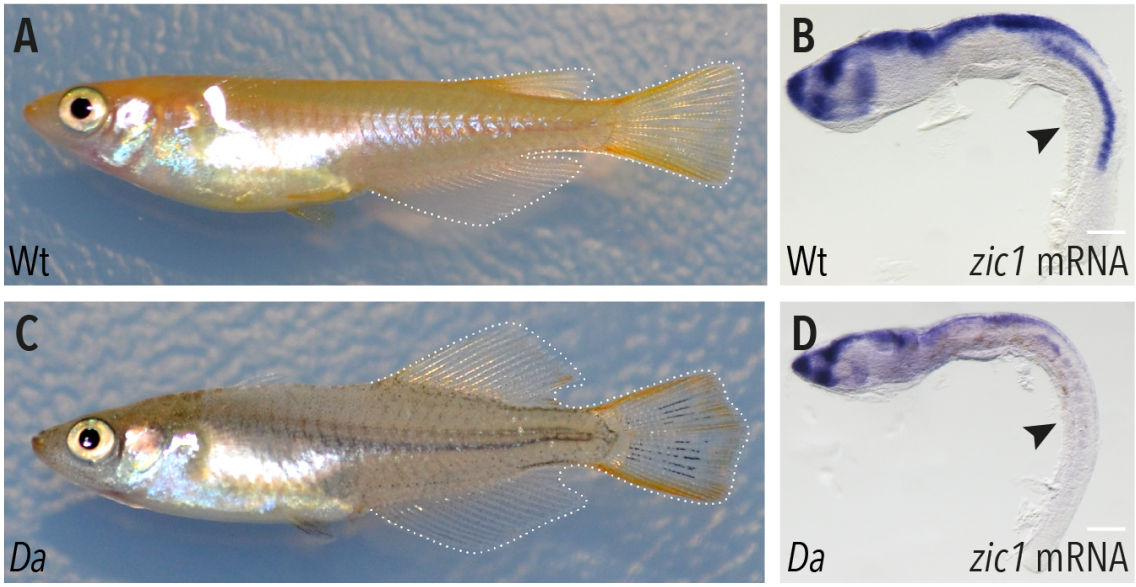

Figure 1.5: Drastic reduction of the somitic expression of *zic1/zic4* causes the ventralized *Da* phenotype.
(A, C) Lateral view of adult medaka. Dorsal and caudal fin shapes are outlined. (B, D) Lateral view of whole-mount *in situ* hybridizations of stage 23 embryos. Arrow heads indicate *zic1* expression in the dorsal somites. (A) The body morphology of Wt medaka is wedge-shaped. The dorsal fin is small and the caudal fin is triangular. (B) In Wt embryos, *zic1* is expressed in the brain, neural tissues and the dorsal somites. (C) The body morphology of an adult *Da* mutant is teardrop shaped. Iridophores, in Wt found on the belly, are found on the dorsal trunk region. The dorsal fin is transformed into a large anal fin. The caudal fin has a rhombic shape. (D) In *Da* mutant embryos the expression of *zic1* in the dorsal somites is drastically reduced. The expression in other tissues in unaffected. Scale bar = 100µm.

For many years the cause of the *Da* phenotype had been a mystery. With the advancement of genetic methods, Ohtsuka and colleagues found that the expression levels of *zic family member 1 (zic1)* and *zic family member 4 (zic4)* are strongly reduced in the dorsal somites

of the *Da* mutant, causing the ventralized mutant phenotype. Interestingly, the expression of *zic1/zic4* in other tissues, including the brain and the neural tube, is unaffected (Figure 1.5B, D). The genes are expressed by a bi-directional promoter, resulting in their similar expression, although *zic4* is expressed more weakly than *zic1* (Aruga et al., 2006; Ohtsuka et al., 2004). Additionally, it was proposed that they have overlapping functions in trunk dorsalization of medaka (Kawanishi et al., 2013; Moriyama et al., 2012), therefore, I will mainly focus on *zic1* in this thesis.
Intriguingly, *zic1* mutant mice show a skeletal defects, spina bifida occulta, which is also observed in the *Da* mutant (Aruga et al., 1999).

Finally, it was discovered that the strong reduction of *zic1/zic4* expression in the dorsal somites is due to the insertion of a large transposon (Teratorn, ca. 180 kb) within the somitic enhancer region of *zic1/zic4*, defining the *Da* mutant as an enhancer mutant (Inoue et al., 2017; Moriyama et al., 2012).

1.7 Zic1/Zic4 in embryonic development

The transcription factors Zic1 and Zic4 belong to the ZIC (zinc finger of cerebellum) gene family and are orthologues of the *Drosophila* pair-rule gene *odd-paired* (Houtmeyers et al., 2013). Zic proteins contain a zinc finger domain consisting of five Cys2His2-type zinc fingers which is closely related to the zinc finger domains found in Glioma-associated oncogene (GLI), Gli-similar (GLIS) and the NK-like (NKL) gene families. It is known that the zinc finger domain is important for DNA and protein/protein interactions, enabling Zic proteins to directly regulate the transcription of target genes or act as co-factors. All Zic genes are evolutionary conserved and can be found in all vertebrates. Fish have seven Zic genes, whereas the other vertebrates have five Zic genes (reviewed in (Houtmeyers et al., 2013)).
In fish and *Xenopus*, the earliest expression of *zic1* and *zic4* can be observed in the neuroectoderm during gastrulation, where they induce differentiation of the neuroectoderm (Elsen et al., 2008; Fujimi et al., 2006; Nakata et al., 1998). In mouse, only *zic1*, but not *zic4* expression, can be observed during early embryogenesis, which, together with *zic3,* is required for neural fate acquisition (Marchal et al., 2009). During organogenesis the expression of *zic1* and *zic4* is conserved among vertebrates. *Zic1* and *zic4* are expressed in the brain, neural tissues and dorsal somites (Fujimi et al., 2006; Houtmeyers et al., 2013; Nakata et al., 1998; Sun Rhodes and Merzdorf, 2006). In the brain they positively regulating the proliferation of granule cell progenitors during the development of the cerebellum (Blank et al., 2011) and during sclerotome differentiation they play a role in the formation of vertebral arches, the dorsal parts of the vertebrae (1999). Additionally, Zic1 plays a role in the induction of neural crest cells (Nakata et al., 1998; Plouhinec et al., 2014; Sato, 2005). As introduced in the previous section, the expression of *zic1/zic4*

in the dorsal somites together with the misshaped dorsal myotome in the *Da* mutant propose a function of *zic1/zic4* in myotome development. Yet, no study has addressed the role of *zic1/zic4* during myotome development, and their regulatory function in this context.

During early somite development, *zic1* expression is negatively regulated by BMP and Shh signaling. The zebrafish BMP2 mutant *swirl* has a dorsalized phenotype (Kishimoto et al., 1997). In these mutants, *zic1* expression is not restricted to the dorsal part of the somites, but can be observed throughout the somites. Creating ventralized phenotypes by injecting *bmp2* mRNA led to the loss of *zic1* expressions in the somites. (Rohr et al., 1999). Similarly, in zebrafish embryos injected with *shh* mRNA, which ventralizes somites, *zic1* expression is reduced in the somites (Rohr et al., 1999). Yet, a positive regulator for *zic1/zic4* has not been conclusively determined. Recently, Abe and colleagues proposed that Wnt signaling positively regulates the expression of *zic1/zic4* in the dorsal somites (Abe et al., 2019). This was concluded from experiments inhibiting Wnt signaling and ectopically expressing Wnt ligands followed by the analysis of *zic1* expression. Despite these results, the direct upstream regulator of *zic1/zic4* has not been identified so far.

Aim

The aim of this study was to elucidate the regulation and the developmental process underlying dorsal somite extension which will give rise to the epaxial muscles of the back. Although it is well described how the myotome is patterned during somite differentiation, it is still unclear how the myotome after induction develops to give rise to the muscle morphology found in adults. Recent studies identified the transcription factors Zic1/Zic4 as dorsalization factors during late somite differentiation. Additionally it was shown that they are crucial for the dorsal identity of the epaxial myotome, by analyzing the *Da* mutant which exhibits a ventralized trunk phenotype including misshaped epaxial muscles. These studies mainly focused on the role of the transcription factors to establish and maintain dorsoventral polarity throughout development. Today, it is not completely clear how *zic1/zic4* are regulated during somite differentiation. Moreover the developmental process fundamental for the formation of epaxial muscles from dorsalized myotome and the cellular and molecular mechanisms underlying this process are poorly understood.

First, I wanted to investigate if *zic1/zic4* are regulated by the canonical Wnt signaling pathway as proposed in earlier studies. Therefore, I examined the expression of *zic1* after pharmacological and genetic manipulation of the canonical Wnt signaling cascade. Moreover, I performed a ChIP-seq against β-catenin to determine whether *zic1/zic4* are direct downstream targets of this signaling pathway.

Second, I wanted to investigate the developmental process of dorsal somite extension to give rise to the epaxial musculature of the trunk. To determine whether the observed characteristics are due to dorsalization of the myotome by *zic1/zic4*, I compared the dorsal somite extension in Wt medaka to the process in the ventralized *Da* mutant using *in vivo* imaging and time-lapse imaging. I further observed whether dorsalization has an effect on the size of the myotome and the proliferative capacity of the dermomyotome by immunohistochemistry.

Third, I wanted to analyze the molecular mechanism underlying dorsal somite extension. Thus, I identified *wnt11r* as potential dorsalization factor downstream of *zic1/zic4*. I examined its dorsalization capacity by knockdown experiments in Wt embryos and a rescue experiment in the *Da* mutant. To investigate through which pathway Wnt11r acts, I inhibited the Wnt/Ca^{2+} signaling pathway and analyzed dorsalization characteristics in treated embryos.

2 Results

2.1 The somitic expression of *zic1/zic4* is directly regulated by the canonical Wnt signaling pathway

2.1.1 The canonical Wnts *wnt1* and *wnt3a* are expressed in the dorsal neural tube during somite differentiation

It had been suggested that *zic1/zic4* are expressed downstream of the canonical Wnt signaling pathway during somite differentiation. Previous experiments performed in the lab (including inhibition of the canonical Wnt signaling pathway and ectopic the expression of Wnt3a) proposed that canonical Wnt signaling is necessary for the activation of *zic1* expression in the somites (Abe et al., 2019). Additionally, observation of a Wnt/β-catenin-reporter line in zebrafish indicated Wnt activity in young somites in a graded fashion, high activity in dorsal somites and a reduction of activity towards the ventral somites. This graded activity in young somites, and the restriction to the dorsal somites in older somites, correlates well with the expression pattern of *zic1*, which is expressed also in a graded fashion in young somites and restricted to the dorsal somites in older somites (Abe et al., 2019; Kawanishi et al., 2013; Shimizu et al., 2012). Several canonical Wnt ligands are expressed in the dorsal neural tube, but expression analysis of canonical Wnt ligands had been done mostly by whole-mount *in situ* hybridization in medaka. Unfortunately this does not provide the necessary spatial resolution to conclusively describe the expression pattern of canonical Wnt ligands during somite differentiation.
To determine the expression of the canonical Wnts *wnt1* and *wnt3a* at stage 26 (22-somite stage), I performed whole-mount *in situ* hybridizations with subsequent vibratome sectioning of the stained embryos. *Wnt*1 and *wnt3a* are expressed in a few cells at the top of the neural tube (Figure 2.1A-B'), these cells co-express *zic1* (Figure 2.1C-C').

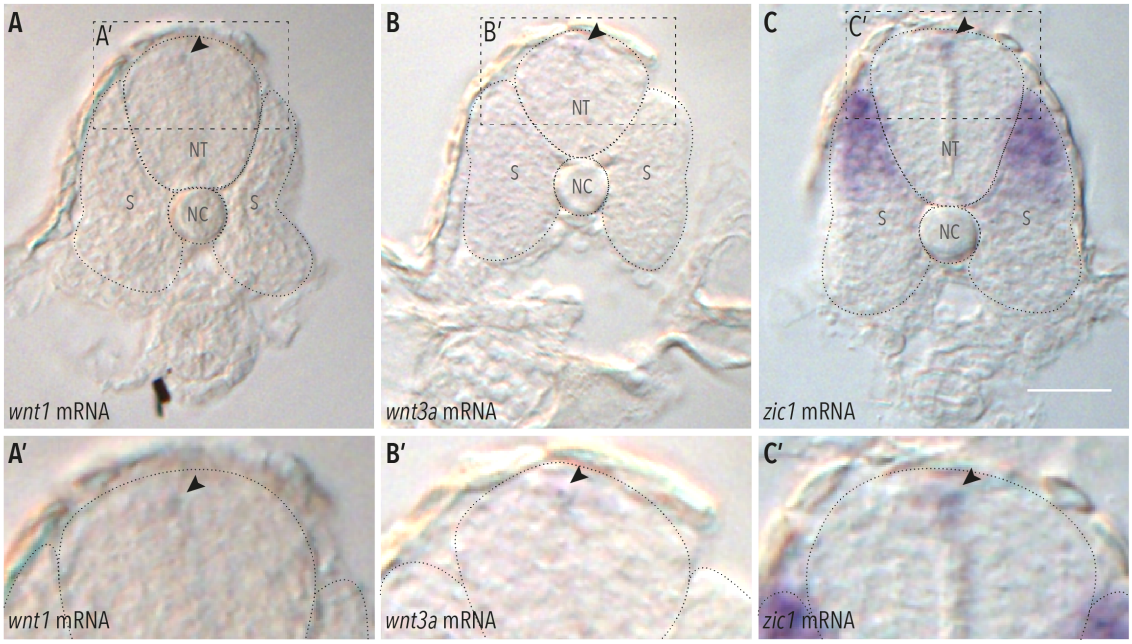

Figure 2.1: Expression of canonical Wnt proteins and *zic1* during somite differentiation.
(A-C') Vibratome sections of whole-mount *in situ* hybridizations of stage 26 embryos. (A-A') *Wnt1* is expressed at the top of the neural tube. (B-B') *Wnt3a* is also expressed at the top of the neural tube. (C-C') *Zic1* is expressed at the top of the neural tube and in the dorsal somites. NC = notochord, NT = neural tube, S = somites, scale bar = 38 µm, sections = 40 µm.

The *in situ* hybridizations validated the expression of *wnt1* and *wnt3a* in the dorsal neural tube during somite differentiation, this is consistent with findings in other vertebrate species.

2.1.2 Up- and downregulation of the canonical Wnt signaling pathway alters *zic1* expression pattern

To investigate a functional relationship between canonical Wnt signaling and *zic1* expression in the dorsal somites, I manipulated the canonical Wnt signaling pathway using chemical inhibitors and activators.
I used the drugs IWR-1 to inhibit the canonical Wnt signaling pathway and 1-Azakenpaullone to over activate the canonical Wnt signaling pathway. Both drugs are widely used in fish (Abe et al., 2019; Meyers et al., 2012; Shimizu et al., 2012). Embryos of the transgenic line *zic1::GFP* were treated with 10 µM IWR-1 from 9-somite stage until stage 24 (16-somite stage), while embryos in the control group were treated with DMSO in parallel. To over activate the canonical Wnt signaling pathway, embryos of the transgenic line *zic1::GFP* were treated with 2.5 µM 1-Azakenpaullone at stage 22 (9-somite stage) for 3 h and raised until stage 24. Embryos in the control group were treated with DMSO in parallel. To investigate the effect of the drug treatments, intensity of the GFP expression (corresponding to the endogenous *zic1* expression (Kawanishi et al., 2013)) was investigated (Figure 2.2A'-B"). Embryos treated with IWR-1 showed a

decrease in GFP intensity in the trunk (10/10 embryos) (Figure 2.2A"), whereas embryos treated with 1-Azakenpaullone show an increase in GFP expression (8/11 embryos) (Figure 2.2B"), compared to GFP intensity of embryos in the control groups.

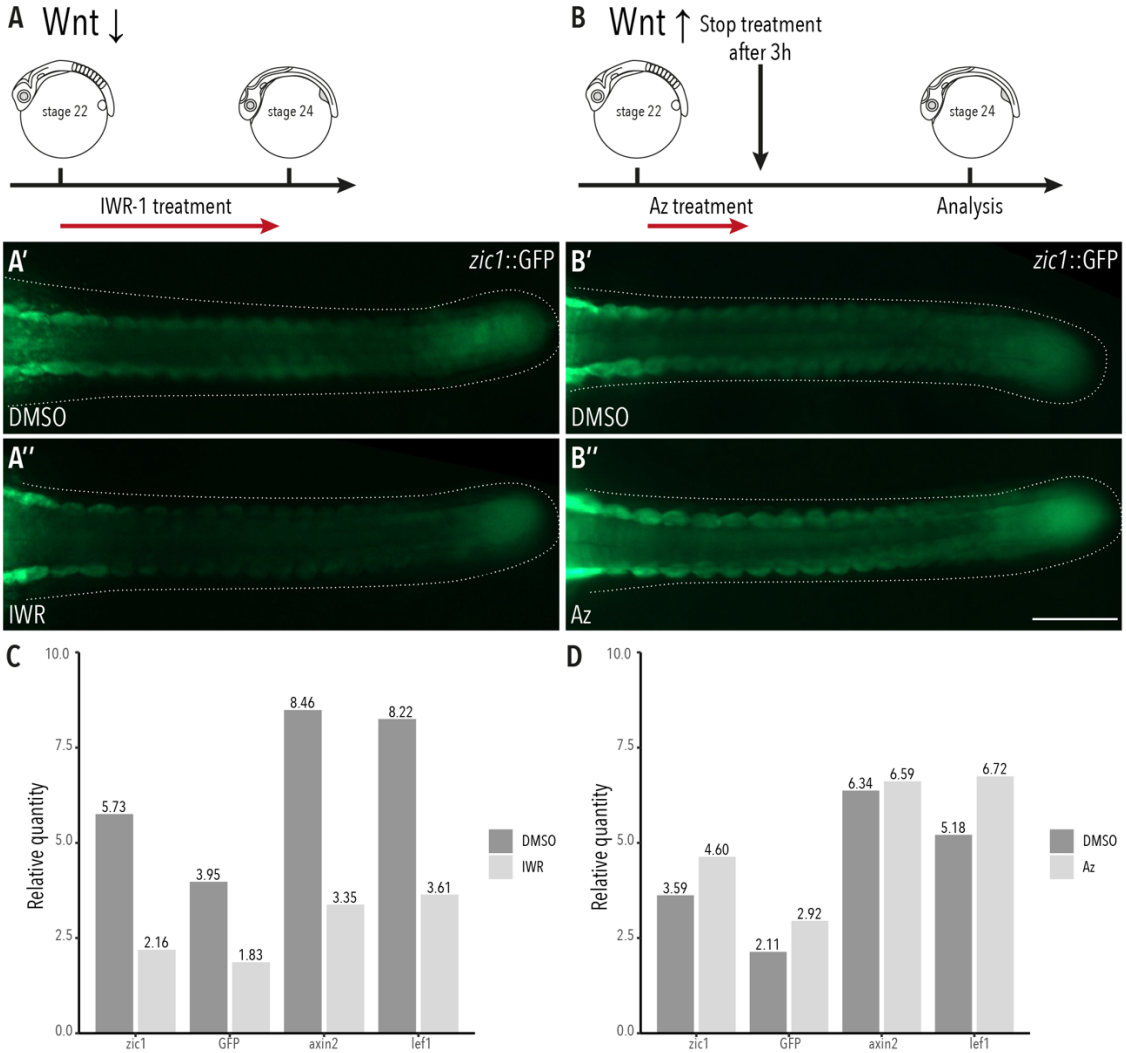

Figure 2.2: Up- or downregulation of the canonical Wnt signaling pathway using chemical compounds leads to the respective up- or downregulation of *zic1*.

(A) To downregulate the canonical Wnt signaling pathway, stage 22 embryos were treated with IWR-1 until stage 24. (B) Canonical Wnt signaling was upregulated by treating stage 22 embryos with (Az) for 3h. Embryos were analyzed at stage 24. (A'-A") Dorsal view of stage 24 embryos. The GFP signal, corresponding to *zic1* expression is reduced in embryos treated with IWR-1 compared to control embryos. (B'-B") Dorsal view of stage 24 embryos. Embryos treated with Az show stronger GFP expression compared to control embryos. (C-D) qPCR quantification of gene expression in tails of embryos after manipulation of Wnt signaling. (C) *Zic1,* GFP and Wnt target gens are downregulated in IWR-1 treated embryos. qPCR was performed on pooled RNA isolated from 10 tails per condition (D) In tails of embryos treated with Az, *zic1*, GFP and the expression of Wnt target genes is upregulated. qPCR was performed on pooled RNA isolated from 10 tails per condition. Az = 1-Azakenpaullone, IWR = IWR-1, scale bar = 100 µm.

To quantify of changes in gene expression after the drug treatments, RT-PCR was performed on cDNA of RNA isolated from dissected tails of treated embryos. RT-PCR confirmed that *zic1*, GFP and known Wnt downstream targets *axin2* and *lef1* (Behrens

et al., 1996; Huber et al., 1996; Ikeda et al., 1998; Sakanaka et al., 1998) were downregulated in tail pieces of IWR-1 treated embryos in comparison to expression levels of control embryos (Figure 2.2C). In embryos treated with 1-Azakenpaulone I confirmed by RT-PCR that the expression levels of *zic1*, GFP, *axin2* and *lef1* were upregulated in comparison with control embryos (Figure 2.2D).

Azakenpaullone-1acts by inhibition of GSK3β, which is also involved in other signaling cascades beside the canonical Wnt signaling pathway (Kunick et al., 2004). To over activate the Wnt signaling pathway more specifically, I additionally manipulated the signaling pathway genetically. I used heat stress inducible constructs containing 8 heat shock elements and a bi-directional promoter. Heat shock leads to the expression of GFP and a gene of interest (Bajoghli et al., 2004). To upregulate the canonical Wnt signaling pathway I used two different constructs, one containing *240ΔLef1VP16* and the other construct containing *61ΔTCF3* (Doenz et al., 2018) (Figure 2.3B). Embryos were injected at 1-cell stage with one of the constructs, followed by a heat shock at stage 20 (4-somite stage). At stage 26, embryos were fixed and whole-mount *in situ* hybridizations against *zic1* were performed to evaluate changes in the expression level. In 12/14 embryos injected with the construct containing 240ΔLef1VP16 and in 7/8 embryos injected with the construct containing 61ΔTCF3 an increase in *zic1* expression could be observed in the trunk region, in comparison to embryos injected with a construct only expressing GFP after heat shock (10/10 embryos showed normal *zic1* expression) (Figure 2.3C-E'). Taken together, the chemical and genetic manipulations of the canonical Wnt signaling pathway further indicate that the somitic expression of *zic1* is regulated by the Wnt signaling pathway.

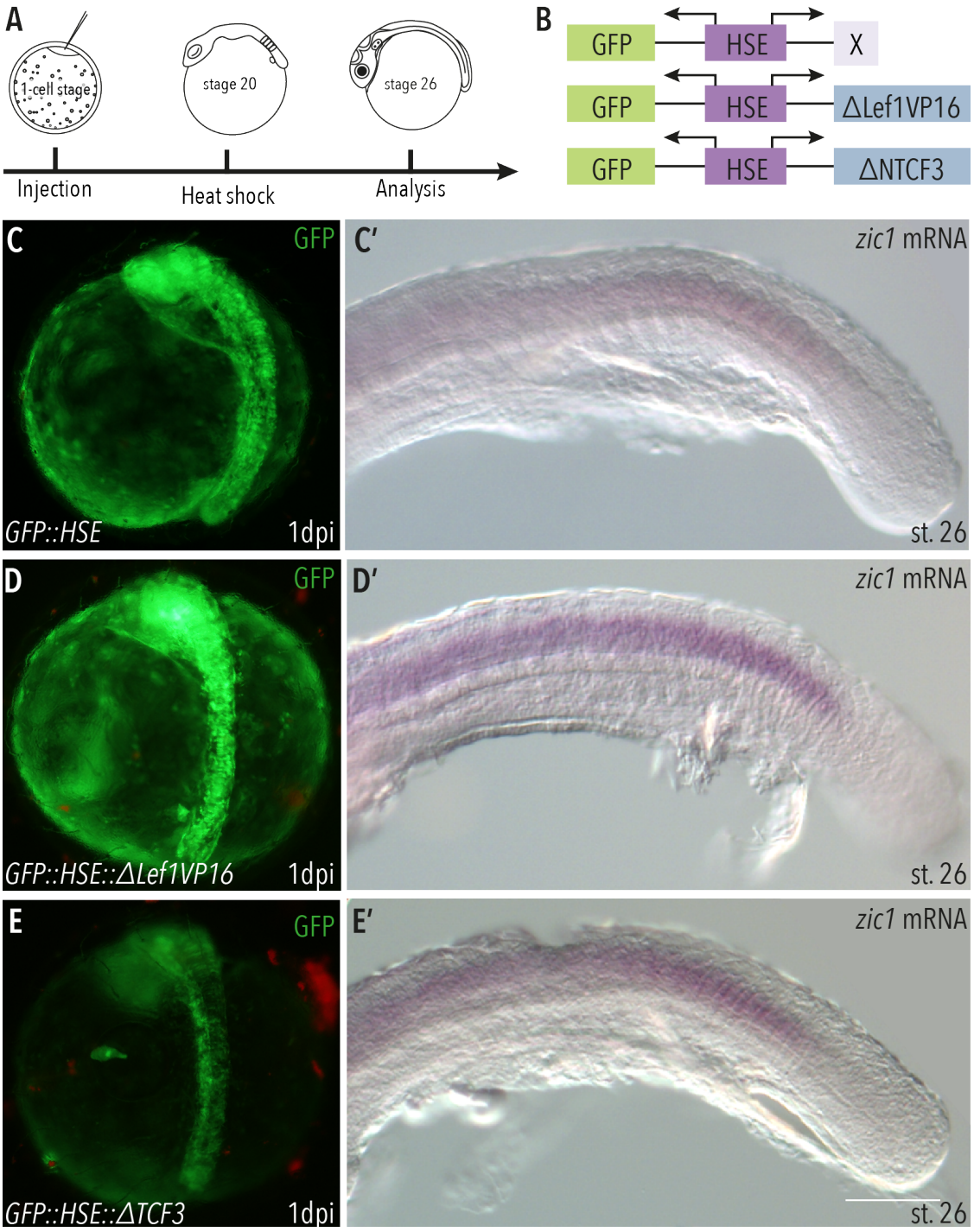

Figure 2.3: Genetic upregulation of the canonical Wnt signaling pathway leads to the upregulation of *zic1* expression in the tail.

(A) Embryos were injected at 1-cell stage with constructs containing heat shock inducible elements. Heat shock was performed at stage 20 and embryos were analyzed at stage 26. (B) List of constructs used in this experiment. (C, D, E) GFP expression 1 day after heat shock (dorsal view). (C', D', E') Whole-mount *in situ* hybridization against *zic1* indicates that *zic1* expression is upregulated in the dorsal somites of embryos with overactivated Wnt signaling pathway (lateral view of tails). HSE = heat shock element, dpi = days past induction, scale bar = 100 µm.

2.1.3 Identification of a suitable antibody for ChIP-seq against β-catenin

So far, it has been confirmed that *zic1* is expressed downstream of the canonical Wnt signaling pathway in the somites. To investigate whether *zic1* is a direct downstream target of the canonical Wnt signaling pathway I planned to perform Chromatin-Immunoprecipitation (ChIP) experiments against β-catenin. β-catenin is a core protein of the canonical Wnt signaling pathway, which translocates from the cytoplasm to the nucleus where it acts as a transcriptional co-activator, binding to the transcription factors TCF/LEF, in the presence of Wnt ligands. While different TCFs and LEFs induce transcription context dependent, β-catenin always acts as co-activator in the canonical Wnt signaling cascade. Although ChIP is established in medaka and widely used in fish (Lindeman et al., 2009; Nakamura et al., 2014), no ChIP against β-catenin had been performed so far. To identify a suitable antibody for the ChIP, I performed a mini screen of different antibodies against β-catenin. Antibodies were pre-selected after the following criteria: 1. Previous use in zebrafish, 2. Similarity of sequence alignment to the medaka β-catenin gene and 3. If possible, the antibody should be monoclonal. I performed ChIP with 300 embryos stage 16 (late gastrula stage) using three different antibodies against β-catenin (Cell signaling #8814, Abcam 227499, Abcam 32572). After the ChIP, I examined the enrichment of recovered DNA at known canonical Wnt target genes by RT-PCR using primers amplifying known β-catenin binding regions in *axin2* and *lef1*. Primers against gene desert regions (Ishikawa et al., 2018) served as negative controls. Two antibodies seemed to be specific for β-catenin (Cell signaling #8814, Abcam 227499), and the Cell Signaling antibody showed higher specificity and efficiency compared to the Abcam antibody (Figure 2.4).
I decided to continue with the Cell Signaling antibody to test if this antibody is suitable to perform ChIP-seq against β-catenin.

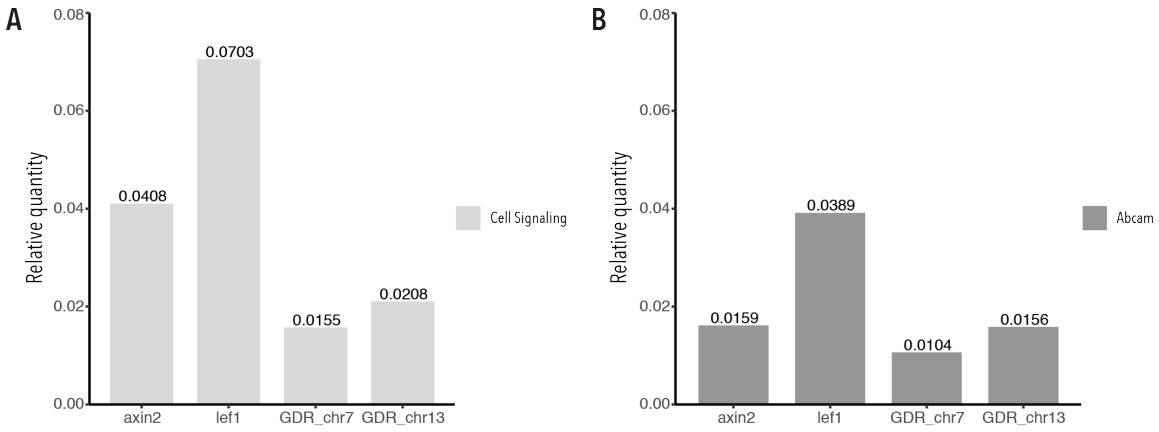

Figure 2.4: ChIP-qPCR comparing the efficiency of different antibodies against β-catenin.
(A) ChIP-qPCR using Cell signaling #8814 antibody. (B) ChIP-qPCR using Abcam 227499 antibody. chr = chromosome, GDR = gene desert region.

After ChIP-seq, computational analyses were carried out to interpret the results. I used the peak calling algorithm of MACS2 (Zhang et al., 2008) to identify regions where β-catenin is significantly enriched. These regions are displayed as peaks when mapped to the genome.

In the nucleus β-catenin binds to DNA bound TCF transcription factors to initiate the expression of Wnt target genes. To further test the specificity of the β-catenin antibody, I wanted to investigate whether TCF binding motifs are enriched under β-catenin ChIP peaks. I performed ChIP-sequencing (ChIP-seq) using 600 stage 16 embryos. Motif analysis of the ChIP-seq results was performed using the MEME-ChIP tool (Ma et al., 2014). 30,000 peaks were analyzed and I compared the enriched motifs to known β-catenin binding motifs (Bottomly et al., 2010; Nakamura et al., 2016). I identified several TCF binding motifs. Interestingly, I also identified a *zic1* binding motif which has a great similarity to the TCF binding motif (Figure 2.5A). To evaluate the specificity of the antibody further, I performed ChIP-seq against β-catenin on 200 embryos stage 26 treated with IWR-1 (an inhibitor of canonical Wnt signaling) or treated with DMSO in the control group. I compared the heights of β-catenin binding peaks in the treated and control condition indicating less enrichment of β-catenin. In embryos with downregulated Wnt signaling pathway, I observed a decrease in height of several peaks from known Wnt target genes (*axin2*, *lef1*, *sp5l*), compared to control embryos (Figure 2.5 B-B", grey boxes).

In summary, I identified an antibody against β-catenin, which is specific in medaka and can be reliably used in ChIP-seq experiments to identify potential direct downstream target of the canonical Wnt signaling pathway.

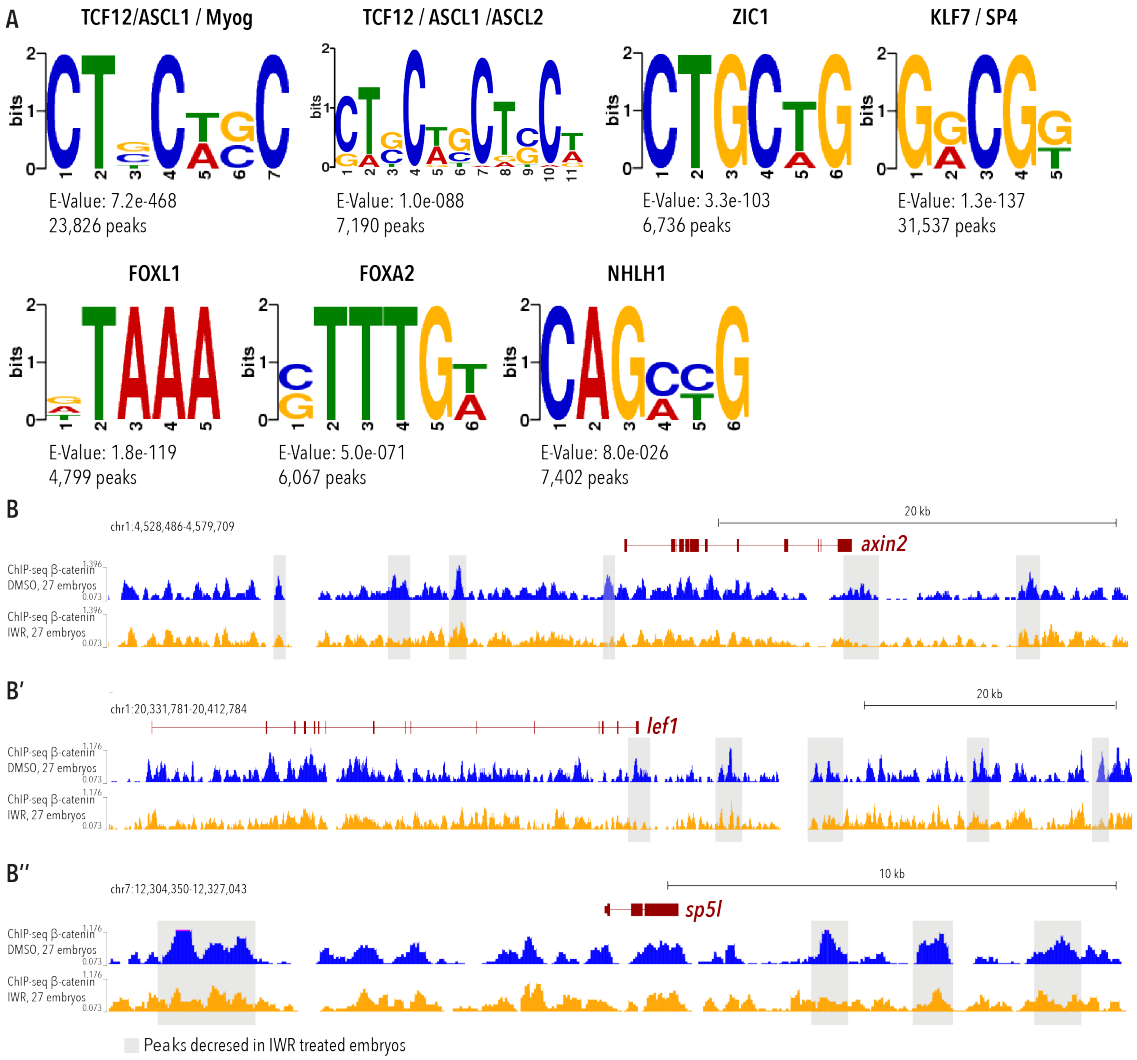

Figure 2.5: Testing of the specificity of the β-catenin antibody for ChIP-seq.

(A) Enriched motifs under β-catenin peaks. Below each motif, statistical significance (E-Value) and number of β-catenin peaks are indicated. Two TCF binding motifs were enriched. (B-B") ChIP-seq performed on embryos with downregulated Wnt signaling (orange track) show reduced height in β-catenin binding peaks compared to peaks from ChIP-seq performed on control embryos treated with DMSO (blue track). Peaks with decreased height are shaded grey. IWR = IWR-1.

2.1.4 The canonical Wnt signaling pathway directly regulates *zic1/zic4*

Next, I wanted to investigate whether the expression of *zic1/zic4* is directly regulated by the canonical Wnt signaling pathway during somite differentiation. I performed ChIP-seq using 200 embryos stage 26. To be able to draw conclusions about the regulation of *zic1/zic4* in the dorsal somites, I compared my ChIP-seq result to somite specific ATAC-seq (Assay for Transposase-Accessible Chromatin using sequencing) data, previously produced in the lab (Y. Hashimoto and R. Nakamura, in preparation). The ATAC-seq was performed on isolated dorsal and ventral somites to determine open chromatin regions in dorsal and ventral somites respectively. Results of the ATAC-seq (Figure 2.6 blue and orange track) enabled me to identify putative promoter regions and putative enhancer regions of *zic1/zic4*, which potentially play a role on the regulation of *zic1/zic4* expression

in the dorsal somites (these regions have accessible chromatin in the dorsal but not the ventral somites). Overlaying the ATAC-seq data with my ChIP-seq against β-catenin (Figure 2.6 black track) showed that peaks of the ChIP-seq can be found in the putative promoter region (Figure 2.6 boxed grey shaded regions) and several putative enhancer peaks (Figure 2.6 grey shaded regions). Interestingly, no β-catenin ChIP peak was observed at the site where the transposon is inserted in the *Da* mutant. Together, these results points towards a possible direct regulation of *zic1/zic4* by the canonical Wnt signaling pathway in the dorsal somites.

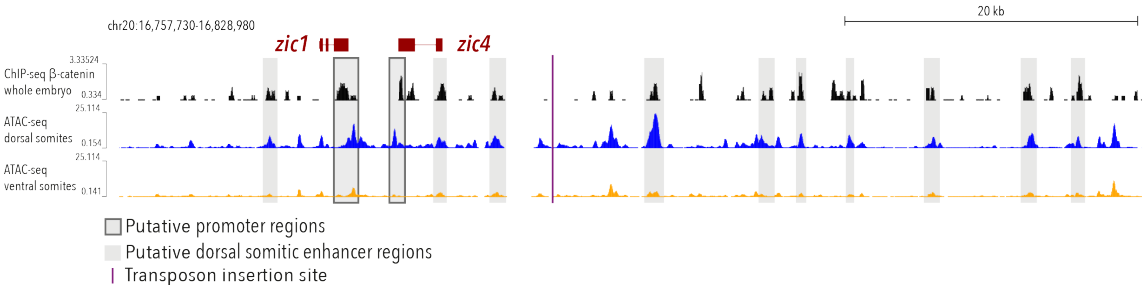

Figure 2.6: ChIP-seq against β-catenin identifies *zic1/zic4* as direct targets of the canonical Wnt signaling pathway in the dorsal somites.

Black track: Potential β-catenin binding sites identified by ChIP-seq against β-catenin in whole-mount embryos. Blue track: ATAC-seq performed on dorsal somites. Orange track: ATAC-seq performed on ventral somites. Putative promoter regions (boxed grey shaded regions) and putative dorsal somite enhancer regions (grey shaded regions) of *zic1/zic4* are identified by comparison of ChIP-seq data and ATAC-seq data. Transposon insertion site is marked by a purple line.

Combining the results obtained from the ChIP-seq against β-catenin and the results from the chemical and genetic manipulation of the canonical Wnt signaling pathway, allowed me to identify that the transcription factors *zic1/zic4* as direct downstream targets of the canonical Wnt signaling pathway during somite differentiation.

2.2 Dorsal-specific morphogenesis of the myotome during late development

2.2.1 The dorsal dermomyotome in the *Da* mutant shows a higher proliferative activity than in Wt

Not much is known about how the trunk myotome is dorsalized during embryonic development. This lab previously reported that Zic1/Zic4 are dorsalization factors by analyzing the *Da* mutant, which has a ventralized trunk phenotype (Kawanishi et al., 2013; Moriyama et al., 2012; Ohtsuka et al., 2004). How the myotome is dorsalized and what are distinct characteristics of a dorsalized myotome has not been fully understood, yet. By closely investigating the morphology, tissue dynamics and molecular characteristics, I intended to shed light on the dorsalization of the myotome.

In the lab it had been assumed that the ventralized dorsal myotome of the *Da* mutant is larger than the dorsal myotome of Wt medaka, and thus resembling the ventral myotome. To investigate the size of the dorsal myotome, I labeled the myotome using phalloidin and investigated the cross sectional area of the dorsal somites in Wt medaka and *Da* mutant at different stages (Figure 2.7). I performed whole-mount immunostaining, and obtained z-stack images of the trunk of the embryos.

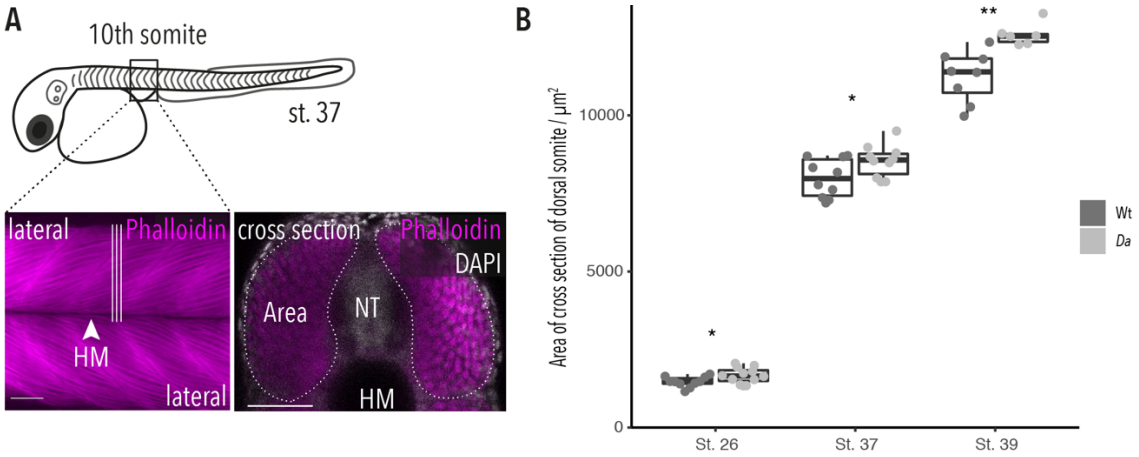

Figure 2.7: The cross sectional area of the dorsal myotome is larger in *Da* mutant embryos than in Wt embryos.

(A) Schematic representation of dorsal myotome area measurements. Embryos were imaged using a confocal microscope. Three consecutive optical cross sections of the 10th somite were analyzed. (B) Measurements of cross sectional area of dorsal somites of Wt and *Da* embryos at stage 26 (Wt n = 10, *Da* n = 12), stage 37 (Wt n = 10, *Da* n = 10) and stage 39 (Wt n = 8, *Da* n = 6). The cross sectional area of the ventralized dorsal myotome of the *Da* mutant is larger than the Wt dorsal myotome in all measured stages (median, first and third quartiles, *$P_{st.26}$ = 0.038, *$P_{st.37}$ = 0.044, **$P_{st.39}$ = 0.0019). HM = horizontal myoseptum, NT = neural tube, scale bar = 50 µm.

The area of the dorsal myotome was measured by analyzing optical cross sections of the 10th somite. To assure the accuracy of the measurements, I measured the area in three consecutive cross sections and calculated the average (Figure 2.7A)(similar to the analysis performed by Ganassi and colleagues (Ganassi et al., 2018)). At the observed stages (stage 26, 37 (7 days post fertilization) and 39 (hatching stage)) the dorsal myotome of the *Da* mutant was significantly larger than in Wt medaka (Figure 2.7B), confirming the assumption.

There are several possible explanations for an enlarged dorsal myotome in the *Da* mutant. One possible explanation is that the myofibers have a larger diameter in the *Da* mutant myotome compared to the Wt myotome. Another possibility is a higher number of myofibers in the dorsal myotome of the *Da* mutant. I investigated the diameter of the myofibers in the dorsal myotome in Wt and *Da* mutant embryos, but failed to find a difference (data not shown). As previously described, the myotome is surrounded by the dermomyotome. The dermomyotome contains proliferative active cells, which will give rise to myoblasts. A higher proliferative activity of cells in the dorsal dermomyotome could ultimately lead to a higher number of myofibers and an enlarged dorsal myotome. To examine the proliferative activity of dorsal dermomyotome cells, I performed immunostainings against phospho-histone H3 (pH3) in *Da* mutant and Wt embryos. PH3 is a mitotic marker, labelling condensed chromatin (Goto et al., 1999; Mendieta-Serrano et al., 2013) (Figure 2.8A).

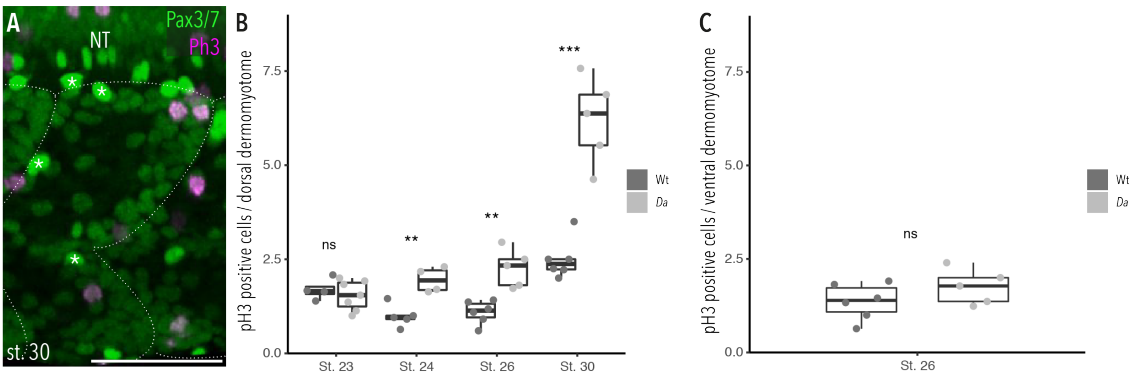

Figure 2.8: The dorsal dermomyotome of the *Da* mutant shows a higher proliferative activity compared to Wt dorsal dermomyotome after the onset of *zic1/zic4* expression.

(A) Lateral view of a maximum projection of the 10th somite of a Wt stage 30 (35-somite stage) embryo stained with antibodies against Pax3/7 (green) to label the dermomyotome and pH3 (magenta) to label proliferating cells. Somites are indicated by dotted lines. * mark neural crest exemplary (B) Quantification of pH3-positive cells in the dorsal dermomyotome per somite of Wt and *Da* embryos. From stage 24 onwards, a higher number of pH3-positive cells can be observed in the dorsal dermomyotome of *Da* mutants (Stage 23: 95 somites from 7 embryos, stage 24: 42.5 somites from 4 embryos, stage 26: 40.5 somites from 5 embryos, stage 30: 47.5 somites from 5 embryos) compared to Wt (Stage 23: 46.5 somites from 4 embryos, stage 24: 54.5 somites from 5 embryos, , stage 26: 66 somites from 6 embryos, stage 30: 49 somites from 6 embryos) embryos (median, first and third quartiles, $^{ns}P_{st.23}$ = 0.48, $^{**}P_{st.24}$ = 0.0038, $^{**}P_{st.26}$ = 0.0035, $^{***}P_{st.30}$ = 0.0008). (C) Quantification of pH3-positive cells per somite of the ventral dermomyotome in Wt (66 somites of 6 embryos) and *Da* mutant (51 somites of 5 embryos) embryos (median, first and third quartiles, ^{ns}P = 0.2). NT = neural tube, scale bar = 50 µm.

Interestingly, after the onset of *zic1/zic4* expression in the dorsal somites at stage 23 (12-somite stage), ergo from stage 24 onwards, dorsal dermomyotome cells of the *Da* mutant show a significantly higher proliferative activity compared to dorsal dermomyotome cells in the Wt (Figure 2.8B). PH3-positive cells were observed throughout the dorsal dermomyotome, without a bias towards a specific region. To investigate whether this increased proliferation in the dorsal dermomyotome of the *Da* mutant is due to its ventralization, I analyzed the proliferative activity of ventral dermomyotome cells in Wt and *Da* embryos. No difference in proliferative activity was observed, suggesting that the previously examined difference in proliferative activity in the dorsal dermomyotome of the *Da* mutant might be due to its ventralized character (Figure 2.8C).

Taken together, these results suggest that the increase in dorsal dermomyotome size in the *Da* mutant is due to a higher proliferative activity of cells in the dorsal dermomyotome.

2.2.2 The dorsal ends of the *Da* myotome extend insufficiently and therefore fail to cover the neural tube

As previously introduced, one prominent trait of the ventralized dorsal myotome of the *Da* mutant is its inability to extend its dorsal ends sufficiently to cover the neural tube (Tamiya et al., 1997). In all animals containing epaxial and hypaxial muscles, the dorsal end of epaxial muscles cover the neural tube by the end of embryonic development (Schilling, 2011; Sefton and Kardon, 2019). However, so far it has not been investigated how the dorsal ends of the myotome extend to cover the neural tube. To investigate this tissue extension in Wt and *Da* mutant embryos, I stained the muscle fibers with phalloidin and investigated the tissue morphology of the myotome from stage 35 (5.5 days post fertilization) to stage 39 (Figure 2.9). In Wt medaka, the right and left dorsal ends of the myotome extend dorsally, and first come into contact at stage 37. The ends extend further dorsally, resulting in the full coverage of the neural tube by stage 39 (Figure 2.9A-A””). Additionally, it can be observed that the ends of the myotome acquire a pointy shape (Figure 2.9A”’-A””). In the *Da* mutant, the dorsal ends of the myotome do also extend dorsally, but to a less extent, leading ultimately to an incomplete coverage the neural tube (Figure 2.9B-B””). Furthermore, at stage 39, the ends of the dorsal myotomes remain round in the *Da* mutant. To quantify the extent of the neural tube coverage, I measured the closest distance between the right and left dorsal tips of the myotome in optical cross sections. As described in 2.2.1, the distance between myotome ends was measured in three consecutive cross-sections and the average distance between the myotome ends was calculated (Figure 2.9C). In both, Wt medaka and the *Da* mutant, a decreased distance between the dorsal ends can be observed, indicating the dorsal extension of the myotome ends. By comparing the medians, it appears that the progress of tissue extension in the *Da* mutant is always lagging 1-2 stages behind the progress observed in Wt embryos (Figure 2.9D). Already at stage 35, the distance between the dorsal ends of the myotome is

smaller in Wt than in the *Da* mutant, raising the question of what is the earliest point that a difference in myotome dorsal end extension can be observed.

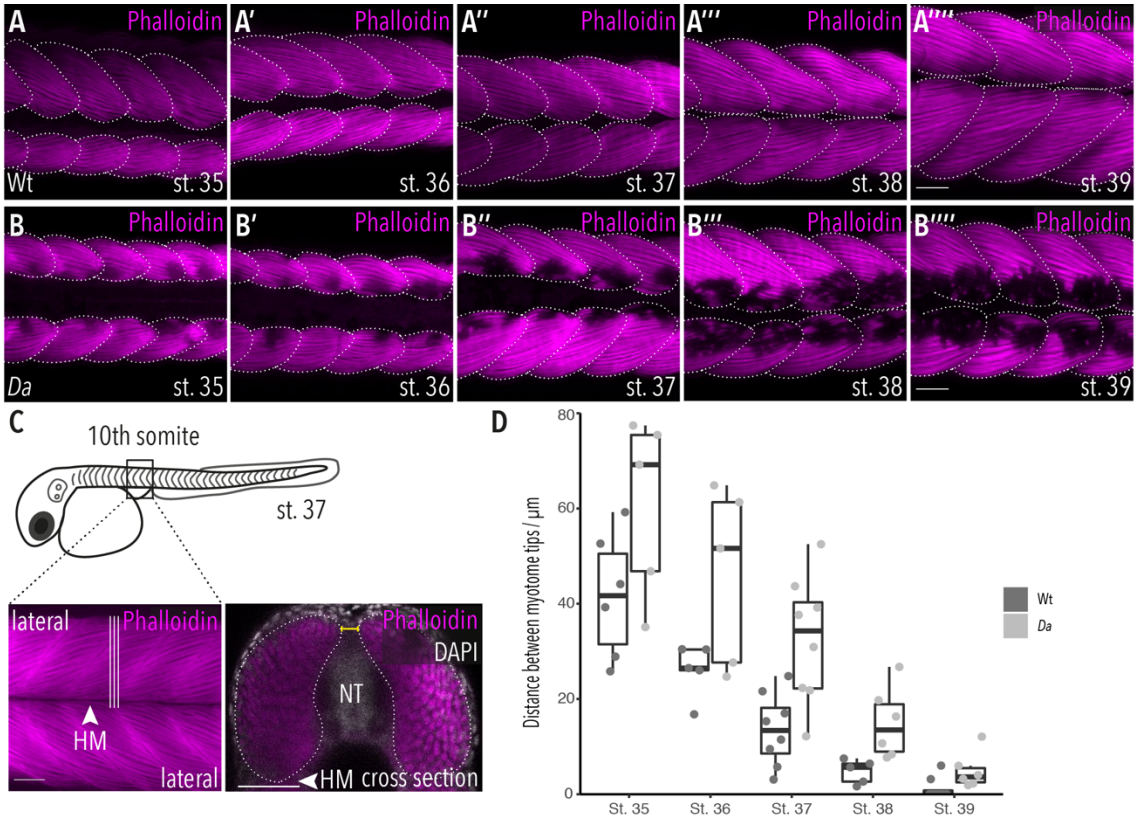

Figure 2.9: The dorsal dermomyotome of the *Da* mutant fails to completely cover the neural tube at the end of embryonic development.

(A-B⁗) Dorsal view of maximum projections of embryonic tails. Phalloidin (magenta) staining labels myotome. (A-A⁗) In Wt embryos, the ends of the dorsal myotome continuously extend dorsally, coming in first contact at stage 37 and cover the neural tube completely by stage 39. (B-B⁗) In the *Da* mutant, the dorsal ends of the myotome continuously extend dorsally, but never cover the neural tube completely. (C) Schematic representation of the measurements of the distance between dorsal ends of the myotome. Embryos were imaged using a confocal microscope. Three consecutive optical cross sections of the 10th somite were analyzed. (D) Measurements of distance between dorsal ends of the myotome in Wt and Da embryos at stage 35 (Wt n = 6, *Da* n = 5), stage 36 (6 days post fertilization, Wt n = 5, *Da* n = 5), stage 37 (Wt n = 8, *Da* n = 8), stage 38 (Wt n = 5, *Da* n = 6) and stage 39 (Wt n = 8, *Da* n = 6). From stage 35 onwards, the dorsal ends of the myotome are in closer proximity in Wt embryos than in *Da* mutant embryos. HZ = horizontal myoseptum, NT = neural tube, scale bar = 50 µm.

To determine the first embryonic stage where a difference in dorsal myotome extension between Wt and *Da* mutant can be observed, I labelled the dermomyotome with the dermomyotome marker Pax3/7 and measured the distance between the dorsal tip of the dermomyotome and the center of the neural tube as indicated in Figure 2.10A. Again, the distance was measured in consecutive optical cross sections and the average distance was calculated. In Wt embryos, the distance between the neural tube and the dorsal tip of the dermomyotome only marginal increases. This is opposing to the observations made in the *Da* mutant, where the distance between the center of the neural tube and the dorsal tip of the dermomyotome increases as development proceeds. From stage 24 onwards,

the distance between the tip of the dorsal dermomyotome and the neural tube is significantly different between Wt and the *Da* mutant. To further access dorsal somite extension and to rule out any bias of the data due to neural tube size, the height of dorsal somites was analyzed (Figure 2.10C). With advancing age, the somite height increases in Wt embryos and *Da* mutant embryos. From stage 24 onwards, the height of dorsal somites of Wt embryos is significantly larger, compared to *Da* mutant dorsal somites (Figure 2.10D). Both measurements (Figure 2.10B, D) show significant differences from stage 24 onwards, one stage after the initiation of *zic1/zic4* expression in the dorsal somites at stage 23.

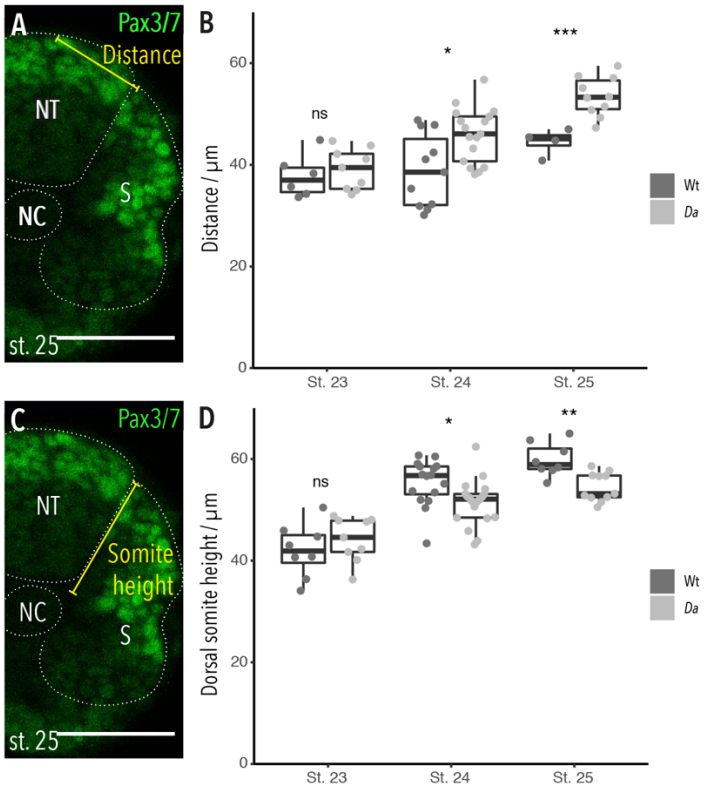

Figure 2.10: Differences in the dorsal extension of somites between Wt and *Da* mutant embryos can be observed from stage 24 onwards.

(A,C) Cross sections of Wt stage 25 (18-19-somite stage) embryos. Pax3/7 (green) labels the dermomyotome. (A) Schematic representation of how the distance between the dorsal tip of the dermomyotome and the central part of the neural tube was measured for the analysis in (B). (B) Quantification of the distance between the dorsal tip of the dermomyotome and the top of the neural tube in Wt (Stage 23: 6 somites from 3 embryos, stage 24: 11 somites from 6 embryos, stage 25: 10 somites from 5 embryos) and *Da* mutant (Stage 23: 9 somites from 5 embryos, stage 24: 17 somites from 9 embryos, stage 25: 12 somites from 6 embryos) embryos. Significant differences in distance between Wt and *Da* mutant embryos can be observed from stage 24 onwards (median, first and third quartiles, ^{ns}Pst.23 = 0.55, **Pst.24 = 0.0068, ****Pst.25 = 3.5e-0.6). (C) Schematic representation of how the height of the dorsal somites was measured for the analysis in (D). (D) Quantification of dorsal somite height of Wt (Stage 23: 8 somites from 4 embryos, stage 24: 16 somites from 8 embryos, stage 25: 8 somites from 4 embryos) and *Da* mutant (Stage 23: 9 somites from 5 embryos, stage 24: 19 somites from 10 embryos, stage 25: 11 somites from 6 embryos) embryos. Significant differences in dorsal somite height between Wt and *Da* mutant embryos can be observed from stage 24 onwards (median, first and third quartiles, ^{ns}Pst.23 = 0.38, *Pst.24 = 0.013, **Pst.25 = 0.0021). NT = neural tube, NC = notochord, S = somite, scale bar = 50 µm.

This is similar to the differences in proliferative activity of the dorsal dermomyotome observed in Figure 2.8.

In summary, one stage after the onset of *zic1/zic4* expression in the dorsal somites, differences in proliferative activity of the dorsal dermomyotome as well as differences in tissue morphology become evident in Wt dorsal somites and ventralized dorsal somites of the *Da* mutant, suggesting that dorsal patterning of the myotome starts right after the expression of *zic1/zic4*.

2.2.3 Wt dorsal somite tip cells form more protrusions which also extend more dynamically than protrusions observed in the Da mutant

The previous results suggest differences in the onset of dorsal somite extension (Figure 2.10) as well as potential differences in extension behavior (Figure 2.8) comparing ventralized *Da* dorsal somites to Wt dorsal somites. To better understand the onset of somite extension, I performed time-lapse imaging. Since Zic1 is a marker for dorsal somites (Ohtsuka *et al.*, 2004; Moriyama *et al.*, 2012; Kawanishi *et al.*, 2013), I used the transgenic line *zic1::GFP* (Kawanishi et al., 2013) to investigate the onset of dorsal somite extension in the Wt background. To visualize the onset of dorsal somite extensions in the *Da* mutant, I used a transgenic *Da* mutant line similarly expressing GFP under the control of the *zic1* promoter (*Da-zic1::GFP*). For this, I generated the transgenic line by crossing *Da* mutants with fish of the *zic1::GFP* transgenic line. Cells expressing GFP in the *Da-zic1::GFP* line would express *zic1* in Wt embryos. I performed time-lapse imaging for 10-15 h, z-stacks were taken in a 600 sec interval. Soon after the onset of imaging the *zic1::GFP* line, I observed that cells at the tip of dorsal somites form numerous protrusions extending towards the top of the neural tube (Figure 2.11A-A"", Movie 2.1). In the *Da* background, cells at the tip of the dorsal somites seemed to begin later with the formation of protrusions and the protrusions seemed less numerous (Figure 2.11B-B"", Movie 2.2). To investigate the protrusions in greater detail, I performed *in vivo* imaging of the transgenic lines (Figure 2.11C-D'). Protrusions were classified into "small protrusions" (<8 µm, arrow head Figure 2.11C') and "large protrusions" (>8 µm, arrow Figure 2.22C') according to their length. Quantification of protrusions revealed that in the *Da* mutant background dorsal somite tip cells form a significantly larger number of "small protrusions", whereas tip cells in the Wt background form significantly more "large protrusions", additionally, the overall number of protrusions was significantly larger in the Wt background than in the *Da* mutant background (Figure 2.11E-E").

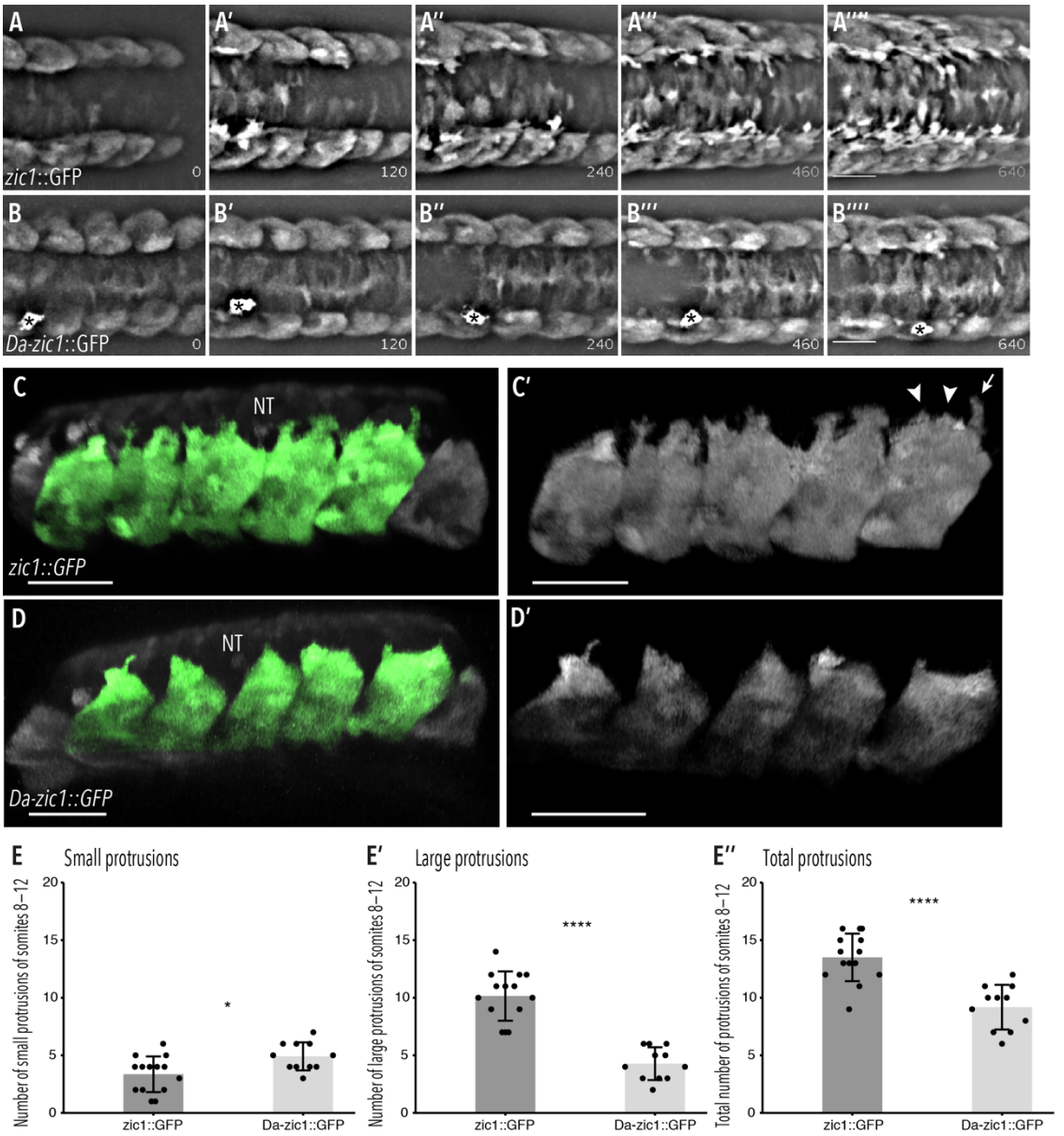

Figure 2.11: Wt dorsal somite tip cells form a higher number of large protrusions and in total more protrusions than *Da* mutant the dorsal somite tip cells.

(A-B"") Dorsal view of time-lapse imaging of *zic1::GFP* (A-A"") and *Da-zic1::GFP* (B-B""). Z-stacks were taken every 10 minutes. 15th somite is in the center. Time is displayed in min. (C-D') Lateral view of 3D-reconstruction of live imaging of *zic1::GFP* (C-C') and *Da-zic1::GFP* (D-D'). * marks migrating melanophore. Embryos were imaged at stage 27 (24-somite stage), 10th somite is in the center. Arrow heads in (C') indicate "small protrusions". Arrow in (C') indicate "large protrusions". Extraction of dorsal somites colored (green) in (C) and (D) are depicted in (C') and (D'). (E-E") Quantification of protrusions of the 8th to the 12th somite of embryos from the *zic1::GFP* line (n = 14 embryos) and the *Da-zic1::GFP* transgenic line (n = 11 embryos) (mean ± SD, *$P_{small\ protrusions}$ = 0.01, ****$P_{large\ protrusions}$ = 3.3e^{-08}, ****$P_{total\ protrusions}$ = 2.1e^{-05}). NT = neural tube, scale bar = 50 µm.

Video 2.1: Time-lapse imaging of onset of somite extension in the transgenic line *zic1::GFP.*

Dorsal view of time-lapse imaging of *zic1::GFP* stage 27 (at the onset of imaging) embryo. Anterior is oriented to the left, 15th somite is positioned in the center. Z-stacks were taken every10 min. Time is displayed in min, scale bar = 50 µm.

Video 2.2: Time-lapse imaging of onset of somite extension in the transgenic line *Da-zic1::GFP*.
Dorsal view of time-lapse imaging of *Da-zic1::GFP* stage 27 (at the onset of imaging) embryo. Anterior is oriented to the left, 15th somite is positioned in the center. Z-stacks were taken every 10 min. Bright migrating cell at the left bottom is a melanophore. Time is displayed in min, scale bar = 50 µm.

I further investigated the protrusions of the dorsal tip cells in Wt and *Da* mutant embryos more closely. The large protrusions found in Wt dorsal somite tip cells tend to branch at their dorsal ends (Figure 2.12A). To observe the underlaying actin cytoskeleton of the protrusions, I injected Wt and *Da* embryos with *Actin-chromobody GFP* mRNA (*AC-GFP*) at 4-cell stage to label actin fibers in a mosaic manner. Large protrusions of dorsal tip cells in Wt and *Da* mutant embryos consists of a lamellipodia (protrusions with branched actin networks at their motile edges) with several thin filopodia (protrusions consisting of parallel actin filaments) branching outwards (Figure 2.12B,D, arrow heads point to filopodia) (Mejillano et al., 2004). However, less and shorter filopodia were observed in the *Da* mutant. Next, I studied the dynamics of the protrusions by examining newly formed protrusions investigating the Video 2.1 and Video 2.2. In the Wt background, the protrusions extend rapidly and the dorsal tips of the protrusions form branches extending in different directions (Figure 2.12 E-E""). In the *Da* mutant background, at the onset of somite extension the protrusions are transient and don't branch (Figure 2.12F-F"").

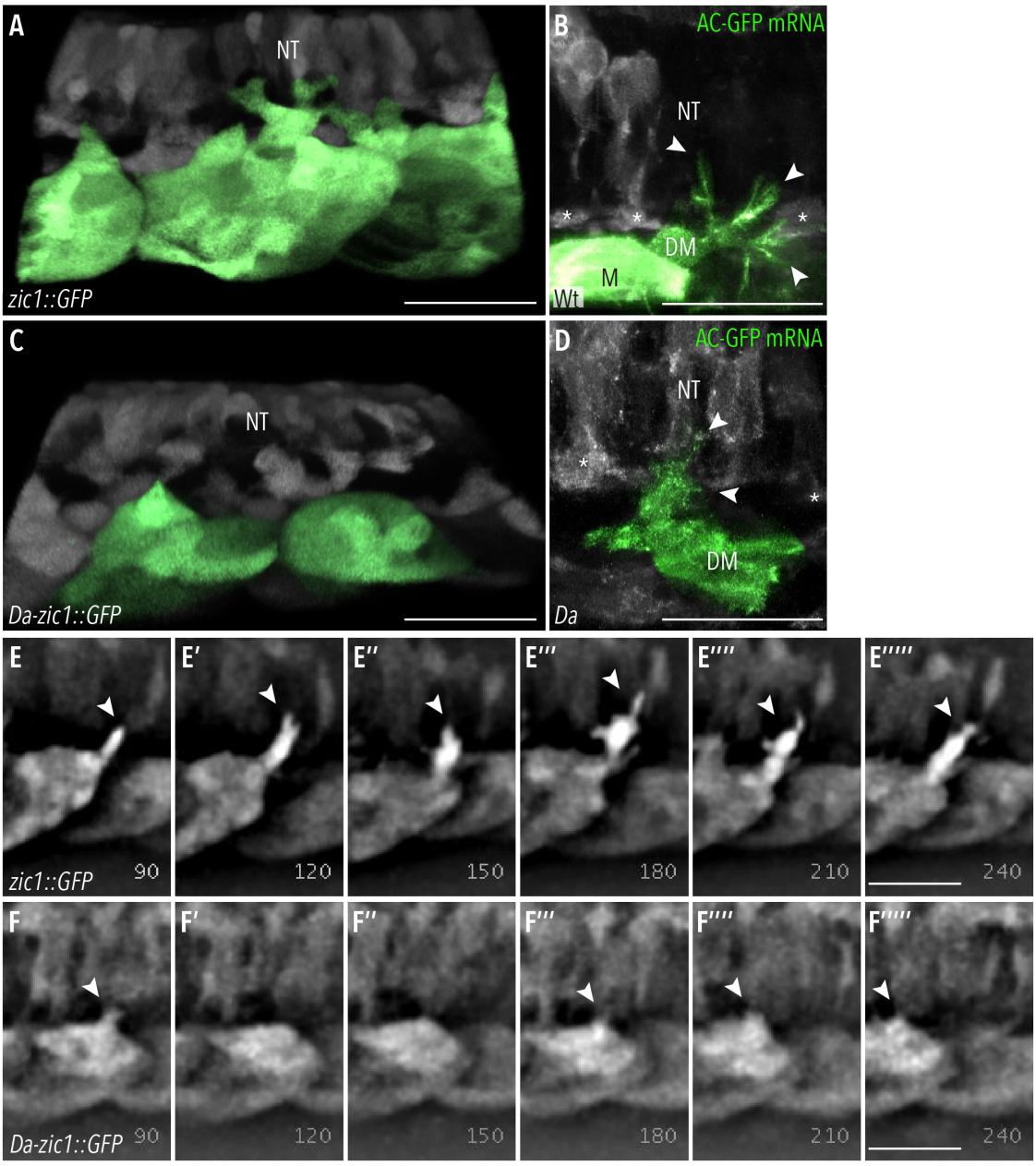

Figure 2.12: Analysis of the actin-cytoskeleton and dynamics of protrusions.

(A-D) Lateral view of 3D-reconstruction of *in vivo* imaging of dorsal somites. (A) *Zic1::GFP* and (C) *Da-zic1::GFP* transgenic embryos were imaged at stage 27, 10th somite in the center, dorsal somites are colored in green. (B) Wt embryos and Da mutant embryos (D) injected with AC-GFP mRNA. A large protrusion is colored in green. Arrow heads point to filopodia branching out from the lamellipodia. * make sclerotome cells. (E-F''''') Dorsal view of somite forming a protrusion. Extractions from time-lapse imaging of *zic1::GFP* (Video 2.1, E-E''''') and *Da-zic1::GFP* (Video 2.2, F-F'''''). Arrow heads point to protrusions. Time is displayed in min. DM = dermomyotome, M = myotome, NT = neural tube, scale bar = 25 µm.

In summary, the data shows that at the onset of dorsal somite extension, cells at the tip of the ventralized dorsal somites of the *Da* mutant form less and shorter protrusions than dorsal somite tip cells observed in Wt embryos. Additionally, the large protrusions of Wt dorsal somite tip cells seem to be very dynamic in terms of branching and the direction of extension.

2.2.4 Cells at the tip of the dorsal somites undergo EMT

Cells undergoing repositioning within or at the periphery of the tissue often change from an epithelial character to a mesenchymal character. This process is called epithelial-mesenchymal transition (EMT) and is essential for several processes during embryonic development, including mesoderm formation and neural crest cell delamination (Ciruna and Rossant, 2001; Lamouille et al., 2014; Theveneau and Mayor, 2012; Thiery et al., 2009). To investigate whether cells at the dorsal tip of the somite undergo EMT during dorsal extension, I performed immunostaining against N-cadherin (antibody against Cadherin2), a marker for epithelial cells in the dorsal dermomyotome in chicken (Cinnamon et al., 2006; Zhou et al., 2018). No marker for epithelial cells in the dorsal dermomyotome is known in fish, thus, downregulation of N-cadherin was considered as a sign for EMT in medaka embryos.

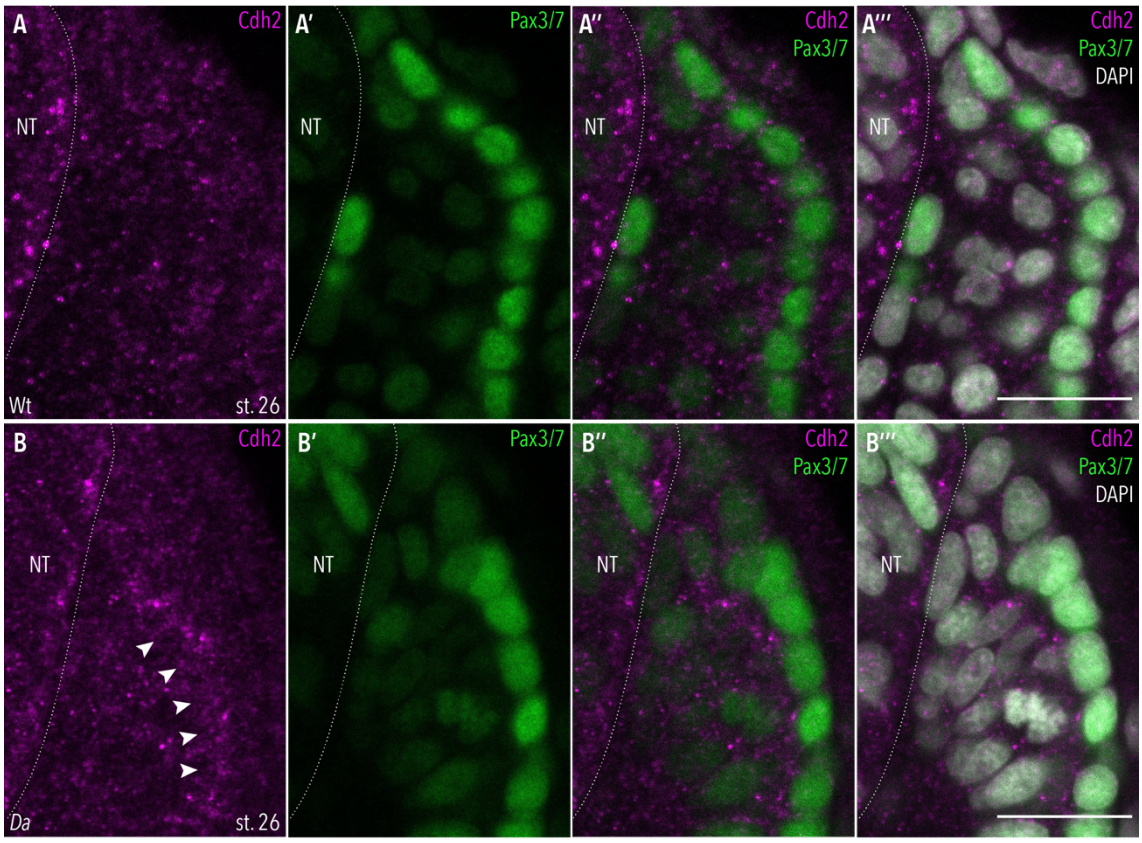

Figure 2.13: N-cadherin is expressed at the apical side of dorsal dermomyotome cells in the *Da* mutant.

(A-B''') Vibratome sections of dorsal somites of Wt (A-A''') and *Da* mutant embryos (B-B'''). Staining against N-cadherin (magenta) marks epithelialized calls, staining against Pax3/7 (green) labels dermomyotome cells. (B) Arrow heads point to increased Cdh2 signal at the apical side of dorsal dermomyotome cells in the *Da* mutant. NT = Neural tube, scale bar = 15 µm, sections = 200 µm.

Although the N-cadherin staining is weak in medaka dorsal somites, the *Da* mutant exhibited an higher accumulation of N-cadherin signals at the apical side of dermomyotome cells (Figure 2.13 B, arrow heads). This suggests that the cells at the tip of the dorsal

dermomyotome have a stronger epithelial character in the *Da* mutant, compared to Wt dorsal dermomyotome cells.

Since the tip cells of the dorsal somites of *Da* mutants behave differently (Figure 2.11, 2.12) and have different molecular characteristics (Figure 2.13) compared to Wt dorsal somite tip cells, I wanted to further elucidate the cellular phenotype of these cells using transmission electron microscopy (TEM)(Figure 2.14). TEM provides high resolution images enabling the detailed observation of tissue, cell and subcellular morphology. I investigated cells at the tip of dorsal somites from Wt and congenic *Da* embryos. The congenic *Da* line was created by backcrossing *Da* mutants with Wt (*d-rR*) medaka to eliminate the bias of strain background. Strikingly, the dorsal tip cells of Wt somites have wavy cell membranes (Figure 2.14A', arrow heads), whereas the cell membranes of dorsal tip cells of the conjenic *Da* are rather straight (Figure 2.13B', arrow heads).

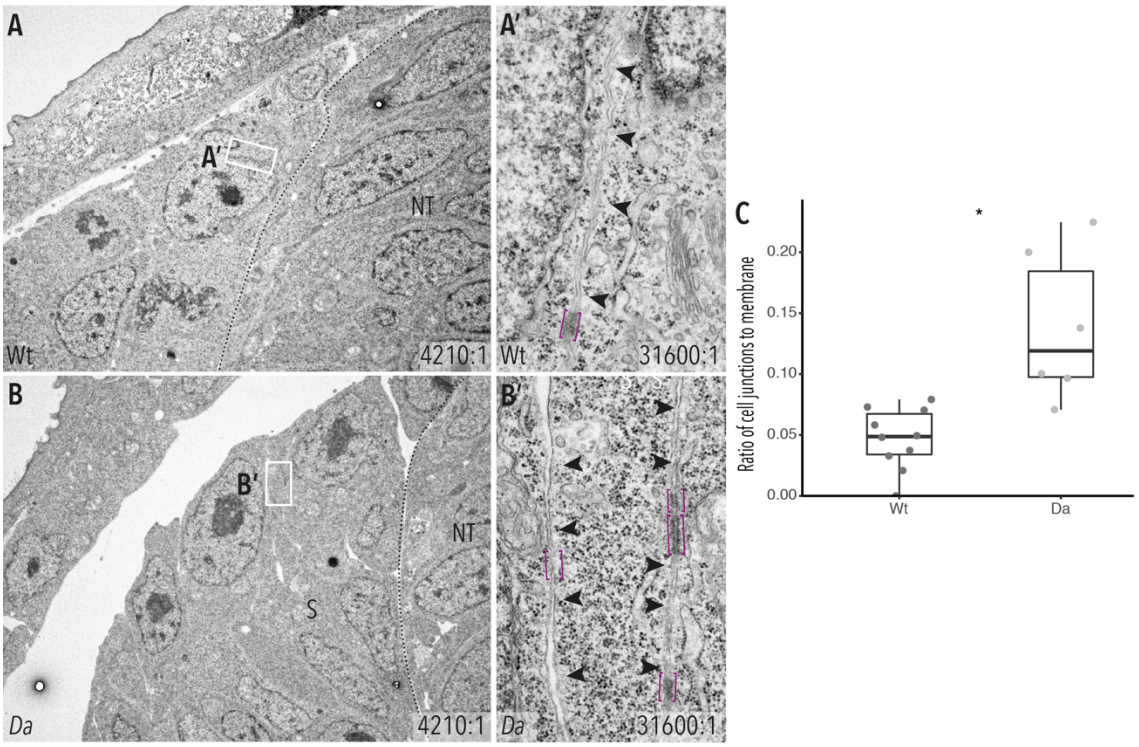

Figure 2.14: Tip cells of Wt dorsal somites have wavy cell membranes.
(A-B') TEM images of the tip of Wt (A-A') and congenic *Da* dorsal somites (B-B'). (A) and (B) are magnified 4210:1. (A') and (B') are magnified 31600:1. Arrow heads indicate cell membranes, magenta brackets mark cell junctions. (A')Zoom-in of (A) indicated by a white square. (B') Zoom-in of (B) indicated by a white square. (C) Quantification of ratio of cell junctions to plasma membrane (Wt: n = 10 sections from 2 smites, congenic *Da*: n = 6 sections from 1 somite). The cell junction to membrane ratio is higher in sections of the congenic *Da* than in sections of Wt somites (median, first and third quartiles, *P = 0.013). NT = neural tube.

The wavy cell membranes of Wt dorsal somite tip cells might be the result of less tight cell-cell contact in this tissue. To further investigate this, I determined the density of cell junctions at the plasma membranes by measuring the length of cell membranes and of

cell junctions in sections of dorsal somite tip cells in Wt medaka and the congenic *Da.* These measurements allowed me to calculate the ratio of cell junctions to plasma membrane in both conditions. The density of cell junction to membrane seems to be higher in the investigated sections of the congenic *Da*, compared to Wt (Figure 2.14C). A higher ratio of cell junctions to membrane would indicate closer cell-cell contact. The number of samples is too small, however, to draw a definite conclusion. Nethertheless, the wavy cell membranes seem to be a characteristic of dorsal somites.

2.2.5 Dermomyotome cells interact with the opposing myotome at the end of somite extension

After describing the onset of dorsal somite extension, I was curious about how at the end the left and right dorsal myotome come together to form a gap-less muscle layer on top of the neural tube in Wt medaka. I examined histological sections of the trunk of stage 37 embryos stained with hematoxylin. At that stage, the dorsal myotomes from both sides come in first contact with each (Figure 2.9A").

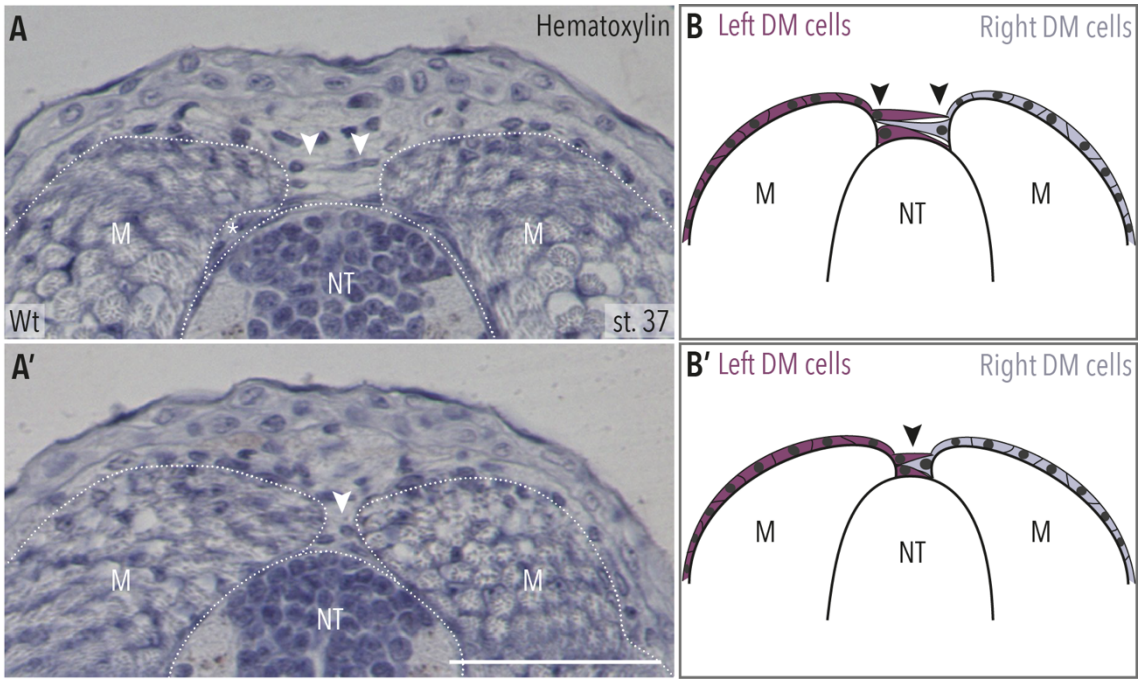

Figure 2.15: At the end of somite extension, dermomyotome cells extend towards the opposing myotome.

(A-A") Hisological cross sections of the trunk of stage 37 Wt embryos. The sections were stained with hematoxylin. (A) Dermomyotome cells at the dorsal tip of the somites extend towards the oposing myotome, this results in the stacking of dermomyotome cells on top of each other. (A') As the myotomes come closer, the cell bodies of the dermomyotome cells between the myotomes seem to be contracted. Arrow heads point to dermomyotome cells between the myotomes extending towards the oposing myotome. * marks sclerotome cells. (B) Schematic drawing of (A). (B') Schematic drawing of (A'). M = myotome, NT = neural tube, scale bar = 25 µm.

As the dorsal tips of the left and right somite come in close contact to each other, the dermomyotome cells at the dorsal tip of each myotome seem to extend towards the opposing myotome. This resulted in dermomyotome cells which previously were surrounding the myotome to be stacked horizontally on top of each other (Figure 2.15A, B). As the left and the right myotome came closer, it seemed that the cell body of the stacked dermomyotome cells shortened (Figure 2.15A', B').

Taken together, the presented results demonstrate that in Wt embryos, the dorsalization of somites during somite differentiation leads to a decrease in proliferative activity of cells in the dorsal dermomyotome and an increase in protrusion formation of dorsal somite tip cells. These processes are impaired in the ventralized somites of the *Da* mutant

2.3 Wnt11r is a somite dorsalization factor

2.3.1 A direct downstream target of *zic1* is *wnt11r* which is also downregulated in the *Da* mutant

After investigating the process of somite extension in detail, I was interested in the molecular background of dorsal somite extension during somite differentiation. Genes potentially involved in this process would be expressed downstream of *zic1* and also differentially expressed in the dorsal somites of the *Da* mutant. In the lab, a ChIP-seq against Zic1 was performed (Hashimoto, Nakamura, unpublished) to identify potential direct downstream targets of *zic1*. Among these genes was *wnt11r*, a non-cononical Wnt, which was previously in the focus of the lab, since it is also downregulated in the dorsal somites of the *Da* mutant (Figure 2.16A) (Kawanishi et al., 2013). qPCR performed on cDNA generated from RNA extracted from tails (including somites) of Wt embryos and *Da* mutant embryos additionally confirmed that *wnt11r* is downregulated by 1.4-fold in tails of *Da* mutant embryos.

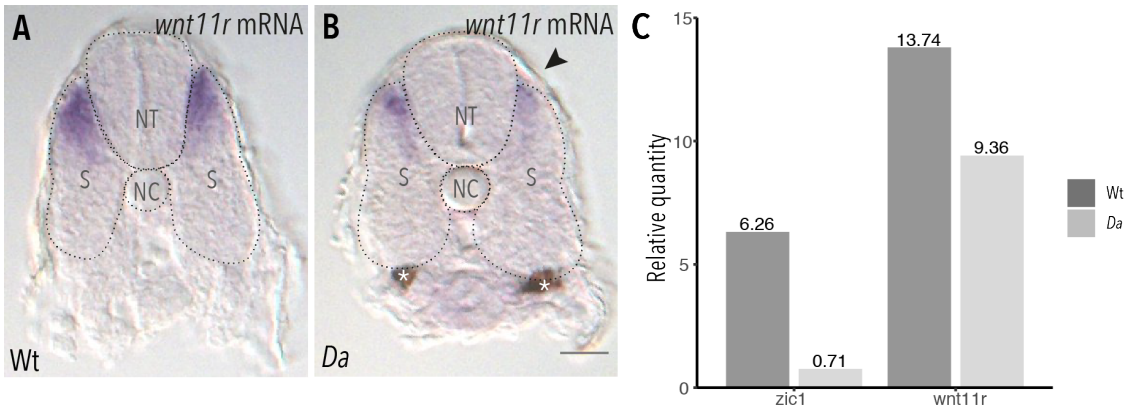

Figure 2.16: Wnt11r is downregulated in the dorsal somites of the *Da* mutant.
(A-B) Vibratome sections of whole-mount *in situ* hybridizations of stage 26 embryos. (A) *wnt11r* is expressed in the dorsal somites of Wt medaka. (B) The expression of *wnt11r* is decreased in the dorsal somites of the *Da* mutant. Arrow head indicated decreased expression. * mark melanophores.(C) qPCR quantification of *zic1* and *wnt11r* in tails of stage 23 Wt and *Da* mutant embryos. *zic1* is downregulated by 8.8-fold in the *Da* mutant and *wnt11r* by 1.4-fold. qPCR was performed on pooled RNA isolated from 10 tails of Wt embryos or *Da* mutant embryos. NT = neural tube, NC = notochord, S = somite, scale bar = 38 µm, sections = 40 µm.

Taken together, *wnt11r* is a promising *zic1* downstream target which could play a role in myotome patterning.

2.3.2 Knockdown of Wnt11r in Wt embryos recapitulates the dorsal somite phenotype of the *Da* mutant

Previously, it had been reported that Wnt11r is involved in EMT events happening at the dorsal somites. In *Xenopus*, a population of neural crest cells and a cell population originating from the dorsomedial somite, migrate dorsally to contribute to the mesenchyme of the dorsal fin. Wnt11r is required for the delamination of these cell populations. Furthermore, *wnt11r* is continuously expressed during dorsal migration of these cells (Garriock and Krieg, 2007). In chicken, the Wnt11r homologue, Wnt11 regulates EMT of cells from the medial dermatome, which migrate dorsally to populate the dorsal feather field (Isabel Olivera-Martinez et al., 2002; Olivera-Martinez et al., 2004). Additionally, Wnt11 also regulates EMT of dermomyotome cells at the dorsal medial lip, which later subsequently migrate dorsally and contribute to the dense dorsal dermis (Morosan-Puopolo et al., 2014). In light of these studies and considering my previous observation of myotome dorsalization, I hypothesized that Wnt11r is an important factor involved in myotome dorsalization during somite differentiation in fish. To investigate the role of Wnt11r in the dorsal somites of medaka, I wanted to knockdown Wnt11r using morpholinos. However, knocking-down Wnt11r during somite differentiation was challenging, since *wnt11r* is also expressed during gastrulation where it plays an essential role in convergent extension (Heisenberg et al., 2000; Ulrich et al., 2003). To tackle this problem, I designed two different experimental approaches. First, I used a Wnt11r antisense morpholino (Wnt11rMO), which blocks the translation of Wnt11r and determined the optimal concentration to mitigate gastrulation defects. Second, I used Photo-Morpholinos (PhotoMOs) to obtain temporal control over Wnt11r knockdown (Tallafuss et al., 2012). Like conventional morpholinos, PhotoMOs are oligomers which are complimentary to a target morpholino; in this case, the PhotoMOs are compliment to the to the antisense Wnt11rMO. In the center of its sequence, however, the PhotoMO contains a nucleotide which is cleavable by UV light. Prior to injection, the Photo-MO and the antisense Wnt11rMO are annealed. The morpholino duplex is injected into 1-cell stage embryos. Upon induction of photo-cleavage of the PhotoMO by UV light, the antisense Wnt11rMO is released from the morpholino duplex and can bind to its target, prohibiting the translation of Wnt11r. In the following experiments, photo-cleavage was induced after gastrulation at stage 20 (Figure 2.17A). Using the PhotoMO, I was able to create Wnt11r morphants exhibiting phenotypes with different degrees of severity. In morphants exhibiting severe phenotypes, the ends of the dorsal myotome of fail to cover the neural tube (n = 7), similar to the dorsal myotome in the *Da* mutant (Figure 2.9). Additionally the myofibers seem to be shorter and less organized, this could be due to the role of Wnt11r during early myogenesis, where Wnt11r is essential for orienting the extension of myocytes (Gros et al., 2008).

To investigate the proliferative activity of dorsal dermomyotome cells in Wnt11r-knockdown embryos, I performed immunostaing against pH3 and quantified the number of mitotic cells per somite (Figure 2.17D). In Wnt11r morphants, created either by the PhotoMO approach or by conventional antisense Wnt11rMO, cells of the dorsal dermomyotome showed a significantly higher proliferative activity, compared to control embryos. This increase in proliferative activity is similar to what was observed when comparing the proliferative activity of *Da* dorsal dermomyotome cells to Wt dorsal dermomyotome cells.
Both approaches to knockdown Wnt11r during somite differentiation seemed efficient.

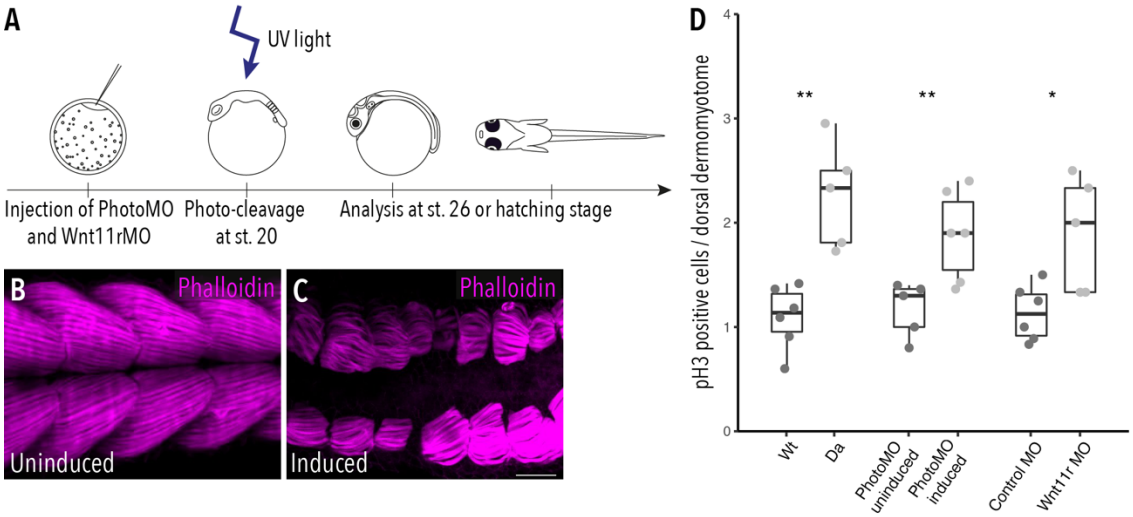

Figure 2.17: Proliferative activity is increased in the dorsal dermomyotome of Wnt11r morphants.
(A) Schematic representation of the knockdown of Wnt11r using PhotoMOs. The annealed antisense Wnt11rMO and sense PhotoMO are injected into an embryo at 1-cell stage. The PhotoMO is cleaved at stage 20 using UV light. (B) Dorsal view of a maximum projection of a stage 39 embryo injected with the morpholino duplex, PhotoMO has not been cleaved. Myotome is labelled with phalloidin (magenta). (C) Dorsal view of a maximum projection of a stage 39 embryo injected with the morpholino duplex. The PhotoMO was photo-cleaved as described in (A). Myotome is labelled with phalloidin (magenta). The dorsal ends of the myotome fail to cover the neural tube. (D) Quantification of pH3-positive cells in the dorsal dermomyotome per somite of Wt (66 somites from 6 embryos), *Da (*40.5 somites from 5 embryos) embryos, embryos injected with the morpholino duplex uninduced (51 somites of 5 embryos) and induced (61.5 somites of 6 embryos) and embryos injected with a control morpholino (65 somites from 6 embryos) or Wnt11rMO (52 somites from 5 embryos). More pH3-positive cells can be observed in the dorsal dermomyotome of embryos with downregulated/knocked down Wnt11r (median, first and third quartiles, $^{**}P_{Wt/Da} = 0.0035$, $^{**}P_{PhotoMO} = 0.0091$, $^{*}P_{MO} = 0.031$). Scale bar = 50 µm.

Next, I wanted to investigate whether the formation of protrusions during dorsal somite extension is altered in embryos with Wnt11r knockdown. If Wnt11r is involved in the regulation of protrusion formation in the dorsal somite tip cells, I expect less and smaller protrusions in the Wnt11r morphants, similar to the observations in the *Da* mutant (Figure 2.11). I performed time-lapse imaging of the transgenic line *zic1::GFP* injected with the morpholino duplex and photo-cleaved at stage 20, as described in Figure 2.17. Time-lapse imaging was performed as described in section 2.2.3. Similar to the results of the time-lapse imaging in the *Da* background, I observed the later onset of protrusion

formation as well as less numerous formation of protrusions compared to Wt embryos (Figure 2.18A-A"", Video 2.3). To quantify the protrusion in Wnt11r morphants, I injected Wt embryos either with a control morpholino (ControlMO) or the Wnt11rMO (Figure 2.18B-C") and live imaged the embryos at stage 27. Wnt11r morphants and control embryos formed a similar number of "small protrusions", whereas the number of "large protrusion" and the total number of protrusions was significantly higher in control embryos (Figure 2.18D-D"). A significantly higher number of "large protrusions" and total protrusions was also observed in Wt dorsal somites, compared to *Da* mutant dorsal somites (Figure 2.11E-E").

In conclusion, I found two ways to knockdown Wnt11r efficiently, without interfering with the expression of Wnt11r before somite differentiation. Similar to what was observed in the *Da* mutants, in Wnt11r morphants generated by the PhotoMO approach, the ends of the dorsal myotome don't elongate sufficiently and fail to cover the neural tube at the end of embryonic development. Furthermore, cells in the dorsal dermomyotome of Wnt11r morphants have a high proliferative activity compared to control embryos and the cells at the tip of the dorsal somites of Wnt11r morphants form less "large protrusions" and overall less protrusions than control embryos. In summary, knocking-down of Wnt11r during somite differentiation recapitulated the ventralized dorsal somite phenotype of the *Da* mutant.

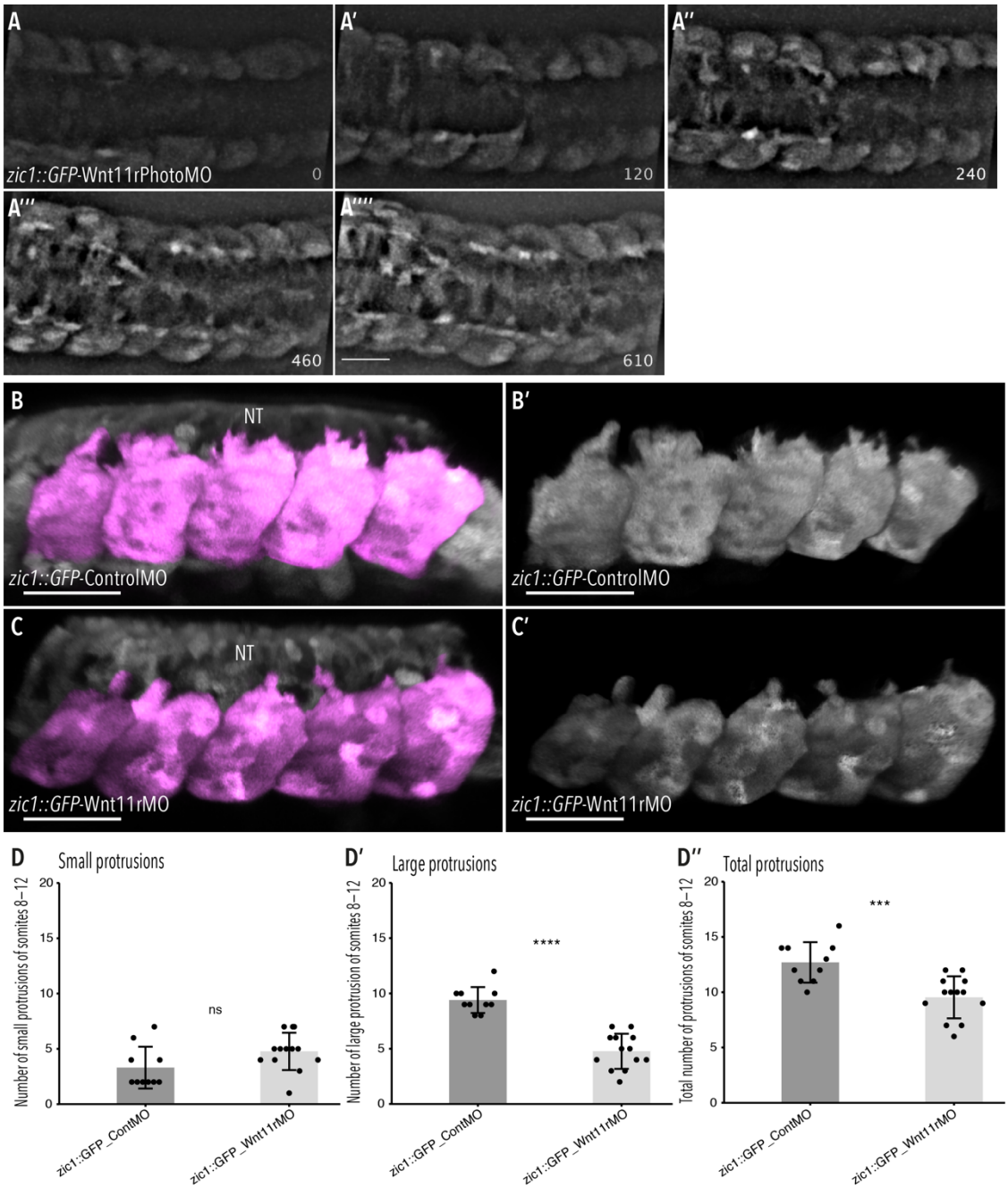

Figure 2.18: Wnt11r morphant dorsal somite tip cells form less large protrusions and less protrusions in total compared to control embryo dorsal tip cells.

(A-A'''') Dorsal view of time-lapse imaging of *zic1::GFP* injected with morpholino duplex and photo-cleaved at stage 20. Z-stacks were taken every 600 seconds. 15th somite is in the center. Time is displayed in min. (B-C') Lateral view of 3D-reconstruction of live imaging of *zic1::GFP* injected with ControlMO (B-B') and *zic1::GFP* injected with Wnt11rMO (C-C'). Embryos were imaged at stage 27, 10th somite is in the center. Extraction of dorsal somites colored (magenta) in (B) and (C) are depicted in (B') and (C'). (D-D'') Quantification of protrusions of the 8th to the 12th somite of embryos from the *zic1::GFP* line injected with ControlMO (n = 10 embryos) and the *zic1::GFP* injected with Wnty11rMO (n = 13 embryos) (mean ± SD, $^{ns}P_{small\ protrusions}$ = 0.069, $^{****}P_{large\ protrusions}$ = 7.7e^{-08}, $^{***}P_{total\ protrusions}$ = 0.00064). NT = neural tube, scale bar = 50 µm.

Video 2.3: Time-lapse imaging of onset of somite extension in Wnt11r morphant.
Dorsal view of time-lapse imaging of *zic1::GFP* injected with morpholino duplex and photo-cleaved at stage 20. At the onset of imaging embryo was at stage 27. Anterior is oriented to the left and the 15th somite is positioned in the center. Z-stacks were taken every 10 minutes. Tome is displayed in min, scale bar = 50 μm.

2.3.3 Wnt11 protein can partially rescue the *Da* phenotype

To further underline the importance of Wnt11r during somite dorsalization, I attempted to rescue the ventralized dorsal somite phenotype of the *Da* mutant. I first tried several genetic approaches to express *wnt11r* in the dorsal somites of the *Da* mutant, but unfortunately they were not successful. I switched my strategy and ectopically provided Wnt11r by injecting human recombinant Wnt11 (hrWnt11) protein directly into the *Da* mutant. I tested the functionality of the hrWnt11 protein by injecting the protein into 1-cell stage embryos. As expected, the hrWnt11r protein interfered with morphogenic movements during gastrulation, resulting in axis formation defects (data not shown) (Djiane et al., 2000; Du et al., 1995; Hardy et al., 2008). To rescue the ventralized dorsal somite phenotype of *Da* mutants, I injected the hrWnt11r protein under the epidermis, above the 10th somite of stage 25 (18-19-somite stage) embryos of the transgenic line *Da-zic1::GFP* (Figure 2.19A). I raised the embryos until stage 27 (24-somite stage embryo) and investigated the number and nature of protrusions formed. To visualize the location of hrWnt11, the protein was co-injected with rhodamine-labeled dextran (Figure 2.19B). Previous transplantation experiments performed in this lab, using beads soaked with hrWnt3a, showed that Wnt proteins diffuse ½ to 1 somite far. I assume that the hrWnt11r protein behaves in a similar way to the previously used Wnt3a because of their similar structure and size. I quantified the protrusions of the 10th somite and its neighboring somites (somite 9 and 11). *Da-zic1::GFP* embryos injected with BSA served as control. The number of small protrusions was similar in embryos injected with hrWnt11 or BSA, but dorsal somite tip cells of embryos injected with hrWnt11 formed significantly more “large protrusions” and significantly more protrusions in total, compared to dorsal tip cells of embryos injected with BSA.
These results further strengthen the hypothesis that Wnt11r is an important factor during somite dorsalization and influences the number and nature of protrusions formed by the dorsal somite tip cells.

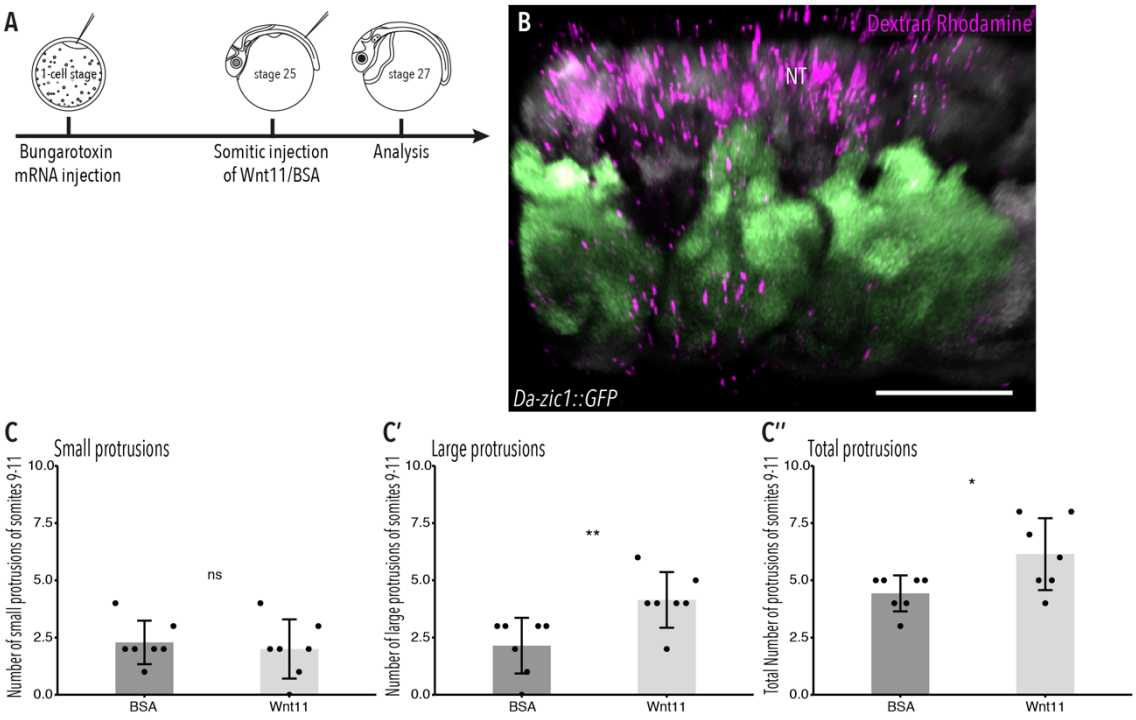

Figure 2.19: Wnt11 protein injections are able to rescue the *Da* mutant dorsal somite protrusion phenotype.

(A) Schematic representation of hrWnt11 protein injection. Embryos are injected with α-bungarotoxin mRNA at 1-cell stage to inhibit muscle movement. At Stage 25, embryos are injected with either hrWnt11 protein or BSA under the dermis on top of the 10th somite. Embryos are raised until stage 27 and analyzed. (B) Lateral view of 3D-reconstruction of live imagined *Da-zic1::GFP* embryos injected with hrWnt11r and Dextran-Rhodamine (magenta). Somites are colored in green. (C-C") Quantification of protrusions of the 9th to the 11th somite of *Da-zic1::GFP* embryos injected with BSA (n = 7 embryos) and hrWnt11 (n= 7 embryos) (mean ± SD, $^{ns}P_{small\ protrusions} = 0.65$, $^{**}P_{large\ protrusions} = 0.0095$, $^{*}P_{total\ protrusions} = 0.03$). NT = neural tube, scale bar = 50 µm.

2.3.4 Wnt11r may act through the Wnt/Ca^{2+} signaling pathway

After identifying Wnt11r as an important dorsalization factor of the myotome during somite differentiation, I wanted to know how exactly Wnt11r acts. During early myogenesis, Wnt11 acts through the planar cell polarity (PCP) pathway to orient the extension of myocytes (Gros et al., 2008). I investigated the expression levels of PCP components in embryonic tails using qPCR but I was not able to observe a differential expression of PCP components in *Da* mutant tails, compared to Wt tails (data not shown). In *Xenopus*, Wnt11r is important for the migration of neural crest cell population and cells from the dorsal somites into the dorsal fin. In this context, it was shown that Wnt11r acts through the Wnt/Ca^{2+} signaling pathway (Garriock and Krieg, 2007). The Wnt/Ca^{2+} pathway belongs, like the PCP pathway to the non-canonical Wnt signaling pathways, since β-catenin is not involved in the signaling cascades. Activation of Wnt/Ca^{2+} signaling leads to increased intracellular Ca^{2+} levels and can lead to the modulation of cell movement and the actin cytoskeleton (Kühl et al., 2001; Wang et al., 2010). In *Xenopus*, CaMKII (Calcium/calmodulin-dependent protein kinase type II), a player of the Ca^{2+}

signaling cascade, is activated by Wnt11 (Kühl et al., 2001). To investigate if in the dorsal somites of medaka, Wnt11r also acts through the Wnt/Ca^{2+} signaling pathway, I inhibited CaMKII with KN-93 (Figure 2.20). KN-93 had previously been shown to specifically inhibit CaMKII (Garriock and Krieg, 2007; Rothschild et al., 2013; Wu and Cline, 1998). To inhibit CaMKII, I incubated embryos from stage 20 until stage 26 in KN-93, embryos of the control group were treated with DMSO (Figure 2.20A). I examined the proliferation activity of dorsal dermomyotome cells in treated and control embryos by performing an immunostaining against pH3. Embryos treated with KN-93 showed a significantly higher proliferative activity per somite, compared to control embryos. This result is similar to that observed in the dorsal dermomyotome of *Da* mutants (Figure 2.8) and in Wnt11r morphants (Figure 2.17). To examine the formation of protrusion of dorsal somites tip cells, I treated embryos of the transgenic line *zic1::GFP* with KN-93 or DMSO and performed live imaging afterwards (Figure 2.20 C-C"). While there was no observable difference in the number of "small protrusions", embryos treated with KN-93 formed significantly less "large protrusions" and the overall number of protrusions was significantly decreased in these embryos, compared to embryos from the control group. Again, the formation of significantly less "large protrusions" and less protrusions in general was observed in Wnt11r morphants (Figure 2.18) as well.

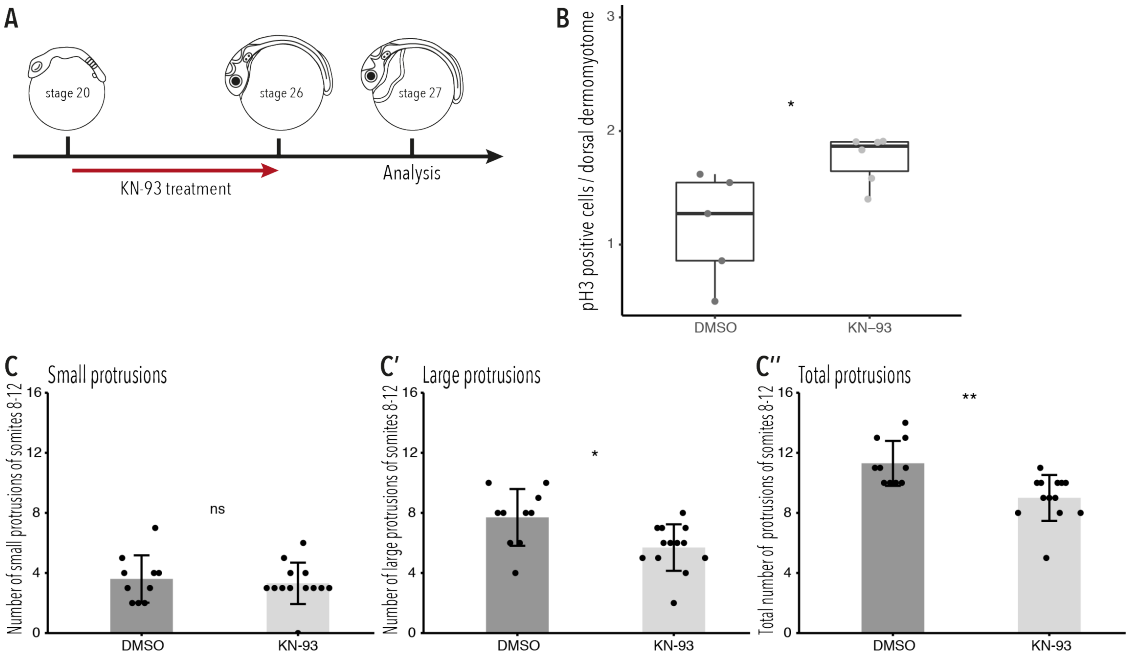

Figure 2.20: Dorsal dermomyotome cells of embryos with inhibited Wnt/Ca^{2+} signaling pathway show cellular features of Wnt11r morphants.

(A) Schematic representation of KN-93 treatment. Treatment was started at stage 20 and embryos were incubated in KN-93 until reaching stage 26. (B) Quantification of pH3-positive cells in the dorsal dermomyotome per somite of embryos treated with DMSO (52.5 somites from 5 embryos) or KN-93 *(*65.5 somites from 6 embryos) embryos (median, first and third quartiles, *P = 0.045). (C-C") Quantification of protrusions of the 8th to the 12th somite of *zic1*::*GFP* embryos treated with DMSO (n = 10 embryos) or KN-93 (n= 13 embryos) (mean ± SD, $^{ns}P_{small\ protrusions}$ = 0.65, $^{*}P_{large\ protrusions}$ = 0.014, $^{**}P_{total\ protrusions}$ = 0.0017).

These results suggest that Wnt11r probably acts through the Wnt/Ca^{2+} signaling pathway, since embryos treated with KN-93, showed an increase in dorsal dermomyotome cell proliferation and a decrease in formation of protrusions, as previously observed in Wnt11r morphants.

In summary, by knocking-down Wnt11r I could recapitulate the ventralized somite phenotype of the *Da* mutant. This phenotype was partially rescued by hrWnt11 protein injected onto the somites. During somite dorsalization, Wnt11r probably acts through the Wnt/Ca^{2+} signaling pathway as inhibition experiments suggested. It is thus highly likely that Wnt11r is a potent somite dorsalization factor that functions downstream of Zic1/Zic4.

3 Discussion

In this thesis, I investigated the regulation of *zic1/zic4* expression in the dorsal somites during somite differentiation. Additionally, I described the process of dorsal myotome extension during secondary myogenesis and identified Wnt11r as a novel dorsalization factor in this context.
Using different gain- and loss-of-function approaches, I demonstrated that *zic1* is expressed downstream of the canonical Wnt signaling pathway. To elucidate whether *zic1* is directly regulated by the canonical Wnt signaling pathway, I performed a ChIP-seq experiment against β-catenin which demonstrated that the expression of *zic1/zic4* in the dorsal somites is directly regulated by the canonical Wnt signaling pathway.
In the *Da* mutant, the expression of *zic1/zic4* is drastically reduced in the dorsal somites. This leads to a ventralized myotome which fails to elongate its dorsal ends sufficiently to cover the neural tube at the end of embryonic development. I described the morphological process of dorsal myotome extension and observed differences between the dorsal somites of Wt embryos and the ventralized dorsal somites of *Da* mutant embryos after primary myogenesis is completed, at the onset of dorsal somite extension. In the *Da* mutant, the onset of somite extension is delayed and cells at the tip of the dorsal somites form less and shorter protrusions extending towards the neural tube, compared to Wt somites. Furthermore, the dorsal dermomyotome of the *Da* mutant shows a higher proliferative activity than that of Wt.
While investigating myotome dorsalization on a molecular level, I identified Wnt11r as a potential dorsalization factor. Strikingly, knockdown of Wnt11r in Wt embryos could phenocopy the *Da* myotome phenotype. Additionally, Wnt11 protein injection could rescue the altered protrusion formation observed in *Da* dorsal somite tip cells. I showed that Wnt11r probably acts through the Wnt/Ca^{2+} signaling pathway, since inhibition of this pathway in Wt embryos led to a mild form of the *Da* dorsal somite phenotype.

3.1 The somitic expression of *zic1/zic4* is directly regulated by the canonical Wnt signaling pathway

Prior to access the somitic regulation of *zic1/zic4*, I examined the expression patterns of *wnt1*, *wnt3a* and *zic1* in cross sections of the trunk region. Interestingly, the expression pattern of all three genes during somite differentiation seem to be widely conserved among vertebrates. In *Xenopus*, chicken and mouse, *wnt1* and *wnt3a* are also expressed in the dorsal neural tube and *zic1* is also expressed in the dorsal neural tube and in the dorsal somites (Houtmeyers et al., 2013; Marcelle et al., 1997; Parr et al., 1993; Sun Rhodes and Merzdorf, 2006; Wolda et al., 1993). Considering that many signaling pathways are

conserved during embryonic development, the regulation of *zic1* in the dorsal somites might also be conserved among vertebrates. Furthermore, since the expression of *zic1* is conserved, its function might be conserved among vertebrates, too. Presumably, Zic1 acts as a somite dorsalization factor not just in fish, but also in other vertebrates. Conditional knockout of *zic1/zic4* in the dorsal somites in other vertebrate model organisms, and a consecutive analysis of the mutant myotome will shed light on this hypothesis.

In the ChIP-seq experiments several putative binding sites of the transcription factor complex involving β-catenin were identified around the *zic1/zic4* locus. The ChIP-seq against β-catenin was performed on whole embryos at stage 26 . To draw conclusions about peaks specific for the regulation of *zic1/zic4* in the dorsal somites, the ChIP-seq results were aligned to ATAC-seq data from dorsal or ventral somites. The ATAC-seq data revealed open chromatin regions specific for the dorsal and ventral somites. β-catenin binding peaks overlapping with open chromatin regions in the dorsal somites but not the ventral somites were considered as potential binding sites specific for the regulation of *zic1/zic4* in the somites. These putative binding sites were found in the predicted promoter region of *zic1/zic4*, additionally in a predicted enhancer site and several uncharacterized sites, proximal to the locus. The prediction of the putative enhancer region was performed by comparing different vertebrate species and identifying conserved noncoding elements (Moriyama et al., 2012). Certainly, the identification of putative binding sites is not a proof of direct regulation. It is important to additionally perform experiments which provide functional evidence for this regulation. It would be interesting to investigate whether dorsal specific open chromatin regions co-localized with β-catenin ChIP peaks become closed upon IWR treatment. Taken together, from the results of the experiments manipulating the canonical Wnt signaling pathway, which clearly prove that *zic1* is downstream of the canonical Wnt signaling pathway, and the identification of β-catenin binding peaks in putative promoter and enhancer regions, it is reasonable to conclude that *zic1/zic4* are direct downstream targets of the canonical Wnt signaling pathway in the dorsal smites. β-catenin peaks, which do not overlap with open chromatin regions of the somites could regulate *zic1/zic4* expression in a different tissue. This regulation of *zic1* was reported in a different context. In *Xenopus*, it is suggested that canonical Wnt signaling is necessary for the mutual induction of *pax3* and *zic1* during neural crest induction (Sato, 2005). On the contrary, during neurula stage, Zic1 induces the expression of *wnt* genes which in turn induce the expression of *engrailed* (Merzdorf and Sive, 2006). Interestingly, this regulatory pathway is conserved among vertebrates and even in *Drosophila*. During segmentation, *odd-paired*, the *Drosophila* homologue to the vertebrate *zic* genes, induces *wingless* expression, the *Drosophila* homologue of *wnt* genes, and Wnt signaling activates the expression of *engrailed* (Benedyk et al., 1994). This indicates that depending on the developmental context, the regulatory role between the canonical Wnt signaling pathway and *zic1* might reverse, or they form a feedback loop.

Considering the dramatic decrease of *zic1/zic4* expression in the dorsal somites of the *Da* mutant, no β-catenin binding peak was observed around the transposon insertion site. This strengthens the hypothesis that the misregulation of *zic1/zic4* in the dorsal somites is not due to the loss of a regulatory site but probably due to a change in the chromosomal architecture, induced by the insertion of the large transposon. To test this further, chromosome confirmation capture techniques like 4C or Hi-C need to be performed. Comparing the chromosome conformation profile of Wt and *Da* mutant embryos will provide insights into how the transposon insertion influenced the long range interaction between enhancer and promoter elements. Additionally, a ChIP-seq against β-catenin in *Da* mutants would elucidate if the regulation of *zic1/zic4* by the canonical Wnt signaling pathway is altered in the mutants.

3.2 The roles of cell protrusions during dorsal somite extension

In all jawed vertebrates epaxial muscles are the fundamental muscles of the back which cover the neural tube at the end of embryonic development. This is achieved by the dorsal extension of the epaxial myotome after it differentiated from the somites. To date, this process is not well understood. Using *in vivo* time-lapse imaging and histological analysis of tissue and cell morphology of sequential embryonic stages, I made the following observations regarding the dorsal extension of the epaxial myotome. During the dorsal extension the myotome is covered by a one-cell thick epithelial layer, the dermomyotome. The dermomyotome cells at the top of the dorsal somite form motile protrusions, extending towards the neural tube, and subsequently leading the myotome dorsally (Figure 3.1A). At the top of the neural tube the left and the right myotome will not fuse with one another, but form a gapless muscular tissue layer. In Wt medaka, the left and right myotome come in first contact at stage 37, the proceeding dorsal movement leads to the compaction of the myotome on top of the neural tube. In the ventralized *Da* mutant, the ends of the left and right myotome fail to come in contact at the top of the neural tube. Meanwhile, the dermomyotomes, covering the left and right myotomes in Wt and *Da* mutant, fuse on top of the neural tube, forming an epithelial layer beneath the ectoderm. *In vivo* imaging of Wt embryos, just before the fusion of dermomyotome layers, revealed that dermomyotome cells from the left and the right somite form protrusions extending towards each other. In Wt, the fusion of dermomyotomes takes place at stage 36 (6 days post fertilization), and in the *Da* mutant at stage 38 (8 days post fertilization, data not shown) (Figure 3.1B). Although, the term fusion might be misleading, here it implements the creation of a continuous epithelium by two epithelial cell layers coming in close proximity and forming *de novo* cell-cell contacts. In general, the fusion of epithelial sheets can be observed in numerous morphological processes. The most prominent examples might

be dorsal closure in *Drosophila*, neural tube closure in vertebrates and wound healing. All of these processes have in common that cells at the leading edge of the epithelial sheets form filopodia and lamellipodia during this process (Hayes and Solon, 2017; Nikolopoulou et al., 2017; Rolo et al., 2016; Wood et al., 2002). A recent study examining neural tube closure in mouse found that cells from the epithelium overlaying the neuroepithelium, which will later be incorporated into the neural tube, form protrusions. Those cells are known to be crucial for neural tube closure; perturbation of the protrusions led to a failed neurulation and resulted in spina bifida (Rolo et al., 2016). This suggests that the fusion of overlaying epithelial cell layers might exert a pulling force to the underlaying tissues, promoting their approximation. I indeed observed something similar in histological sections from stage 37 embryos. After the first dermomyotome cells formed a continuous epithelial cell layer in Wt embryos, dermomyotome cells covering the dorsal ends of each myotome extend towards the opposing myotome. This leads to a horizontal stacking of dermomyotome cells from each myotome on top of the neural tube. Later, a shortening of the cell bodies of these cells was observed, forming a tight myotome layer on top of the neural tube, which led me to the idea that those cells pull the dorsal ends of the myotomes closer together. (Figure 3.1B). This, however, was not observed in sections of *Da* mutants, probably due to impaired behavior of dorsal tip cells; they fail to come together close enough.

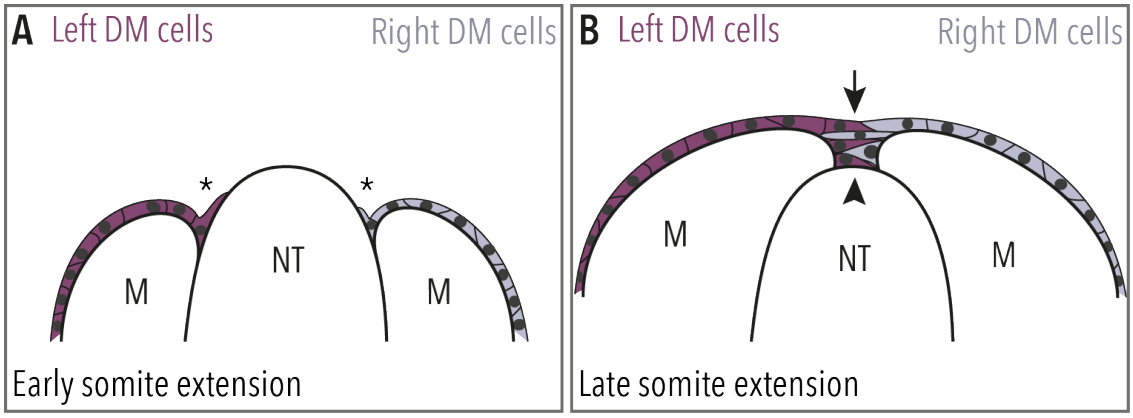

Figure 3.1: Roles of dermomyotome cells during somite extension.

(A) Schematic drawing of cross section of the trunk during early somite extension. Dermomyotome cells at the tip of the dorsal somites form protrusions extending dorsally (*). This will guide the myotome towards the top of the neural tube. (B) Schematic drawing of cross section of the trunk during late somite extension. Dermomyotome cells from the left and right somite have fused and formed an epithelial cell layer (arrow). Dermomyotome cells at the dorsal tip of the myotomes have extended to the opposing myotome. This result in horizontal stacking of dermomyotome cells (arrow head). These cells potentially generate a pulling force, by contracting their cell bodies, binging the myotomes closer together. DM = dermomyotome, M = myotome, NT = neural tube.

Taken together, the dorsal dermomyotome plays a crucial role for the proper morphology of epaxial muscles. First, in the beginning of somite extension, the dorsal dermomyotome guides the myotome dorsally. Second, later during this process, fusion of dermomyotomes from opposing myotomes and the contraction of stacked dermomyotome cells on top of

the neural tube might exert a pulling force bringing the myotomes close together (Figure 3.1).

To further characterize dorsal somite extension and the importance of dorsoventral patterning, I compared the onset of dorsal somite extension between Wt and *Da* mutant embryos. Already at stage 24, one stage after the induction of *zic1* expression in the dorsal somites, differences in somite extension towards the neural tube became evident. *In vivo* imaging of the onset of dorsal somite extension revealed that formation of protrusions starts after primary myogenesis is completed. In the *Da* mutant, the onset of somite extension was delayed. Additionally, *Da* mutants exhibit a higher number of short protrusions and less protrusions in total, as compared to Wt embryos. Generally, the protrusions observed in *Da* mutants were transient and did rarely form additional branches at the top of a protrusion, in opposite to the very motile, readily branching protrusions observed in Wt embryos. The reduced number of protrusions could result in a slower dorsal extension of somites, leading to the incomplete coverage of the neural tube by epaxial myotome in the *Da* mutant. This indicates that late dorsoventral patterning during somite differentiation is crucial for the successful establishment of epaxial muscles.
Ras-related C3 botulinum toxin substrate 1 (Rac1) and Cell division control protein 42 homolog (Cdc42) are small GTPases belonging to the Rho family which are known to modulate the actin cytoskeleton in cell protrusions. Rac1 is important for the formation of lamellipodia and membrane ruffles by promoting the formation of branched actin networks, whereas Cdc42 is crucial for filopodia formation by promoting the formation of straight actin bundles (Heasman and Ridley, 2008; Ridley, 2011). During neural tube closure in mouse, it was recently shown that, early in this process, leading-edge cells predominantly formed filopodia, but at later stages, mostly membrane ruffles, which are related to lamellipodia (Rolo et al., 2016). This suggested that different types of protrusions fulfill different functions. Additionally, during mesenchymal cell migration, the formation of lamellipodia is associated with fast migration, whereas filopodia carry out an exploratory role leading to slow migration with high directionality (Innocenti, 2018; Leithner et al., 2016). At the onset of dorsal somite extension in medaka, dorsal tip cells form a mixture of lamellipodia and filopodia. In Wt and *Da* mutant embryos, the large protrusions of dorsal tip cells consist of a lamellipodia with filopodia branching out from its edge. In Wt, more and longer filopodia were observed at the lamellipodia. Furthermore, they extend the large number of long protrusions, which could be beneficial for the invasion of the confined space between ectoderm and neural tube at the top of the neural tube. It would be interesting to investigate whether the composition of actin filaments changes in the protrusions during the course of somite extension. This could be achieved by *in vivo* imaging of embryos injected with *AC-GFP* mRNA, which labels actin filaments, at several different time points during somite extension. The dependency of the protrusions on Rac1 and Cdc42 can be studied by knocking these factors down. Along these

lines, it would be interesting to investigate the nature of protrusions upon conditional knockdown Rac1 or Cdc42.

That the extracellular matrix (ECM) influences movements of cells and tissues by providing guiding or restraining cues, is a widely accepted concept. Intriguingly, recent studies have also shown that the ECM can be remodeled by cells, facilitating their own movement. During gastrulation of zebrafish embryos, dorsal migrating endoderm cells express the *metalloproteinase Matrix metalloproteinase 14* (*mmp14)* which proteolytically deforms the ECM by degrading fibronectin and laminin (Hu et al., 2018). Zic1/Zic4 are transcription factors, regulating a wide variety of genes. Given the diverse phenotype of the *Da* mutant, Zic1/Zic4 should regulate multiple processes in the dorsal somite. The transcription factors might initiate the expression of a molecule which proteolytically remodels the surrounding ECM. In Wt embryos this would facilitate dorsal extension, while in *Da* mutants potentially less of this factor would be produced, resulting in an onerous dorsal somite extension. Studying the ECM remains a challenge to this day, even though major advancements can be recalled in this field. Revisiting the data from the ChIP-seq against Zic1 could provide hints if Zic1 regulates the expression of proteases in the dorsal somites. Immunostainings of various ECM components and scanning electron microscopy will reveal differences in ECM composition around dorsal somites of Wt and *Da* mutant embryos.

3.3 Upregulation or maintenance of *wnt11r* expression by Zic1 is crucial for dorsal-specific morphogenesis of the late somite

During somite differentiation in amniotes, *wnt11* is a marker for the DML and its expression is regulated by the canonical Wnt signaling pathway. This regulatory relationship is not reported in teleost and *Xenopus*, even though the homologue of *wnt11, wnt11r*, is also expressed in their dorsal somites. As somite differentiation proceeds in medaka, Zic1/Zic4 exert somite dorsalization, responsible for the late dorsoventral patterning during somite differentiation. The importance of the patterning by Zic1/Zic4 is well supported by the phenotype of the *Da* mutant, as loss of *zic1/zic4* expression in the dorsal somites leads to the ventralization of the trunk, including the myotome (Kawanishi et al., 2013; Ohtsuka et al., 2004). ChIP-seq against Zic1 revealed that *wnt11r* is potentially directly regulated by Zic1 (Y. Hashimoto and R. Nakamura, in preparation).

Zic1/Zic4 seem to act through Wnt11r to induce late somite and myotome dorsalization. This was experimentally evidenced by knocking-down Wnt11r in Wt embryos using morpholinos. These Wnt11r morphants recapitulated the ventralized somite phenotype of the *Da* mutants. Additionally, in morphants with extreme phenotypes, shorter and less organized myofibers were observed. This might be due to the earlier role of Wnt11r during

myogenesis, where it serves as a cue for the orientation and elongation of myocytes (Gros et al., 2008). Indeed, *wnt11r* is expressed earlier than *zic1/zic4* in the dorsal somites of medaka, at that point the expression levels of *wnt11r* in Wt and the *Da* mutant are the same (data not shown).
From the expression pattern of *wnt11r* in the dorsal somites of the *Da* mutant, Zic1 seems to be essential for the maintenance or upregulation of *wnt11r* during late somite differentiation. Intriguingly, the ChIP-seq against β-catenin detected a peak at the promoter region of *wnt11r*, suggesting a potential β-catenin-dependent additional regulation of *wnt11r* in the dorsal somites during late somite differentiation.

3.4 Dorsal somite tip cells undergo partial EMT during dorsal somite extension

Collective cell migration is a process in which multiple cells move together in a coordinated fashion. This process is frequently adopted throughout embryonic development including gastrulation, the elongation of the body axis in vertebra embryos, neural tube closure, neural crest migration, and additionally in wound healing (reviewed in (Lamouille et al., 2014; Thiery et al., 2009)). By performing *in vivo* imaging of dorsal somite extension, I observed that cells of the dorsal somites move together in a coordinated manner, a typical manner for collective cell migration. However, the question arose as to what enables the dorsal somite cells to start extending dorsally?
During dorsal closure and wound healing in *Drosophila*, cells at the leading edge lose their apico-basal polarity and undergo partial EMT (partial EMT implements that not all cell-cell contacts are lost and the cell displays both epithelial and mesenchymal properties). The loss of cell-cell adhesions at the leading edge leads to an accumulation of phosphatidylinositol 3,4,5-trisphosphate (PIP3), which promotes the formation of actin protrusions (Bahri et al., 2010; Pickering et al., 2013). To examine the role of EMT during the onset of dorsal somite extension, I performed N-cadherin staining in dorsal dermomyotome cells of Wt embryos and *Da* mutant embryos. N-cadherin is a marker for epithelial dermomyotome cells (Cinnamon et al., 2006; Zhou et al., 2018). Overall, the staining of N-cadherin was weak in the dorsal somites, but an accumulation of N-cadherin signal was indeed observed at the apical side of dorsal dermomyotome cells in the *Da* mutant. On the contrary, no accumulation of N-cadherin signal was detected in Wt dorsal dermomyotome. This suggests that these cells lost their apico-basal polarity and might have undergone incomplete EMT. In light of the studies introduced earlier, the loss of cell-cell adhesions could promote protrusion formation and might explain the high number of protrusions observed in Wt dorsal somite tip cells during *in vivo* imaging. This contrasts with the lower number of protrusions observed in the *Da* mutant.

To investigate differences of the cellular morphology of dorsal dermomyotome cells of Wt medakas and the ventralized dorsal dermomyotome cells of *Da* mutants, I performed TEM analysis. Intriguingly, the cell membranes of dorsal dermomyotome cells in Wt embryos showed wavy cell membranes and seemingly, the cell contact between neighboring cells was loose. By contrast, the cell membranes of dorsal tip cells in *Da* mutants appeared straight and cells seemed to be in close contact with their neighboring cells. In sections of Wt and *Da* mutant embryos, I also examined tight junctions and adherence junctions based on their size and location. Adherence junctions were especially prominent in sections of *Da* dorsal somites. Additionally, the density of cell junctions at the plasma membrane was higher in sections of the *Da* mutant compared to Wt sections. A higher ratio of cell junctions to membrane implies closer cell-cell contact. Although it is not possible to draw definite conclusions from the observed cell junctions, since the sample number was too small. Nevertheless, the observed wavy cell membranes in Wt dorsal dermomyotome cells seem to be a characteristic of dorsal somites. They might result from looser cell contact between neighboring cells, a possible consequence of partial EMT. To further access the role of EMT during dorsal somite extension, it will be necessary to deplete PIP3 in the dorsal dermomyotome of Wt embryos and observe if the number of protrusions is reduced and the cell membranes display a straight and not a wavy morphology.

Strikingly, Wnt11r also plays a role in promoting EMT in various developmental contexts. In chicken, Wnt11 promotes EMT of cells from the medial dermomyotome to undergo EMT to migrate dorsally and contribute to the dorsal feather field and the dermis (Morosan-Puopolo et al., 2014; Olivera-Martinez et al., 2004). In *Xenopus*, Wnt11r supports the delamination of cells from the dorsal dermomyotome and neural crest cells from the neural tube to migrate dorsally and become mesenchyme of the dorsal fin fold (Garriock and Krieg, 2007). Potentially, Wnt11r supports cells undergoing partial EMT in the context of dorsal somite extension as well.

3.5 Self-generated gradients and the guidance during somite extension

During embryonic development, directional cell and tissue movement is often guided by diffusible chemicals. This process is called chemotaxis. In the classical sense, source cells secrete a diffusible attractant which diffuses over a distance to the target sink cells. This generates an attractant gradient which is detected by the sink cells which migrate towards the attractant expressing cells (Insall and Andrew, 2007; Zigmond, 1977). However, this classical model has major limitations in terms of robustness over a range of concentrations. Additionally it works over short distances, only. In recent years, the view on chemotaxis has changed. It was observed that the sink cells have a more active role and adjust the

gradient using enzymatic degradation or replenishment of the attractant by endocytosis (Tweedy et al., 2016). Taking this principle further, by replenishing an attractant, cells are able to fully self-generate gradients in an environment where the chemoattractant is uniformly distributed. These gradients have been shown to be especially robust over a range of concentrations and function over long distances because cells locally generate their own steep gradient (Norden and Lecaudey, 2019; Tweedy and Insall, 2020). In zebrafish embryos, self-generated gradients work during the migration of the lateral line primordium (Donà et al., 2013; Venkiteswaran et al., 2013). Very recently, a striking paper was published which showed that using self-generated gradients, collectively migrating cells of the slime mold *Dictyostelium discoideum* and mouse metastatic pancreatic cancer cells were able to solve complex mazes and made decisions over the optimal route. This study indicates that self-generated gradients enable migrating cells to pilot complex paths accurately (Tweedy et al., 2020).

And what could guide the dermomyotome cells dorsally during somite elongation? It is very unlikely that cells at the top of the neural tube secrete an attractant to generate an imposed gradient which attracts the dorsal somite tip cells towards the neural tube. The large distance to covered, additionally the curved nature of the neural tube and its constant growth, would make it difficult to set up a robust gradient. It is more likely that cells at the tip of the dorsal dermomyotome generate their own gradient, by removing an attractant from the extracellular environment. So far, 33 chemokine receptors and 89 chemokine genes have been identified in zebrafish (Bussmann and Raz, 2015; Nomiyama et al., 2013). Candidate chemokines and receptors could be identified by their differential expression in dorsal somites of Wt and *Da* mutant embryos. Differences in chemokine levels or abundance of membrane receptors could lead to alterations in elimination of the chemokines from the extracellular environment. This would result in the generation of gradients with different degrees of steepness and potentially influence the speed or directionality of the tissue movement.

Wnt11r is known to control cell migration and morphogenesis during gastrulation. Recent studies have provided evidence that endocytosis is crucial for efficient Wnt signaling. During gastrulation, cell migration is regulated by the non-canonical PCP pathway. Cadherins and Procadherins form adhesive plaques adhering to the substrate and neighboring cells. Binding of Wnt11 to its Fz receptor enhances the endocytosis of the receptor-ligand complex and the associated Cadherins and Procadherins. These Cadherins and Procadherins are either recycled and redistributed at the plasma membrane or degraded. Overall, the interaction of Wnt11 with its receptor influences the adhesiveness of the cell (Brunt and Scholpp, 2018; Kraft et al., 2012; Witzel et al., 2006). To investigate if the internalization of Wnt11r plays a role during dorsal somite extension, the protein could be endogenously tagged with a fluorescent protein containing a short half-life. This would enable to visualize the location and decay of Wnt11r *in vivo*. Additionally, since Wnt proteins seem to be internalized by Clathrin-mediated endocytosis (Blitzer and Nusse,

2006; Hagemann et al., 2014; Ohkawara et al., 2011). To further elucidate if this internalization of Wnt11r is crucial for somite elongation, I definitely need to block the internalization by inhibiting Clathrin-mediated endocytosis and observe the dorsal somite extension and protrusion formation behavior.

3.6 The roles of Wnt11r during late somite development

The morpholino and the rescue experiments have shown clearly that Wnt11r acts as a direct dorsalization factor during late somite differentiation. A characteristic of dorsal somites is the formation of large and numerous protrusions by the dermomyotome cells located at the dorsal tip of the somites. These protrusions seem to be important for successful dorsal somite extension. Analysis of the Wnt11 zebrafish mutant "*silberblick*" revealed that Wnt11 plays a crucial role in the orientation of cell protrusions as well as in directed cell movement. The analysis of mutant hypoblast cells demonstrated that Wnt11 supports the formation and stabilization of directed protrusion. (Ulrich et al., 2003). Additionally, in migrating neural crest cells, Wnt11 promotes the stabilization of lamellipodia. Morpholino mediate knockdown of Wnt11 led to the inhibition of neural crest cell migration, while the induction and maintenance of neural crest cell migration was not influenced (De Calisto et al., 2005; Matthews et al., 2008a). These studies indicate that Wnt11 is involved in the stabilization of protrusions and their oriented elongation, leading to the idea that it also acts in the same way during somite extension.
Comparison of the proliferative activity of dorsal dermomyotome cells between Wt and *Da* mutant embryos revealed one characteristic of dorsalized somites; the proliferative activity of dorsal dermomyotome cells is reduced after the onset of the somitic expression of *zic1/zic4*. A control experiment confirmed that the proliferative activity of Wt and *Da* mutant ventral dermomyotome cells is not significantly different, indicating that the reduced proliferative activity in the dorsal dermomyotome is probably a result of late dorsoventral somite pattering mediated by Zic1/Zic4. This is further supported by knockdown of Wnt11r which increases the proliferative activity of dorsal dermomyotome cells. In the dorsal dermomyotome, Wnt11r directly or indirectly reduces the proliferation activity. So far, not much is known about the negative regulation of cell proliferation by Wnt11r. In the neonatal heart in mouse, Wnt11 regulates cell proliferation in a chamber specific manner. Downregulation of Wnt11 induced myocyte proliferation (Touma et al., 2017). On the other hand, it was proposed that Wnt11 stimulates cell proliferation in mouse intestinal epithelial cells in cell culture (Ouko et al., 2004). Thus, the effect of Wnt11r on cell proliferation is context-dependent. The results of this thesis provide another example of Wnt11r negatively regulating cell proliferation.

Taken all obtained results together, I propose the following two hypotheses explaining dorsal somite extension in medaka, which is essential for the epaxial myotome to form a gapless myotome layer on top of the neural tube at the end of embryonic development. In the first hypothesis, Wnt11r balances between proliferation and protrusion formation of dorsal dermomyotome cells.

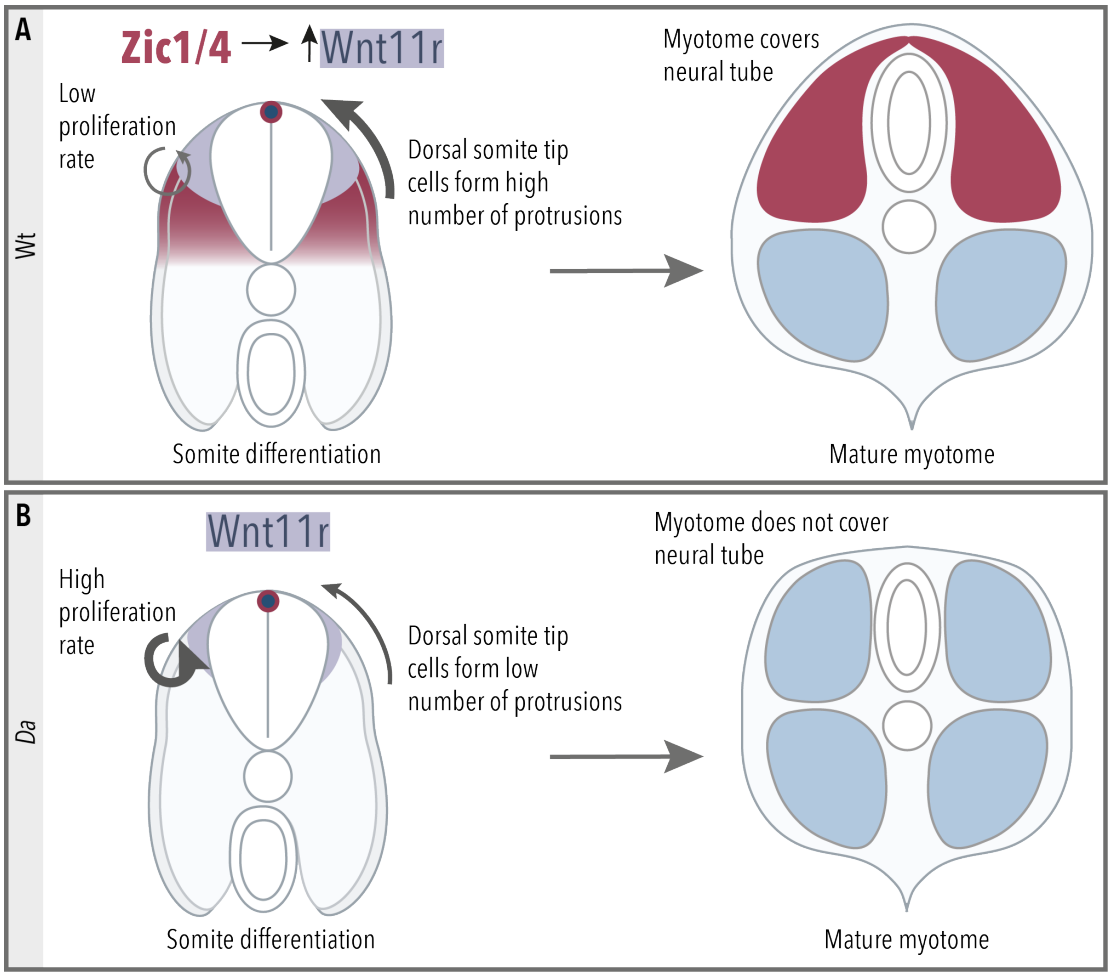

Figure 3.2: Wnt11r balances between proliferation and protrusion formation in dorsal dermomyotome cells.

(A-B) Schematic representation of somite dorsalization during late somite differentiation and the subsequent effect of epaxial muscle morphology at the end of embryonic development. (A) In Wt embryos Zic1/Zic4 maintain or upregulate the expression of *wnt11r* in the dorsal somites. This results in the decrease of proliferative activity in the dorsal dermomyotome and promotes the formation of large protrusions of dorsal somite tip cells. Somites extend properly and at the end of embryonic development a layer of epaxial muscles will cover the neural tube. (B) In the *Da* mutant only low levels of *wnt11r* are expressed in the dorsal somites. This leads to high proliferative activity in the dorsal dermomyotome and impaired protrusion formation of dorsal somite tip cells. This results in perturbed somite extension and the mature epaxial muscles will not cover the neural tube in the *Da* mutant.

The great reduction of *zic1/zic4* expression in the dorsal somites of the *Da* mutant leads to low levels of Wnt11r in the dorsal somites. This results in an imbalance in favor of proliferation at the cost of protrusion formation in the dorsal dermomyotome cells. Ultimately, the dorsal dermomyotome cells form less and shorter protrusions, leading to

insufficient dorsal somite extension and a failure of epaxial myotome to cover the neural tube (Figure 3.2). This hypothesis is supported by the coupled observation of increased proliferation and perturbed protrusion formation of dorsal dermomyotome cells in the Wnt11 morphants.
The second hypothesis proposes that the regulation of proliferation in the dorsal dermomyotome cells and the formation of protrusions happens independent from each other. During normal development, the proliferative activity in the dorsal dermomyotome might be suppressed to simply adapt to the limited space at the dorsal side of the trunk which is cause by the large neural tube. This situation is in contrast to the ventral side, where the growth of the myotome is less restricted spatially. Wnt11r may participate in the pathway sensing the confined space. It would be interesting to observe if blocking the proliferation in the dorsal dermomyotome of the *Da* mutant could rescue the perturbed protrusion formation.

Wnt11r can act through the PCP pathway and the Wnt/Ca^{2+} signaling pathway. In the previously listed examples, it was shown that Wnt11 acts through the PCP pathway during neural crest cell migration in zebrafish and *Xenopus* (De Calisto et al., 2005; Matthews et al., 2008b). Whereas the protein acts through the Wnt/Ca^{2+} signaling pathway while regulating the EMT of dorsal somite cell which are destined to migrate into the dorsal fin fold in *Xenopus* (Garriock and Krieg, 2007) and during the proliferation and migration of mouse intestinal epithelial cells in culture (Ouko et al., 2004). To determine which signaling pathway is active during dorsal somite extension, I examined whether genes of the PCP signaling cascade (*prickle1a* and *ror2* (Butler and Wallingford, 2017; Jussila and Ciruna, 2017)) were differentially regulated in tails of *Da* mutant embryos by qPCR (data not shown). This was not the case, suggesting that the PCP pathway is not active during somite extension. Next, I investigated the involvement of the Wnt/Ca^{2+} signaling pathway. I downregulated the pathway by inhibiting CaMKII, a molecule which is activated after the Wnt induced release of intracellular Ca^{2+}. The results were not as drastic as observed in the *Da* mutant or the Wnt11r morphants, but inhibition of Wnt/Ca^{2+} signaling pathway led to an increase in the proliferation of dorsal dermomyotome cells and dorsal somite tip cells formed significantly less large protrusions and less protrusions in total. These results strongly suggest that Wnt11r acts through the Wnt/Ca^{2+} signaling pathway during somite extension.
Garriock and colleagues argue that Wnt11r acts cell-autonomous in the dorsal somites of *Xenopus* (Garriock and Krieg, 2007). I found that in medaka during late somite dorsalization, Wnt11r acts in a cell non-cell-autonomous manner, since I was able to rescue the *Da* mutant protrusion phenotype by Wnt11 protein injection into the extracellular space above the dorsal somites.

4 Conclusions

In this thesis, I investigated the developmental mechanism of how Zic1/Zic4 mediate the dorsal muscle morphology in medaka embryos. The results from the manipulation of the canonical Wnt signaling pathway and the ChIP-seq analysis show that somite dorsalization factors *zic1/zic4* are direct downstream targets of the canonical Wnt signaling pathway during somite differentiation. Furthermore, subsequent analysis suggest that these dorsalization factors act through the non-canonical Wnt *wnt11r*. Knockdown of Wnt11r in Wt embryos recapitulated the ventralized somite phenotype of the *Da* mutant and Wnt11 protein injection were able to partially rescue the *Da* mutant. On a cellular level, dorsalized dermomyotome cells show a reduced proliferative capacity, the dorsalized somite tip cells have the ability to form multiple and large protrusions, and additionally, their plasma membranes have a wavy character. By acquiring these characters, dermomyotome cells surrounding the myotome could guide the myotome dorsally towards the top of the neural tube.

Based on the results presented in this thesis, I propose following model to describe dorsal somite extension to give rise to epaxial muscles of the trunk. Prior to dorsal somite extension, cells have to acquire dorsal identity by expressing *zic1/zic4*, which are induced by the canonical Wnt signaling pathway. *Zic1/zic4* expressing dorsal dermomyotome cells then reduce their proliferative activity, and the cells at the tip of the dorsal somites form protrusions extending dorsally, to ultimately cover the neural tube. *Wnt11r*, whose expression is maintained or upregulated by *zic1*, might maintain a balance between proliferation and protrusion formation of dorsal dermomyotome cells. I found for the first time the key developmental process underlying the formation of epaxial trunk myotome in medaka.

Since expression of canonical Wnts, *zic1/zic4* and *wnt11r* during late somite differentiation are highly conserved among vertebrates, it would be interested if a similar developmental process could be observed in other vertebrates, too.

5 Materials & Methods

5.1 Materials

5.1.1 Organisms

Medaka fish lines

Medaka stocks and transgenic lines used and/or generated for this thesis are summarized in Table 5.1.

The transgenic line *Da-zic1::GFP;zic4::dsRed* was generated by crossing *Da* mutants with fish from the transgenic line *zic1::GFP;zic4::dsRed*. The transgenic lines *Da-like*, *zic1EnhD35bp* and *zic1EnhD346bp* were generated by the CRISPR/Cas9 system.

Table 5.1: Medaka stocks and transgenic lines used in this thesis.

Name of fish line	Internal stock number	Source
wildtype Cab	7239, 7524, 7796	(Wittbrodt et al., 2002)
wildtype d-rR	S181018, S190307, S190718, S191122, S200211, S200605, S200915	(Yamamoto, 1975)
Double anal fin (Da) mutant	7633, 7838, 7958, 8105, 8389, S180918, S190117, S190913, S200122, S200818	(Ohtsuka et al., 2004)
Da-like	17j, 22j	this thesis
congenic *Da*	26j	lab stock
zic1::GFP;zic4::dsRed	S190125, S190717, S200609, S201127	(Kawanishi et al., 2013)
Da-zic1::GFP;zic4::dsRed	25J	this thesis
zic1EnhD35bp$^{-/-}$	1J	this thesis
zic1EnhDΔ35bp$^{+/-}$	2J	this thesis
zic1EnhD346bp$^{-/-}$	5J	this thesis
zic1EnhDΔ346bp$^{+/-}$	6J	this thesis

Bacteria

Bacteria used in this thesis are listed in Table 5.2.

Table 5.2: Bacteria used in this thesis.

Designation	Source
DH5αCompetent Cells	Thermo Fisher Scientific
MachT1 chemically competent *E. coli*	Thermo Fisher Scientific

5.1.2 Plasmids

Plasmids used in this thesis are listed in Table 5.3.
The plasmid pGGEV5_+(ocean pout terminator)+_+1_BK was generated by releasing the ocean pout terminator element from the plasmid pGGEV4_-(ocean pout terminator)-_+1_BK (plasmid stock #5346) and subcloning it into the pGGEV5 vector. For the generation of the plasmids pGEM-Teasy(Wnt11r_ISH) and pGEM-Teasy(Wnt3a_ISH), *wnt11r* and *wnt3a* cDNA was amplified and cloned into a pGEM-Teasy vector as described in the section 5.2.39. The sgRNA template vectors DR274(sgRNA_zic1/zic4_EnhancerD_T1) and DR274(sgRNA_zic1/zic4_EnhancerD_T2) were generated as described in (Stemmer et al., 2015). The plasmids pSPORT6.1(Wnt1-ISH) and pSPORT6.1(zic1-ISH) come from the lab cDNA library.

Table 5.3: Plasmids used in this thesis.

Plasmid name	Plasmid stock number	Source
pSGH2	1599	lab stock
DR274 sgRNA backbone (T7)	3632	lab stock
pCS2+Inv X_Cas9	5197	lab stock
pGGEV5_+(ocean pout terminator)+_+1_BK	5337	this thesis
DR274(sgRNA 57 Oca2_ex9_T1)	5357	lab stock
DR274(sgRNA 58 Oca2_ex9_T3)	5358	lab stock
pGEM-Teasy(Wnt11r_ISH)	5374	this thesis
DR274(sgRNA_zic1/zic4_EnhancerD_T1)	5402	this thesis
DR274(sgRNA_zic1/zic4_EnhancerD_T2)	5403	this thesis
pSPORT6.1(zic1-ISH)	5404	this thesis
pSPORT6.1(Wnt1-ISH)	5408	this thesis
pGEM-Teasy(Wnt3a_ISH)	5409	this thesis

Plasmid name	Plasmid stock number	Source
pSGH2_+(delta61_NTCF3 cDNA)+_+1_PCR	5410	lab stock
pSGH2-lef1delta240VP16	J1	lab stock
pMTB-memCherry	J2	lab stock
pCS2+AC-TagGFP2	J3	lab stock
pmtb-t7-alpha-bungarotoxin	J4	lab stock

5.1.3 Primers

Primers used in this thesis are listed in Table 5.4. Primers with a number starting with "JW" were ordered from Eurofins MWG Operon and primers with a number starting with "AKH" were ordered from Invitrogen.

Table 5.4: Primers used in this thesis.

Number	Name	Source	Sequence 5'–3'
JW6919	Wnt11r-FW	this thesis	CATGAA-GAGCCGCTCTCACA
JW6920	Wnt11r-RV	this thesis	TCCCTGAGGTCTTGGAG-TCC
JW7712	EnhancerD-seq-F	lab stock	TGTTTCCAA-GCTTCTCGACG
JW7713	EnhancerD-seq-R	lab stock	GTGGAGCAGCGAA-GAAACTC
JW7576	Wnt3a_ISH_FW	this thesis	TCAACCTATTCTTT-GTGGGAGCATA
JW7577	Wnt3a_ISH_RV	this thesis	CTTGTCTTTCATGTAG-TCACCGATG
JW8002	OceanPout-seq-down-F	lab stock	GTACAGCTACCAGAGAA-GCTTGA
JW8003	OceanPout-seq-down-R	lab stock	GGTTTTGACATGTTCAG-TTAACGG
AKH030	Axin2_LefBS-1_FW	this thesis	TGTGAG-TGCCTTTCTGCCTC
AKH031	Axin2_LefBS-1_RV	this thesis	TTCTGTGTGAACCCGGT GAG
AKH038	Lef_LefBS-2_FW	this thesis	TGGCCTGGAAAGGAA-GATCAA

Number	Name	Source	Sequence 5'–3'
AKH039	Lef_LefBS-2_RV	this thesis	TGTCCCTTTACAGCAG-TGACTC
AKH051	zic1ol.F-rt	lab stock	AGCCCTTTCCGTGTCCG TTCC
AKH052	zic1ol.R-rt	lab stock	CCGACGTGTGGACGTG-CATGT
AKH066	qPCR-chr7-FW	this thesis	GTGACTGTAATGGCTAC-CGATCT
AKH067	qPCR-chr7-RV	this thesis	TGTCCTG-CATGTCAGCCAATA
AKH070	qPCR-chr13-FW	this thesis	CTTTACGCGCTTT-GGTGCTG
AKH071	qPCR-chr13-RV	this thesis	AGGTAGATTTCAG-TGACACGGG
AKH094	wnt11r-qPCR2-FW	this thesis	CGCTGGAACTGCTCCTC-TAT
AKH095	wnt11r-qPCR2-RV	this thesis	GCAGCG-GACAAGGCATAAAC
AKH098	axin2-CDS1-FW	this thesis	GGACTGTCCGCAAA-GAACCT
AKH099	axin2-CDS1-RV	this thesis	AGCCAGAGTT-GACAAAGTAGGG
AKH104	lef1-CDS1-FW	this thesis	GAAGAGGAGGGAGACTT-GGC
AKH105	lef1-CDS1-RV	this thesis	TGGTATTTGG-GACTGCCTAGC
AKH186	qPCR-EGFP Fv1	lab stock	AGGACGACGGCAAC-TACAAG
AKH187	qPCR-EGFP Rv1	lab stock	TTCTGCTT-GTCGGCCATGAT

5.1.4 RNAs

Table 5.5 lists sgRNAs used in this thesis. Transcription of sgRNAs was performed according to protocol in section 5.2.43.

Table 5.5: sgRNAs used in this thesis.

Name	Source	Target	Comment
sgRNA EnhD_T1	this thesis	*zic1/zic4* enhancerD, next to transposon insertion site	Transcribed from plasmid #5402
sgRNA EnhD_T2	this thesis	*zic1/zic4* enhancerD, next to transposon insertion site	Transcribed from plasmid #5403
sgRNA 57 Oca2_ex9_T1	lab stock	*oca2* exon9	Transcribed from plasmid #5357
sgRNA 57 Oca2_ex9_T3	lab stock	*oca2* exon9	Transcribed from plasmid #5358

Table 5.6 lists the mRNAs used in this thesis. Transcription of mRNAs is described in section 5.2.44.

Table 5.6: mRNAs used in this thesis.

Name	Source	Comment
α-bungarotoxin	lab stock	Transcribed from #J4
AC-GFP	lab stock	Transcribed from #J3
mmCherry	lab stock	Transcribed from #J2

5.1.5 Morpholinos

Morpholino oligonucleotides used in this thesis were ordered from Gene Tools and are listed in Table 5.7.

Table 5.7: Morpholinos used in this thesis.

Name	Source	Target	Sequence
Standard control	lab stock	Mutated Intron of human *beta-globine* causing beta-thalassemia	CCTCTTAC-CTCAGTTACAATTTATA
wnt11r MO1	lab stock	wnt11r promoter region	CTTCATGATGGATGGAGGCTCCGGT
Wnt11r_Photo-MO	this thesis	wnt11r MO	CGGAGCCTP-CATCCATCATG

5.1.6 Chemicals and reagents

Chemicals and reagents used in this thesis are listed in Table 5.8.

Table 5.8: Chemicals and reagents used in this thesis.

Chemical/Reagent	Company
1-Azakenpaullone	Sigma-Aldrich
2-Propanol	Sigma-Aldrich, Wako
Adenosine triphosphate (ATP)	Thermo Fisher Scientific
Agarose	Funakoshi co., LTD, Sigma-Aldrich, Solana
Agarose Low Melt	Sigma-Aldrich
Alexa Fluorophore 488, Phalloidin	Invitrogen
AmPureXP magnetic beads	Beckman Coulter
Anti-Digoxigenin-AP Fab fragments	Roche
Bacto-Agar	BD Difco, Roth
Bacto-Trypton	BD Difco, Gibco
Bacto-Yeast extract	BD Difco
BCIP (5-bromo-4-chloro-3-indolyl phosphate)	Roche
Blocking reagent	Roche
Bovine Serum Albumin (BSA)	Sigma-Aldrich
Calcium chloride ($CaCl_2$)	AppliChem, Wako
Calcium chloride dihydrate ($CaCl_2 \cdot 2\ H_2O$)	AppliChem, Wako
Chloroform	Sigma-Aldrich, Wako
DAPI (4',6-Diamidino-2-Phenyindole, Dilactate)	Sigma-Aldrich
Deoxyadenosine triphosphate (dATP)	Thermo Fisher Scientific
Deoxynucleotide triphosphates (dNTPs)	Sigma-Aldrich, TaKaRa, Thermo Fisher Scientific
Dextran Rhodamine	Thermo Fisher Scientific

Chemical/Reagent	Company
digoxigenin deoxyuridine triphosphate (digUTPs)	Roche
Dipotassium phosphate (K2HPO4)	Wako
Disodium hydrogen phosphate (Na_2HPO_4)	Nacalai tesque, Sigma-Aldrich
Disodium hydrogen phosphate dihydrate ($Na_2HPO_4 \cdot 2\ H_2O$)	Sigma-Aldrich, Wako
Dimethyl sulfoxide (DMSO)	Sigma-Aldrich
Dithiothreitol (DTT)	Thermo Fisher Scientific
DNA Purple loading dye	Thermo Fisher Scientific
Dynabeads Protein A	Invitrogen
Ethanol 70 % (denatured) (EtHO)	Roth, Wako
Ethanol 96 % (denatured) (EtHO)	Roth, Wako
Ethanol 99 % (EtHO)	Sigma-Aldrich, Wako
Ethachinmate	Nippon Gene
Ethidium Bromide (EtBr)	Sigma-Aldrich
Ethylenediaminetetraacetic acid (EDTA)	Dojindo, Roth
EGTA	Dojindo
Formamide	Sigma-Aldrich, Wako
Gel Loading Dye Purple (6x)	NEB
GeneRuler DNA Ladder Mix	Thermo Fisher Scientific
Glacial acetic acid 96 %	Merck, Wako
Glucose	Sigma-Aldrich, Wako
Glycerin (Glycerol)	Merck, Wako
Glycine	Sigma-Aldrich, Wako
Heparin	Gibco, Sigma-Aldrich
HEPES (4-(2-hydroxyethyl)-1-piperazineethanesulfonic acid)	Roth, Sigma-Aldrich

Chemical/Reagent	Company
Hydrogen Chloride (HCl)	Merck, Wako
ISOGEN	Nippon Gene
IWR-1	Sigma-Aldrich
KN-93	Wako
Magnesium chloride ($MgCl_2$)	AppliChem, Wako
Magnesium sulphate heptahydrate (MgSO4·7 H2O)	Merck, Wako
Methanol (MeOH)	Roth, Wako
Methylene blue trihydrate	Sigma-Aldrich
Midori GreenXtra	Nippon Genetics
NBT (4-nitro blue tetrazolium chloride)	Roche
Normal Goat Serum (NGS)	Gibco
Paraformaldehyde (PFA)	Sigma-Aldrich
Paraformaldehyde Phosphate Buffer Solution	Wako
Phenol	Nippon Gene
Phenylmethylsulfonyl fluoride (PMSF)	Roche
Polyethylene glycol - 4000 (PEG-4000)	Thermo Fisher Scientific
Potassium acetate (KAc)	AppliChem, Wako
Potassium chloride (KCl)	AppliChem, Wako
Potassium dihydrogen phosphate (KH_2PO_4)	Merck, Wako
Protease Inhibitor	Sigma-Aldrich
Red sea salt	Red Sea
Rhodamine Phalloidin	Life Technologies
RiboLock RNase Inhibitor	Thermo Fisher Scientific
RNA from torula yeast Type VI	Sigma-Aldrich
RNA Loading Dye 2x Rapid	Thermo Fisher Scientific, Ambio
RNase-free water	Sigma-Aldrich
rNTPs (ribonucleoside triphosphate) (ATP, CTP, GTP, UTP)	Roche
Roti	Roth

Chemical/Reagent	Company
Sheep Serum (SS)	Sigma-Aldrich
Sodium acetate (NaOAc)	Grüssing, Nippon Gene
Sodium butyrate (Na-butyrate)	Sigma-Aldrich
Sodium chloride (NaCl)	Sigma-Aldrich, Wako
Sodium citrate	Sigma-Aldrich
Sodium citrate tribasic ($C_6H_5Na_3O_7 \cdot 2\ H_2O$)	Sigma-Aldrich
Sodium deoxycholate (Na-Deoxycholate)	Wako
Sodium dodecyl sulphate sodium salt (SDS)	Serva, Sigma-Aldrich
Sodium hydrogen carbonate ($NaHCO_3$)	Merck, Wako
Sodium hydroxide (NaOH)	Sigma-Aldrich, Wako
Tricaine (MS-222)	Sigma-Aldrich
Tris base	Roth, Sigma-Aldrich
Tris-hydrochloride (Tris-HCl)	Sigma-Aldrich
Triton X-100	Sigma-Aldrich
Trizol	Invitrogen
Tween20	Sigma-Aldrich
X-Gal	Thermo Fisher Scientific
Yeast Extract	Roth

5.1.7 Enzymes and proteins

Enzymes used in this thesis are listed in Table 5.9.

Table 5.9: Enzymes and corresponding buffers used in this thesis.

Enzyme	Company
Ex Taq DNA Polymerase and 10x Ex Taq Buffer	TaKaRa
Hatching enzyme	lab made
I-SceI Meganuclease and 10x I-SceI buffer	NEB

Enzyme	Company
Phusion High-Fidelity DNA Polymerase and 5x Phusion HF Buffer	NEB
PrimeSTAR GXL DNA Polymerase and 5x PrimeStar GXL Buffer	TaKaRa
Proteinase K	Roche
Q5 High-Fidelity DNA Polymerase and 5x Q5 Reaction Buffer	NEB
Restriction enzymes and buffers	NEB/TaKaRa/Thermo Fisher Scientific/TOYOBO
RNase A, DNase- and protease-free (10 mg/ml)	Thermo Fisher Scientific
T4 DNA Ligase and 10x T4 DNA Ligase Buffer	NEB, Thermo Fisher Scientific
Taq Roboklon 5 U/ml and 10x PolBufferB	Roboklon
THUNDERBIRD SYBR qPCR Mix and50x ROX reference Dye	TOYOBO
Turbo DNaseI (2 U/ml)	Invitrogen
Ligation High Ver.2 ligation Mix	TOYOBO

Proteins used in this thesis are listed in Table 5.10.

Table 5.10: Proteins used in this thesis.

Protein	Company
EnGen® Spy Cas9 NLS	NEB
Recombinant Human Wnt11 protein (hrWnt11)	R&D

5.1.8 Antibodies

Primary antibodies used in this thesis are listed in Table 5.11.

Table 5.11: Primary antibodies used in this thesis.

Primary antibody	Species	Concentration	Company
Anti-Cdh2	rabbit	0.18055556	Gene Tex, GTX125885
Anti-Pax3/7 (DP312)	mouse	0.11111111	Davis et al., 2001
Anti-pH3	rabbit	0.18055556	Millipore, 06-570

Secondary antibodies used in this thesis are listed in Table 5.12.

Table 5.12: Secondary antibodies used in this thesis.

Secondary antibody	Species	Concentration	Company
Anti-mouse Alexa 555	goat	0.38888889	Thermo Fisher, A-21422
Anti-rabbit Alexa 488	donkey	0.38888889	Life Technnologies, A-11008

Antibodies used in the ChIP experiments are listed in Table 5.13.

Table 5.13: ChIP antibodies used in this thesis.

Antibody for ChIP	Species	Company
Anti-β-Catenin	rabbit	Abcam Ab227499
Anti-β-Catenin	rabbit	Abcam 32527
Anti-Non-phospho β-Catenin	rabbit	Cell Signaling, 38814

5.1.9 Kits

Kits used in this thesis are listed in Table 5.14.

Table 5.14: Kits used in this thesis.

Kit	Company
Bioanalysis High Sensitivity DNA Analysis Kit	Agilent
HiScribe T7 Quick High Yield RNA Synthesis Kit	NEB
innuPREP PCRpure Kit	Analytik Jena
KAPA Hyper Prep Kit	Roche
MCE-202 MultiNA DNA-500 Reagent Kit	Shimadzu
MCE-202 MultiNA DNA-1000 Reagent Kit	Shimadzu
MEGAscript™ T7 Transcription Kit	Thermo Fisher Scientific
mMessage mMachine® Sp6 Transcription	Thermo Fisher Scientific
mMessage mMachine® T7 Transcription	Thermo Fisher Scientific
pGEM®-T Easy Vector System	Promega
QIAPrep® Spin Miniprep Kit	Qiagen
Qiaquick Nucleotide Removal Kit	Qiagen
RNeasy Mini Kit	Qiagen
SeqCap Adapter Kit A, B	Roche

Kit	Company
Super Script III Kit	Invitrogen
Wizard SV Gel and PCR Clean-Up System	Promega

5.1.10Consumables

Consumables used in this thesis are listed in Table 5.15.

Table 5.15: Consumables used in this thesis.

Consumable	Company
Adhesive Glass Slide	Matsunami
Cell saver tips 200 µl	Roth
Cover slips	Roth, Matsunami
Filter Tips 10 µl, 20 µl, 200 µl, 1.25 ml	Starlab
Filter Tips 10 µl	Vortex
Filter Tips 20 µl, 200 µl	Molecukar Bio Products
Filter Tips 1.25 ml	Thermo Scientific
Glass beads	Roth
Glass bottom dishes for microscopy	IWAKI
Glass dish 40mm	Trade Flat Mark
Glass vials	Roth
Imersol W	Zeiss
Injection molds	homemade
Injection needles GC100F-10	Harvard Apparatus
Latex gloves	Semperguard
Microloader tips	Eppendorf
Micro pestles 0.5/1.5 ml	Laborversand Hartenstein
Micro pestles 1.5/2.0 ml	Eppendorf
Microtome blades C35	Feather
Nail polish	Canmake Tokyo, Essence
Nitrile gloves	Starlab, Kimberly-Clark
Parafilm® M	Bemis

Consumable	Company
Pasteur pipettes	Falcon, Iwaki, Sarstedt
PCR 96 well plate	Nippon Genetics
PCR stripes	BMBio, Sarstedt
PCR tubes	BMBio, Kisker
Petri dishes	Greiner, Rikaken
Pipette tips 10 µl, 200 µl	QSP, Steinbrenner
Pipette tips 1.2 ml	Sorenson, Steinbrenner
Precision glide needle 30G1/2	Becton Dickinson & Co
qPCR plate 96 well plate	FrameStar
qPCR plate seal	Watson
Reaction tubes 1.5 ml, 2 ml	BMBio, Sarstedt, Watson
Sandpaper 1000 grit	Bauhaus
Scalpel blades	Feather, Roth
Sterilized petri dish - Fish dish	Rikaken
Tissue Culture Dish 15mm, 35mm, 60mm	Falcon
Tubes 15 ml, 50 ml	Falcon, Sarstedt
Well plate 4-well	Falcon
Well plates 6-well, 12-well, 24-well	Böttger, Roth, Thermo Scientific

5.1.11 Equipment

Equipment used in this thesis is listed in Table 5.16.

Table 5.16: Equipment used in this thesis.

Equipment	Company
Bacterial Shaker INNOVA 44	New Brunswick
Bacterial Shaker SLI-400	EYELA
Centrifuges 5417C, 5425, 5430R, 5810R	Eppendorf
Centrifuges MX-307, MX-107	TOMY
Cold light source for stereomicroscope CLS 100x	Leica
Cold light source for stereomicroscope KL 1500 LCD	Schott

Equipment	Company
Cold light source for stereomicroscope TL3	Olympus
Cool incubator CN-25C	Mitsubishi Electronics
DeNovix DS-11 spectrophotometer	DeNovix
Dry block heater	Iwaki
Electrophoresis chambers and combs	homemade and Peqlab
FAS-V Gel Dokumentation System	Nippon Genetics
FemtoJet express, 4i and Microinjector 5242	Eppendorf
Fish incubators	Heraeus instruments and RuMed
Focused-ultrasonicator S220	Covaris
Forceps 5, 55 Inox stainless steel	Dumont
Forceps 110 mm, straight	NeoLab
Freezer -20°C	Liebherr, Nihon Freezer
Freezer -80°C	Thermo Fisher Scientific, Nihon Freezer
Fridge 4°C	Liebherr
High-Resolution Automated Electrophoresis 2100 Bioanalyzer	Agilent
HiSeq 1500 System	Illumina
Incubator 32°C, 37°C, 60°C	Binder
InjectMan NI2	Eppendorf
Keyence BZ-9000 Biorevo	Keyence
Leica DFC 7000T	Leica
Leica M165 FC	Leica
Magnetic stand	Invitrogen
Microchip Electrophoresis System 202 MultiNA	Shimadzu
Microwave	Sharp, National
Milli-Q water filtration station	Millipore Corporation
Mini-centrifuge	Sarstedt, TOMY
Mini-centrifuge for PCR tubes	WAKEN

Equipment	Company
Multi 2plus Submarine electrophoresis system	Advance
Multiplex Quantitative PCR System Mx3000P	Stratagene
MS1Minishaker	IKA
NanoDrop 2000 Spectrometer	Thermo Fisher Scientific
Needle puller P-30	Sutter Instrument Co USA
Needle puller PC-10	Narishigen
Nikon DS-Ri1	Nikon
Nikon SMZ18 stereomicroscope	Nikon
Olympus SZX7	Olympus
PCR C100 Touch Thermal Cycler	Bio-Rad
Pharmaceutical Refrigerator with Freezer Sanyo MPR-411F	Sanyo Medicool
pH-Meter	Sartorius, Laqua
PipetBoy	Gilson, Drummond
Pipette 2 µl, 20 µl, 200 µl	Nichiryo
Pipette 1 ml	Gilson
Power supply Power-PAC Basic	Bio-Rad
PowerPac 300	Bio-Rad
Qubit 2.0 Fluorometer	Thermo Fisher Scientific
Rotating arm	homemade
Scale	Sartorius, A&D
Shakers CAT S 20, DRS-12	NeoLab
Shakers Wave-SI, Wave-PR	TAITEC
Slow Stirrer SW-500N	NISSIN
Stereomicroscope Zeiss Stemi 2000	Zeiss
Thermocycler	Bio-Rad
Thermomixer Comfort	Eppendorf
Thermomixer Compact	Eppendorf
Thermomixer F1.5	Eppendorf

Equipment	Company
T Professional Thermocycler	Biometra
UV-Gel Documentation System	Intas
UV table	Vilber Lourmat
Vertical Rotator	Scinics
Vibratome Series 3000 Sectioning System	Vibratome
Vibratome VT1000S	Leica
Vortex	Scientific Industries
Water bath	GFL, EYELA
Zeiss Axio Imager M1	Zeiss
Zeiss AXIO Observer Z1	Zeiss
Zeiss LSM 710	Zeiss

5.1.12 Solutions for fish husbandry

Solutions for fish husbandry and fish work used in this thesis are listed in Table 5.17.

Table 5.17: Recipes for solutions for fish husbandry and work used in this thesis.

Solution	Ingredients	Final concentration
10x Embryo Rearing Medium (ERM)	NaCl	17 mM
	KCl	0.4 mM
	$CaCl_2 \cdot 2\ H_2O$	0.27 mM
	$MgSO_4 \cdot 7\ H_2O$	0.66 mM
	HEPES pH 7.3	17 mM
	pH 7.1	
10x Medaka Hatch Medium	NaCl	17 mM
	KCl	0.4 mM
	$CaCl_2 \cdot 2\ H_2O$	0.27 mM
	$MgSO_4 \cdot 7\ H_2O$	0.66 mM
	HEPES pH 7.3	17 mM
	Methylene blue trihydrate	0.0001%
	pH 7.1	

Solution	Ingredients	Final concentration
100x Hatching buffer	NaCl	100 g/l
	KCl	3 g/l
	$CaCl_2 \cdot 2\ H_2O$	4 g/l
	$MgSO_4 \cdot 7\ H_2O$	16 g/l
10x Yamamoto's Ringer Solution	NaCl	57 g/l
	KCl	2 g/l
	$CaCl_2 \cdot 2\ H_2O$	2.7 g/l
	NaHCO3	2 g/l
20x Tricaine	Tricaine	4 g/l
	$Na_2HPO_4 \cdot 2\ H_2O$	10 g/l
	pH 7.0-7.5	
32 % PFA stock solution	PFA	500 g
	Millipore H_2O	ad 1562 ml
16 % PFA stock solution	32 % PFA stock	200 ml
	Millipore H_2O	ad 360 ml
	solve at 60°C, adjust to pH 7.0 with 1 M NaOH	
	Millipore H_2O	ad 400 ml
1-Azakenpaullone	1-Azakenpaullone	1 mg
stock 30 mM	DMSO	0.102 ml
IWR-1	IWR-1	5 mg
stock 10 mM	DMSO	1.22 ml
KN-93 1	KN-93	1 mg
stock 1.996 nM	DMSO	1 ml

5.1.13 Solutions for bacterial work

Solutions for bacterial work used in this thesis are listed in Table 5.18.

Table 5.18: Recipes for solutions for bacterial work used in this thesis.

Solution	Ingredients	Final concentration
LB-Bacterial Plates	Bacto-Tryptone	10 g/l
	Bacto-Yeast extract	5 g/l
	NaCl	10 g/l
	Bacto-Agar	15 g/l
LB-Medium	Bacto-Tryptone	10 g/l
	Bacto-Yeast extract	5 g/l
	NaCl	10 g/l
SOC medium	Bacto-Yeast extract	0.50%
	Bacto-Tryptone	2%
	NaCl	10 mM
	KCl	2.5 mM
	MgCl2	10 mM
	MgSO4	10mM
	Glucose	20 mM
TB-medium	Bacto-Tryptone	12 g/l
	Bacto-Yeast extract	24 g/l
	Glycerin	0.40%
	KH_2PO_4	2.13 g/l
	K_2HPO_4	12.54 g/l

5.1.14 Antibiotics

Antibiotics used in this thesis for bacterial selection are listed in Table 5.19.

Table 5.19: Antibodies for bacterial selection used in this thesis.

Antibiotic	Working concentration	Company
Ampicillin	50 µg/ml	Roth
Kanamycin	100 µg/ml	Roth

5.1.15 Solutions for DNA and RNA work

Solutions for DNA and RNA work used in this thesis are listed in Table 5.20.

Table 5.20: Recipes for solutions for DNA and RNA work used in this thesis.

Solution	Ingredients	Composition
EtBr bath	EtBr (10 mg/ml)	0.02%
	1x TAE	
Finclip buffer	Tris-HCl pH 8.5	100 mM
	EDTA pH 8	10 mM
	NaCl	200 mM
	SDS	2%
50x Alkaline Lysis Solution	NaOH	1.25 mM
	EDTA	10 mM
Oligo annealing buffer	Tris-HCl pH 7.5-8	10 mM
	NaCl	30 mM
P1 buffer	Glucose	50 mM
	Tris-HCl	25 mM
	EDTA	10 mM
	RNase A	100 µg/ml
	pH 8.0	
P2 buffer	NaOH	0.2 M
	SDS	1%
P3 buffer	KAc	5 M
	pH 5.5	
50x Tris-Acetate-EDTA buffer (TAE)	Tris base	242 g/l
	Glacial acetic acid	5.71%
	EDTA	50 mM
	pH 8.5	

5.1.16 Solutions for immunohistochemistry

Solutions for immunohistochemistry used in this thesis are listed in Table 5.21.

Table 5.21: Recipes for solutions for immunohistochemistry used in this thesis.

Solution	Ingredients	Composition
10x Phosphate-buffered saline (PBS)	NaCl	70.1 g
	Na_2HPO_4	49.8 g
	KH_2PO_4	3.4 g
	de-ionized H_2O	ad 1 l
	pH 7.3	
PBSDT	DMSO	1%
	Triton X-100	0.10%
	1x PBS	
1x PBS with Tween (PTW)	10x PBS pH 7.3	100 ml
	20 % Tween20	5 ml
	Millipore H_2O	ad 1 l
Blocking solution	BSA	2%
	DMSO	1%
	Triton X-100	0.20%
	1x PBS	
DAPI stock solution (2 mg/ml)	DAPI	10 mg
	DMSO	ad 5 ml

5.1.17 Solutions for *in situ* hybridization

Solutions used for *in situ* hybridization used in this thesis are listed in Table 5.22.

Table 5.22: Recipes for *in situ* hybridization solutions used in this thesis.

Solution	Ingredients	Final concentration
20x Saline Sodium citrate	NaCl	3 M
buffer (SSC)	$C_6H_5Na_3O_7 \cdot 2\ H_2O$	300 mM
	pH 7.0	

Solution	Ingredients	Final concentration
4x SSC with Tween (SSCT)	20x SSC	4x
	20 % Tween20	0.10%
2x SSCT	20x SSC	2x
	20 % Tween20	0.10%
0.2x SSCT	20x SSC	0.2x
	20 % Tween20	0.10%
Blocking buffer	Sheep serum	5%
	in 1x PTW	
Hybridization Mix	Formamide	50%
	20x SSC	5x
	Heparin	150 µg/ml
	RNA from torula yeast Type VI	5 mg/ml
	20 % Tween20	0.10%
Pre-staining buffer	Tris-HCl pH 7.5	100 mM
	NaCl	100 mM
	20 % Tween20	0.10%
Staining buffer	Tris-HCl pH 9.5	100 mM
	NaCl	100 mM
	$MgCl_2$	50 mM
	20 % Tween20	0.10%
Staining solution	NBT	337.5 µg/ml
	BCIP	175 µg/ml
	Staining buffer	1 ml

5.1.18Solutions for ChIP

Solutions for ChIP used in this thesis are listed in Table 5.23.

Table 5.23: Recipes for ChIP solutions used in this thesis.

Solution	Ingredients	Final Concentration
Solution A	Protease Inhibitor	1x

Solution	Ingredients	Final Concentration
	Na-butyrate	20 mM
	PMSF	1 mM
	PBS	ad 3 ml
RIPA buffer	Tris-HCl pH 8.0	10 mM
	NaCl	140 mM
	EDTA	1 mM
	EGTA	0.5 mM
	Triton X-100	1%
	SDS	0.10%
	Na-Deoxycholate	0.10%
Lysis buffer	Tris-HCl pH 8.0	50 mM
	EDTA	10 mM
	SDS	1%
TE buffer	Tris-HCl pH 8.0	10 mM
	EDTA	10 mM

5.1.19 Software

Software used in this thesis is listed in Table 5.24.

Table 5.24: Software used in this thesis.

Name	Reference/Vendor
Adobe Illustrator	Adobe
Burrows-Wheeler Aligner mapping software	(Li and Durbin, 2009)
CCTop	(Stemmer et al., 2015)
Fiji	(Schindelin et al., 2012)
FileMaker Pro	FileMaker, Inc.
FluoRender 2.19	(University of Utah, 2020)
Geneious	Biomatters Limited, (Kearse et al., 2012)
ggplot2	(Wickham, 2009)

Name	Reference/Vendor
iTerm2 3.4	(Nachman, 2019)
Microsoft Office	Microsoft
Python 3.8	(WinPython distribution of Python, 2019)
QuEST software	(Valouev et al., 2008)
Rstudio	(RStudio Team, 2020)
SAMtools v1.3	(Li et al., 2009)
ShortRead	(Morgan et al., 2009)
ZEN	Zeiss

5.2 Methods

5.2.1 Fish husbandry

Medaka (*Oryzias latipes*) fish used in this thesis were kept as closed stocks in accordance to Tierschutzgesetz 111, Abs. 1, Nr. 1 and with European Union animal welfare guidelines. Fish were maintained in constantly recirculating systems at 28°C on a 14 h light/10 h dark cycle (Tierschutzgesetz 111, Abs. 1, Nr. 1, Haltungserlaubnis AZ35–9185.64 and AZ35–9185.64/BH KIT). Embryos were staged as previously described in (Iwamatsu, 2004).

5.2.2 Microinjection into fertilized medaka eggs

The transgenic lines *Da-like*, *EnhDΔ35bp* and *EnhDΔ346bp* were generated using the CRISPR/Cas9 system. To generate the *Da-like* mutants, a ocean pout terminator (OPT) cassette was released from the plasmid #5337 by BamHI+KpnI digest and co-injected with sgRNAs and *cas9* mRNA (*cas9* mRNA injection + OPT). Microinjections into medaka embryos were used in several transient experiments to up- or downregulate gene expression. To ectopically express genes, embryos were injecting with meganuclease and plasmids containing a heat shock promoter and the gene of interest. To knockdown Wnt11r, embryos were injected with morpholinos. The rescue experiment in the *Da* mutant was performed by Wn11 protein injections. To immobilize embryos for *in vivo* imaging and time-lapse imaging, embryos were injected with *α-bungarotoxin* mRNA. For the visualization of actin filaments in cell protrusions, embryos were injected with *membrane-mCherry* (*mmCherry*) mRNA and *Actin-Chromobody-GFP*（*AC-GFP*）mRNA. All injection mix recipes are summarized in Table 5.25.

Table 5.25: Injection mix recipes used in this thesis.

***cas9* mRNA injection**	**Concentration**	***cas9* mRNA injection + OPT**	**Concentration**
cas9 mRNA	150 ng/µl	*cas9* mRNA	150 ng/µl
sgRNAs	15 ng/µl	sgRNAs	15 ng/µl
RNase-free H_2O	ad 10 µl	OPT	0.5 ng /µl
		RNase-free H_2O	ad 10 µl
Plasmid injection	**Concentration**	***α-bungarotoxin* mRNA injection**	**Concentration**
Plasmid DNA	10 ng/µl	*α-bungarotoxin* mRNA	25 ng/µl
I-SceI	0.25 U/µl	10x YRS	1x

Plasmid injection	Concentration	*α-bungarotoxin* mRNA injection	Concentration
10x I-SecI buffer	1x	RNase-free H_2O	ad 10 µl
10x YRS	1x		
MilliQ H_2O	ad 20 µl		
Morpholino injection	**Concentration**	**Photo-Morpholino Injection**	**Concentration**
1 mM Morpholino	12.5 µM	Photo-Morpholino-Antisense Morpholino duplex	25 µM
10x YRS	1x	10x YRS	1x
MilliQ H_2O	ad 10 µl	MilliQ H_2O	ad 5 µl
Membrane-mCherry Mix	**Concentration**	**Actin-Chromobody-GFP Mix**	**Concentration**
Membrane-mCherry mRNA	152 ng/µl	*Actin-Chromobody-GFP* mRNA	184 ng/µl
α-bungarotoxin mRNA	25 ng/µl	10x YRS	1x
10x YRS	1x	RNase-free H_2O	ad 10 µl
RNase-free H_2O	ad 10 µl		
hrWnt11 protein Mix	**Concentration**	**BSA Mix**	**Concentration**
hrWnt11r protein	1.7 ng	0.1 % BSA/1x PBS	0.085 %
10x YRS	1x	10x YRS	1x
1 % Dextran Rhodamine	0.05 %	1 % Dextran Rhodamine	0.05 %
RNase-free H_2O	ad 10 µl	RNase-free H_2O	ad 10 µl

Prior to the injection, an injection plate and the injection mix were prepared. The injection plate was prepared in a 9 cm petri dish. The dish was filled with 1.5 % - 1.8 % Agarose/H_2O and an injection mold was placed on top of the agarose to generate grooves for the embryos. The mold was removed once the agarose solidified and covered with 1x ERM or Hatching buffer to prevent dry out. Microinjections were performed into 1-cell stage embryos. To synchronize embryonic development, male fish were separated from female fish the night before the injection. 20 min prior to injection, male and female fish were brought together to mate. Fertilized eggs were collected, washed, separated with forceps and carefully placed into the grooves of the injection plate. The eggs were oriented in a way that the cell was facing up. Injection needles were generated from glass capillaries

using a needle puller, and filled with 2.5-3 µl of injection mix. The needle was opened by carefully scratching an embryo's chorion. Dependent on the needle, 500-850 hPa injection pressure and 80-100 hPa compensation pressure was used for the injection. The needle was inserted in a 23 ° angle into the cell and a small amount (roughly 10 % of the cell's volume) was injected. After the injection, embryos were transferred into dishes containing either 1x ERM, 1x Hatch or Hatching buffer and raised until the desired stage was reached.

5.2.3 Photo-Morpholino mutagenesis

Sense-Photo-Morpholino and Wnt11r antisense morpholino were annealed in a ratio 2:1 for 30 min at RT in the dark. This Photo-Morpholino-antisense morpholino duplex can be stored in the dark at RT for several months. Prior to injection, the duplex was heated up to 65 °C for 10 min. Microinjection into medaka embryos was performed as described in section 5.2.2 while trying to expose the injection mix, containing the morpholino duplex, as short as possible to the daylight. After the injection, embryos were raised to stage 21 in the dark. Photo-cleavage of the Photo-Morpholino was performed using the 10x objective and the DAPI filter of a Keyence BZ-9000 microscope. For the photo-cleavage, six injected embryos were mounted in 1 % Methylcellulose in a glass bottom dish, with the dorsal side facing up, and illuminated for 30 min using the Keyence microscope. After Photo-cleavage, embryos were dechorionated and raised until the desired stage. At the desired stage embryos were either prepared for *in vivo* imaging or fixated for immunostaining.

5.2.4 Injection of hrWnt11 protein onto *Da* mutant somite

Da-zic1::GFP embryos were injected with α-Bungarotoxin mRNA as described in 5.2.2 and raised at 28 °C until stage 25 was reached. Embryos were mounted with the dorsal side facing upwards in 1 % LMA. Mounted embryos were injected directly beneath the dermis above of the 10th somite with either hrWnt11 (human recombinant Wnt11) protein mix or with 0.1 % BSA mix (Table 5.26). Embryos were raised until stage 27 and *in vivo* imaging of dorsal somite extension was performed. Number and size of protrusions were analyzed using FluoRender.

5.2.5 Dechorionation of embryos

Embryos were gently rolled on sandpaper to remove outer surface hair. After hair removal, the embryos were washed three times with hatching buffer and transferred into 1x YRS, previously pre-warmed to 28 °C. Hatching enzyme was added, and the embryos were incubated at 28 °C. After the chorion was digested, embryos were carefully transferred

into fresh 1x YRS, excess chorion was removed using forceps and embryos were raised to the desired stage.

5.2.6 1-Azakenpaullone treatment

Embryos were dechorionated and raised to 9 somite stage. For the Azakenpaullone treatment, embryos were incubated in the dark in 2.5 µM 1-Azakenpaullone/1x YRS at 28 °C for 3 h. Embryos belonging to the control group were treated in parallel with 0.12 % DMSO/1x YRS and incubated at 28 °C, in the dark for 3 h. After the treatment, embryos were washed 3x 5 min with 1x YSR and raised in 1x YSR until stage 24 was reached. Once the embryos reached stage 24, they were prepared for RNA extraction from the tails.

5.2.7 IWR-1 treatment

Embryos were dechorionated and raised until 9 somite stage was reached. For the IWR-1 treatment, embryos were incubated with 10 µM IWR-1/1x YRS at 24 °C, in the dark, overnight. In parallel, embryos belonging to the control group were treated with 0.1 % DMSO/1x YRS at 24 °C, in the dark, overnight. The treatment was stopped when the embryos reached stage 24. Embryos were washed 3x 5 min in 1x YRS and prepared for RNA extraction from the tails.

5.2.8 KN-93 treatment

Embryos were dechorionated and raised until 4 somite stage was reached. For the treatment, embryos were incubated in 30 µM KN-93/1x YRS at 28 °C, in the dark, until stage 26 was reached. In the control group, embryos were treated with 1.53 % DMSO/1x YRS, in parallel. After the treatment, embryos were washed 3x 5 min with 1x YRS and fixed for immunostaining or further raised to stage 27 for live imaging.

5.2.9 Heat shock induced upregulation of the canonical Wnt signaling pathway

To manipulate the canonical Wnt signaling pathway, plasmids containing a bi-directional heat shock promoter where injected into 1-cell stage medaka embryos. The bi-directional heat shock promoter controls the expression of GFP and a gene of interest, which is able to upregulate the canonical Wnt signaling pathway. Embryos were raised to 6-somite stage and heat shock was performed using a thermal cycler. Prior to the heat shock, embryos expressing GFP already, were excluded from the experiment. The other embryos were individually placed into a PCR tube, containing 50 µl of 1x ERM, and heat shocked according to the protocol described in Table 5.26.

Table 5.26: Heat shock protocol.

Time	Temperature	Repeats
30 sec	4 °C	1x
10 min 10 min	4 °C 39 °C	6x
5 min	32 °C	1x

After the heat shock, embryos were raised under standard conditions until stage 26. To evaluate changes of *zic1* expression after the upregulation of the canonical Wnt signaling pathway, a whole-mount *in situ* hybridization was performed.

5.2.10 Genotyping of medaka embryos

A medaka embryo was transferred into a PCR tube containing 10 µl 1x Alkaline Lysis Solution and smashed using a P-1000 Pipette tip. The sample was incubated at 95 °C for 15 min and cooled down to 4 °C on ice. 10 µl 40 mM Tris-HCl (pH 8.0) was added, and a genotyping PCR was performed. For the PCR 2 µl genomic DNA was used as input for the 20 µl Phusion PCR reaction, which was performed according to manufacturers' instructions. After the PCR, the sample was incubated for 2 min at 95 °C, followed by a ramp down to 25 °C (-1 °C/sec). The PCR product was analyzed by MultiNA electrophoresis.

5.2.11 Genotyping of adult medaka

Adult medaka were anesthetized and the tip of the caudal fin was cut off using a racer plate. The small fin sample was transferred into a PCR tube containing Hatching buffer. Hatching buffer was removed and 10 µl 1x Alkaline Lysis Solution was added to the fin and incubated at 95 °C for 15 min. Sample was cooled down on ice and 10 µl 40 mM Tris-HCl (pH 8.0) was added. The extracted DNA was either stored at 4 °C or directly used as input for a genotyping PCR (1 µl genomic DNA in a 10 µl Phusion PCR reaction). PCR product was analyzed by conventional agarose gel electrophoresis or MultiNA electrophoresis.

5.2.12 RNA extraction from embryonic tails

Prior to the RNA isolation from embryonic tails, tails have to be dissected. For the dissection, dechorionated embryos were kept in 1x YRS on ice. Batches of 5 embryos were transferred into a 40 mm glass dish containing ice-cold 1x PBS. For the dissection 30G 1/2 precision glide needles were used. The yolk sac was poked to release the yolk. The tail

was cut anteriorly from the first somite and carefully detached from the yolk sac. Five tails were pooled and transferred in 1.5 µl into a 1.5 ml tube containing 500 µl ice-cold ISOGEN and stored on ice. Several batches were pooled in one 1.5 ml tube. After completion of one sample (consisting of several batches of 5 embryos), tails were carefully homogenized using a pestle. Additional 500 µl ISOGEN was added to the sample. The sample was kept at -80 °C, for long-term storage.
From here on, all steps were performed under RNase-free conditions. Samples were vortexed and incubated 5 min at RT followed by a 5 min, 12,000 g centrifugation step at 4 °C. Supernatant was transferred into a new 1.5 ml tube and 200 µl Chloroform was added. The sample was vortexed for 15 sec and incubated for 3 min at RT. This was followed by centrifuging the sample for 15 min, 12,000 g at 4 °C. The upper phase was transferred into a new 1.5 ml tube and 500 µl 100 % EtOH was added. The sample was carefully mixed by pipetting up and down and directly transferred into RNeasy Min Elute columns. Columns were centrifuged for 15 sec, 8000 g at 20 °C and the flow-through was discarded. 500 µl of RPE buffer was added to the column followed by a short centrifugation step for 15 sec, 8000 g at 20 °C. The flow-through was discarded and 500 µl 80 % EtOH was added to the column, followed by a 2 min centrifugation at 8000 g and 20 °C. This step was repeated. To dry off residual EtOH, the column was spun 5 min at 15,000 rpm and 20 °C. The column was transferred into a new collection tube. To elute the RNA, 14 µl of nuclease-free water was added onto the membrane of the column. The column was centrifuged for 1 min at 15,000 rpm. The RNA concentration was measured using a NanoDrop and stored at -80 °C.

5.2.13 Fixation of embryos for *in situ* hybridization

Embryos were washed in 1x PTW and fixed in 4 % PFA/1x PTW while slowly rotating at 4 °C, overnight. Fixed embryos were washed 3x with 1x PTW, followed by the removal of the chorion using forceps. Following the dechorionated, embryos were dehydrated in consecutive dilutions of MeOH/1x PTW (25 %, 50 %, 75 %, 100 %) for 5 min and stored in 100% MeOH at -20 °C.

5.2.14 Fixation of embryos for immunohistochemistry

Embryos were dechorionated and fixed in 4 % PFA/1x PBS for 2 h a RT or at 4 °C overnight, while mildly shaking. After fixation, the embryos were washed 3x with 1x PBS and stored at 4 °C for up to one month.

5.2.15 RNA probe synthesis for *in situ* hybridization

6-10 µg of template DNA plasmids were linearized using EcoRI (*wnt1, zic1) or* SacII (*wnt3a, wnt11r)* and run on a 1 % agarose/TAE gel. Template DNA was cut out and purified using the innuPREP PCRpure kit. NTP-Mix was prepared according to Table 5.27.

Table 5.27: rNTP mix composition.

Component	Concentration
100 mM ATP	15.4 mM ATP
100 mM CTP	15.4 mM CTP
100 mM GTP	15.4 mM GTP
100 mM UTP	10.0 mM UTP
Millipore H_2O	ad 100 µl

For the probe transcription either T7 polymerase (*wnt1, zic1*) or Sp6 polymerase (*wnt3a, wnt11r*) was used.
The transcription reaction was set up in the following order (Table5.28) under RNase-free conditions:

Table 5.28: Transcription reaction to transcribe *in situ* hybridization probes.

Component	Volume per reaction
Linearized template	1 µg
100 mM DTT	2 µl
NTP-Mix	1.3 µl
10mM Dig-UTP	0.7 µl
RiboLock	0.5 µl
10x Transcription buffer	2 µl
RNase-free H_2O	Ad 18 µl
RNA-Polymerase (Sp6/T7)	2 µl

The reaction was incubated for 3 h at 37 °C. 1 µl of Turbo DNaseI (2 U/µl) was added to the transcription reaction, followed by a 15 min incubation at 37 °C. The RNA probe was purified using the RNeasy Kit (Qiagen). The probe was eluted twice in 25 µl RNAse-free H_2O, to end up with a final volume of 50 µl RNA. To analyze the quality of the RNA probe generation, 2 µl of RNA were combined with 5 µl 2x RNA loading buffer

(Ambion) and 1 µl RNase-free H_2O. The sample was denatured at 80 °C for 10min and run on a 1 % agarose/TAE gel instantly. If the quality was sufficient, 150 µl of Hybridization Mix was added to the remaining RNA probe, mixed my careful finger tipping, and stored at -20 °C.

5.2.16 Whole-mount *in situ* hybridization

All steps, until the pre-hybridization, were performed mildly shaking at RT, unless stated otherwise.
Fixated embryos were transferred into a 6-well cell culture dish, volumes of solution per well were between 5-7.5 ml. Embryos were rehydrated by 5 min rehydration steps in 75 % MeOH/PTW, 50 % MeOH/PTW, 25 % MeOH/PTW and two 5 min rinses in PTW. Rehydrated embryos were digested in 10 µg/ml Proteinase K according to Table 5.29. The digest was performed without shaking.

Table 5.29: Duration of Proteinase K treatment for different developmental stages.

Embryonic stage	Time of Proteinase K digestion
17-20	5 min
21-24	7 min
25-27	12 min

After the digest, embryos were rinsed twice with freshly prepared 2 mg/ml Glycine and fixed in 4 % PFA/PTW for 20 min. Fixed embryos were washed 5x for 5 min in PTW. Hybridization Mix was warmed to RT. From here on, all steps were performed in a water bath at 65 °C.
Embryos were transferred to 2 ml tubes and pre-hybridized for 2 h in 2 ml Hybridization Mix. RNA probes were diluted in Hybridization Mix (according to Table 5.30). 100 µl of the diluted probes were denatured at 80 °C for 10 min and directly placed on ice.

Table 5.30: Dilution of *in situ* hybridization probes.

RNA probe	Dilution
anti-*wnt1*	1:10
RNA probe	**Dilution**
anti-*wnt3a*	1:20
anti-*wnt11r*	1:5
anti-*zic1*	1:20

Pre-hybridization solution was carefully removed from the embryos and replaced by 100 µl of diluted RNA probes and incubated at 65 °C, overnight. For the following washing steps, all solutions were pre-warmed to 65 °C and washing steps were performed at 65°C. Probe solution was carefully removed and embryos were washed twice for 30 min with 2 ml 50 % Formamide / 2x SSCT. This was followed by two washing steps with 2 ml 2x SSCT for 15 min and two final washing steps with 2 ml 0.2x SSCT for 30 min.
Embryos were blocked with 1-2 ml 5 % Sheep Serum/PTW for 1-2 h at RT, while mildly shaking. After the blocking, embryos were incubated in 400 µl of a 1:2000 dilution of Anti-Digoxigenin-AP Fab fragments/5 % Sheep Serum, overnight at 4 °C while slowly rotating. Embryos were transferred into a 6-well cell culture dish and washed 6x 10 min with PTW at RT, while mildly shaking. For equilibration, embryos were transferred into a 24-well plate and incubated twice for 5 min, gently shaking with 2 ml of freshly made Pre-staining buffer. The equilibration steps were repeated using the Staining buffer. For the detection reaction, the Staining buffer was replaced by 1 ml freshly prepared Staining solution, containing 337.5 µg/ml NBT and 175 µg/ml BCIP. The reaction was incubated up to 48 h in the dark, at RT without shaking. Color development was checked frequently. To stop the reaction, embryos were washed 3x 5 min in PTW and stored in PTW at 4 °C until imaging or vibratome sectioning.

5.2.17Vibratome sectioning

The sample was mounted in a 6-well cell culture plate in 4 % agarose / 1x PBS. After the agarose hardened, the sample was cut out in a square shaped piece and glued onto the vibratome plate (sample facing up). The vibratome chamber was filled with 1x PBS and sections were cut using the following settings:

Table 5.31: Vibratome setting.

Feature	Setting
Frequency	7
Speed	9
Section thickness	40 µm or 200 µm
Section mode	Single

The sections were retrieved with a brush and placed into a 24-well cell culture dish, each well filled with 1 ml 1x PBS. Using forceps, sections were transferred onto a microscope slide, mounted in 60 % Glycerol, covered with a coverslip and sealed with nail polish. Sections were stored at 4 °C.

5.2.18 Whole-mount immunohistochemistry

The immunostaining was performed in 2 ml tubes, volumes used per tube varied between 1.5-1.8 ml. All steps were carried out a RT while gently shaking, unless stated otherwise. Embryos younger than stage 26 were permeabilized with 0.5 % TritonX-100/1x PBS for 1 h. Embryos stage 27 and older were permeabilized for 2 h. After the permeabilization, embryos were rinsed in 1x PBS and blocked with Blocking solution for 2 h, if younger than stage 27, embryos stage 27 and older were blocked for 4 h. The Blocking solution was replaced by 150 µl of Primary antibody respectively diluted in Blocking solution. Samples were incubated at 4 °C overnight and washed with PBSDT 6x for 15 min. A second blocking step was carried out for 4 h. 150 µl of Blocking solution containing the respectively diluted secondary antibodies, DAPI and, depending in the experiment, phalloidin, was added to the samples and incubated overnight at 4 °C. The antibody solution was washed off by six 15 min washing steps with PBSDT. Embryos were transferred in a 4-well or 24-well cell culture dish, rinsed with 1x PBS and stored at 4 °C in 1x PBS.

5.2.19 Imaging

Whole-mount *in situ* hybridizations and sections of *in situ* hybridizations were imaged using the Zeiss Axio imager M1 (Plan-Apochromat lenses: 10x/0.45, 20x/0.8, DCI filter). Whole-mount *in situ* hybridization samples and sections were mounted in 60 % Glycerol on cover slips.
Imaging of immunohistochemistry was performed at the Zeiss LSM 710 confocal microscope system containing an inverted stand and a Zeiss AXIO Observer Z1 (Objective lenses: objective LD LCI Plan-Apochromat 25x/0.8 multi-immersion, objective LD C-Apochromat 40x/1,1 water; laser lines: 405 nm, 488 nm, 561 nm) and a T-PMT detector. Samples were mounted 1 % LMA/1x PBS in a glass bottom dish and oriented in a way that the dorsal side was facing down. The agarose was covered with 1x PBS to avoid drying out during imaging.
After heat shock induction, embryos were imaged using a Nikon SMZ18 stereomicroscope equipped with a Nikon DS-Ri1 camera.
IWR-1 and Azenkenpaulone treatment embryos were imaged using an Leica M165 FC stereomicroscope equipped with a Leica DFC 7000T camera.

5.2.20 *In vivo* imaging of onset of dorsal somite extension

Stage 27 embryos were live imaged to observe protrusion formation of the dorsal somite tip cells at the onset of the dorsal extension of dorsal somites. The onset of somite externsion was imaged in Wt medaka, *Da* mutant and different experimental conditions (Wnt11r morpholino knockdown, Wnt11r Photo-Morpholino knockdown, Wnt11-protein rescue experiment, KN-93 treatment). To inhibit muscle twitching, embryos were

injected with *α-bungarotoxin* mRNA as described in section 5.2.2. Embryos were dechorionated and raised until stage 27. At late stage 27 the yolk movement has stopped. Embryos were mounted in 1 % LMA/1x YRS in a glass bottom dish, and oriented in a way that the dorsal side was facing down. The agarose was covered with 1x YRS. *In vivo* imaging was performed using the 40x objective of the Zeiss LSM 710 confocal microscope. The 10th somite, counted from anterior, was aligned in the center and z-stacks were taken. Z-stacks were analyzed and protrusions were quantified using the software FluoRender. Statistical analysis and the representation of the statistical data was performed in RStudio.

5.2.21 Time-lapse imaging

Transgenic embryos expressing *zic1::GFP* were injected with *α-bungarotoxin* mRNA as described in section 5.2.2 to inhibit muscle twitching. The injected embryos were dechorionated and raised until stage 27. Embryos were mounted in a glass bottom dish in 1 % LMA/1x YRS and oriented with the dorsal side facing down. The embryos were covered with 1x YRS to avoid drying out the sample during imaging. Time-lapse imaging was performed at the Zeiss LSM 710 confocal microscope using the 40x objective. Embryos were aligned with the 15th somite, from anterior, in the center and z-stacks were imaged in a 600 sec interval for 10 – 15 h. Image analysis was performed in FIJI using the "Image Stabilizer" Plugin and the FFT Bandpass filter.

5.2.22 *In vivo* imaging of actin filaments in cell protrusions

During somite extension, the leading edge cells of the dorsal somites form protrusions. These protrusions are lost, once the embryos are fixed. To observe actin filaments within the protrusions, *in vivo* imaging was performed. Wt and *Da* embryos were injected at 1-cell stage (as described in section 5.2.2) with *mmCherry* and *α-bungarotoxin* mRNA and raised until 4-cell stage. At this stage, one cell was injected with *AC-GFP* mRNA and the embryos were raised until stage 27. Embryos were imaged as described in "Live imaging of onset of dorsal somite migration" and image processing was performed using the FluoRender software.

5.2.23 Image processing and statistical analysis

Images were processed using the image processing software Fiji. Statistical analysis and representation of the data was performed using RStudio. In bar plots mean and error limits, defined by the standard deviation, are indicated. In box plots, median, the first and third quantiles are indicated. In the figure legends, the sample size (n) and number of individuals used in the experiments are stated. Statistical significant was determined by un-paired t-tests, a p-value $p < 0.05$ was considered as significant. P-values can be found

in the figure legends. When comparing experimental groups, the allocation was performed randomly and without blinding. All figures and illustrations were done using Adobe Illustrator CS6. Experiments were quantified as stated in Table 5.32:

Table 5.32: Quantification of data presented in the respective figures.

Figure	Data	Quantification in
Figure 2.7	cross sectional area of dorsal somites	3 Y planes, of the 10th somite counted from anterior
Figure 2.8	pH3^{+} cells in the dorsal dermomyotome pH3^{+} cells in the ventral dermomyotome	all Z planes all Z planes
Figure 2.9	distance between myotome tips	3 Y planes, of the 10th somite counted from anterior
Figure 2.10	distance between dorsal somite tip and neural tube height of dorsal somite	3 Y planes, of the 5th somite counted from anterior 3 Y planes, of the 5th somite counted from anterior
Figure 2.11	number of protrusions	protrusions formed by somites 8-12, counted from the anterior
Figure 2.14	cell junctions/membrane	all cell membranes in contact to neighbouring cells
Figure 2.17	pH3^{+} cells in the dorsal dermomyotome	all Z planes
Figure 2.18	number of protrusions	protrusions formed by somites 8-12, counted from the anterior
Figure 2.19	number of protrusions	protrusions formed by somites 9-11, counted from the anterior
Figure 2.20	pH3^{+} cells in the dorsal dermomyotome number of protrusions	all Z planes protrusions formed by somites 8-12, counted from the anterior
Figure 6.1	quantification of phenotypes	whole embryos

5.2.24Transmission Electron Microscopy (TEM)

Fixation of samples was performed according to company's (Tokai-ema.com) instructions. Embryos were dechorionated and raised util stage 27 was reached. The yolk sac of the embryos was poked to release the yolk and embryos were transferred into a drop of fixation solution. Tails were cut off just before the 10th somite and transferred into a tube

containing fixation solution. Samples were shipped to the TEM company where electron microscopy was performed on cryosections of the tail.
TEM images were analyzed using the Fiji image processing software and Adobe Illustrator.

5.2.25 Crosslinking of embryos for Chromatin immunoprecipitation

Prior to the crosslinking Solution A was prepared and pre-cooled on ice. Unless stated otherwise, all steps were performed on ice. Dechorionated embryos were carefully transferred into a 3 cm dish containing ice-cold 1x PBS. 500 µl of Solution A was added into a 2 ml tube and embryos were transferred in minimal volume, using a 1.2 ml tip into the 2ml tube. Embryos were homogenized using the same 1.2 ml tip by pipetting up and down. Homogenized embryos were centrifuged for 10 min, 500 g at 4 °C. The supernatant was removed carefully and 700 µl of Solution A was added to the pellet. To dissolve the pellet, the sample was briefly vortexed at half speed and spun down. For the crosslinking, 20 µl of 36.5 % Formaldehyde was added followed by a brief vortex at half speed and a short spin down of the sample. The reaction was incubated for exactly 8 min at RT. To quench the Formaldehyde, 40 µl 2.5 mM Glycine was added to the sample. The sample was briefly vortexed at half speed, shortly spun down and incubated for 5 min on ice. After the incubation, the sample was centrifuged for 10 min, 500 g at 4 °C. The supernatant was carefully removed and 500 µl Solution A was added. The sample was resuspended by briefly vortexing at half speed followed by a 10 min centrifugation at 500 g and 4 °C. This washing step was repeated. After the washing step, the supernatant was removed completely and the dry cells were stored at -80 °C.

5.2.26 Chromatin immunoprecipitation (ChIP)

For the preparation of antibody-bead complexes 100 µl of protein A magnetic beads were transferred into a 1.5 ml tube and placed on a magnetic stand. The supernatant was removed and 250 µl of RIPA buffer was added. The beads were vortexed, spun down and placed on the magnetic stand. The supernatant was removed and 200µl of RIPA buffer was added, the sample was vortexed, spun down and again placed on the magnetic stand. This step was repeated. Finally, 250 µl of RIPA buffer and 10 µg of the antibodies was added to the beads. The beads were incubated overnight at 4 °C while slowly rotating.
For the chromatin preparation Protease inhibitor (final concentration 1x), PMSF (final concentration 1 mM) and Na-butylate (final concentration 20 mM) were added to the Lysis buffer and the RIPA buffer. RIPA buffer was pre-cooled on ice. Crosslinked embryos were suspended in 130 µl Lysis buffer and sonicated using the S220 Focused-ultrasonicator (Covaris). Following settings were used for the sonication:

Table 5.33: Sonication settings.

Feature	Setting
Peak incident power	105 watts
Duty factor	4.0 %
Cycles/burst	200
Duration	720 sec

The sonicated sample was transferred into a 1.5 ml tube and centrifuged for 10 min, 12,000 g at 4 °C. The supernatant was transferred into a 2.0 ml tube and 5 µl of the fragmented chromatin was kept at 4 °C until the fragmentation check. The supernatant was diluted 1:10 with RIPA buffer. A 100 µl aliquot was saved as input and kept at 4 °C. The prepared antibody bound magnetic beads were spun down and placed on a magnetic stand. The supernatant of the beads was removed and the fragmented chromatin was added. The sample was incubated at 4 °C, overnight while slowly rotating.
To check the efficiency of chromatin fragmentation, a fragmentation check was performed. To the 5 µl aliquot 95 µl MilliQ H_2O and 1 µl 10 mg/l RNase were added. The sample was incubated for 1 h at 37 °C. After the incubation, 4 µl 5 M NaCl, 2 µl 0.5 M EDTA, 4 µl 1 M Tris-HCl pH 8.0 and 1 µl 20 mg/ml Proteinase K was added. The sample was incubated at 55 °C for 30 min. 110 µl Phenol/Chloroform was added after the incubation, and the sample was vortexed and centrifuged for 5 min at 12,000rpm. The upper layer was transferred into a new tube and 1 µl Ethatinmate, 11 µl NaOAc and 275 µl 100 % EtOH was added. The sample was incubated for 15 min at -20 °C, followed by a centrifugation for 15 min at 15,000 rpm and 4 °C. To wash the pellet, the supernatant was removed and 500 µl 70 % EtOH was added. The sample was centrifuged for 5 min at 15,000 rpm at 4 °C. The supernatant was removed and the pellet was air-dried. The pellet was dissolved in 10 µl H_2O. To check the fragmentation efficiency, an agarose gel electrophoresis was performed, loading 1 µl and 5 µl of the prepared DNA. The expected fragment size should be around 100-700 bp, with an increased intensity around 300-400 bp. If the fragmentation worked well, the ChIP was continued.
After the overnight incubation, the ChIP sample was placed onto a magnetic stand and the supernatant was removed. 1 ml of ice-cold RIPA buffer was added and the sample was mixed by gentle inversion of the tube. The sample was rotated for 4 min at 4 °C and, after placing the sample on a magnetic stand, the supernatant was removed. This washing step was repeated, twice. After the washing, 1 ml ice-cold TE was added to the sample. The sample was rotated tor 4 min at 4 °C, placed on a magnetic stand and the supernatant was removed. 200 µl of Lysis buffer and 13 µl of 5 M NaCL was added to the sample. To the input, 100 µl of Lysis buffer and 13 µl 5 M NACl were added. Both, sample and

input, were incubated at 65 °C, shaking at 800 rpm, overnight. From here on ChIP sample and input are processed in parallel and will be referred to as "the samples". The samples were spun down for 1 min at 14,000 rpm and the supernatant was transferred into new 1.5 ml tubes. 200 µl TE and 8µl 10 mg/l RNase were added and the samples were incubated at 37 °C for 2 h. 4 µl 20 mg/ml Proteinase K was added to the samples, followed by an incubation at 55 °C for 2 h. 400 µl Phenol/Chloroform was added, the samples were vortexed and centrifuged for 10 min at 14,000 rpm. The upper layers were transferred into fresh 1.5 ml tubes. 1 µl Ethachinmate, 16 µl 5 M NaCl and 1 ml 100 % EtOH were added. The samples were incubated at -80 °C for 2 h. This was followed by a centrifugation for 15 min, 15,000 rpm at 4 °C. The supernatant was removed and 1 ml 70 % EtOH was added. The samples were centrifuged for 5 min at 15,000 rpm and 4 °C. The supernatant was removed and the pellets were air-dried. The pellets were dissolved in 40 µl H2O and stored at -20 °C. Concentration of the samples were determined using a Qubit fluorometer. ChIP samples were either analyzed by qPCR (1/25 of the Input is used as standard) or prepared for next generation sequencing.

5.2.27 ChIP-seq library construction

For the library construction, the KAPA Hyper Prep Kit was used. Libraries were constructed according to manufacturer's instruction. 1 ng of ChIP sample and input was used. Concentration of the adapters was 300 nM. To amplify the library, 18 cycles were run. Concentration of the libraries were determined using a Qubit fluorometer. For the quality check an automated electrophoresis was run using a Bioanalyzer and the Bioanalysis High Sensitivity DNA Analysis Kit.

5.2.28 Sample preparation and sequencing of the ChIP

Libraries of the ChIP sample and the Input were diluted to 2 nmol/l. 60 µl of the sample and 40 µl of the input were combined in a 1.5 ml tube for sequencing. Sequencing was performed using a HiSeq1500 (Illumina). The sequencing was done by 50-base single-end sequencing.

5.2.29 Alignment of ChIP-seq data and analysis

Alignment was performed as previously described in (Nakamura et al., 2014). First, reads with low quality (reads containing 5 and more undetectable bases in the 50-base long reads) were removed. Alignment was performed using the Burrows-Wheeler Aligner mapping software, only allowing less than three mismatches and no gaps. The data was represented using the UCSC genome browser and mapped to the *Oryzias latipes* genome assembly 1.0 (Kasahara et al., 2007).

5.2.30 Polymerase chain reaction (PCR)

PCR reactions were carried out according Table 5.34.

Table 5.34: PCR reaction setup.

Component	Volume per 50 µl reaction	Final concentration
5x Q5 Reaction buffer	10 µl	1x
2.5 mM dNTPs	4 µl	200 µM
10 µM Forward primer	1 µl	0.2 µM
10 µM Reverse primer	1 µl	0.2 µM
Template DNA	variable	<1000ng
Q5 High-Fidelity DNA Polymerase	0.5 µl	0.02 U/µl
MilliQ H_2O	ad 50 µl	
5x PrimeSTAR GXL Buffer	10 µl	1x
2.5 mM dNTPs	4 µl	200µM
10 µM Forward primer	1.5 µl	0.3 µM
10 µM Reverse primer	1.5 µl	0.3 µM
Template DNA	variable	<750 ng
PrimeSTAR GXL DNA Polymerase	1 µl	1.25 U/50 µl
MilliQ H_2O	ad 50 µl	
10x Ex Taq Buffer	5 µl	1x
2.5 mM dNTPs	4 µl	200 µM
10 µM Forward primer	4 µl	0.8 µM
10 µM Reverse primer	4 µl	0.8 µM
Template DNA	variable	<500 ng
TaKaRa Ex Taq	0.25 µl	1.25 U/µl
MilliQ H_2O	ad 50 µl	
5x Phusion HF Buffer	10 µl	1x
2.5 mM dNTPs	4 µl	200 µM
10 µM Forward primer	2.5 µl	5 µM
10 µM Reverse primer	2.5 µl	5 µM

Component	Volume per 50 µl reaction	Final concentration
Template DNA	variable	<250 ng
Phusion DNA Polymerase	0.5 µl	1.0 U/50 µl
MilliQ H_2O	ad 50 µl	

PCR reactions were performed according to manufacturers' instructions. To calculate the annealing temperature for a PCR using the Q5 polymerase, the Tm Calculator from NEB was used (http://tmcalculator.neb.com/#!/main, v1.12.0).

5.2.31 Colony PCR

For each colony, a 50 µl Ex Taq PCR reaction was set up in a PCR tube. A single colony was picked, using a tooth pick, and dipped several times into the PCR reaction mix. Prior to the amplification reaction, samples were incubated for 1 min at 94 °C. The PCR was run according to manufacturers' protocol and the PCR product was investigated by gel electrophoresis.

5.2.32 Reverse transcription PCR (RT-qPCR)

RT-PCR was performed with the Stratagene MX3000P system using the THUNDERBIRD SYBR qPCR Mix. For the reaction standard, 4 consecutive 5-fold dilutions were made. RT-PCR reactions were assembled on ice. For each reaction, one technical replicate was performed per run.

Table 5.35: Setup of RT-PCR reaction.

Component	V per 10µl reaction	Final concentration
2x THUNDERBIRD SYBR qPCR Mix	5.0 µl	1x
10µM Forward primer	0.3 µl	0.3 µM
10µM Reverse primer	0.3 µl	0.3 µM
cDNA	1 µl	10 %
MilliQ H_2O	3.4 µl	

Of each reaction, 10 µl were transferred into a RT-PCR plate at RT. The plate was sealed with PCR plate seal, spun down and assembled into the RT-PCR machine. The following "Fast 2 Step" program was run.

Table 5.36: Fast 2 Step qPCR program.

Segment	Number of cycles	Time	Temperature
1	1	10 min	50 °C
2	1	1 min	95 °C
3	40	15 sec	95 °C
		30 sec	60 °C
4	1	1 min	95 °C
		30 sec	55 °C
		30 sec	95 °C

Relative quantities were normalized against *gapdh* expression and analyzed using excel and RStudio.

5.2.33 Oligonucleotide annealing

Annealing reaction was performed in PCR tubes. 1 µl of each oligonucleotide (100 µM) were combined with 18 µl MilliQ H_2O and 20 µl Oligo annealing buffer. The annealing reaction was performed in a thermocycler. The reaction was incubated for 10 min at 95 °C followed by a ramp down to 70 °C (-0.1 °C/ sec), and a 10 min incubation at 70 °C. From 70 °C, temperature was ramped down to 65 °C (-0.1 °C/sec), where the sample was incubated for 10 min. Again, temperature was ramped down to 60 °C (-0.1 °C/sec) followed by a 10 min incubation at 60 °C and a final ramp down to 10 °C (-0.1 °C/sec). Prior to the ligation of the annealed oligonucleotides into a DR274 vector, linearized with BsaI, the annealing reaction was diluted 1:33 (0.075 pmol/µl). The ligation reaction was set up as described in Table 5.37 and incubated for 10 min at RT.

Table 5.37: Setup of ligation reaction after oligonucleotide annealing.

Component	Volume
MilliQ H_2O	5 µl
10x Ligase buffer	1 µl
PEG 4000	1 µl
DR274 (40 ng/µl) linearized with BsaI	1 µl
Annealed oligonucleotides (0.075 pmol/µl)	1 µl
T4 Ligase (5 U/µl)	1 µl

5.2.34 Agarose gel electrophoresis

Gel electrophoresis was used to separate DNA fragments after a restriction enzyme digest, after PCR reactions or as test gel for quality control. DNA samples were combined with 6x DNA Loading dye and loaded into 1-2% agarose/1x TAE gels or 0.8-2% agarose/0.5xTAE gels. Gel chambers were filled with the respective buffer (1x TAE or 0.5x TAE).
To the agarose/1x TAE gels, 100-130 V were applied and the gels were run for 30-45 min. The gels were stained by a 15-40 min incubation in 2 µg/ml Ethidium bromide/1x TAE. The stained gels were imaged in a gel documentation station using UV-light (λ = 254 nm).
Agarose gel electrophoresis for agarose/0.5x TAE gels was carried out at 100 V for 30-45 min. Gels were stained by incubation in 1:10,000 Midori GreenXtra/0.5x TAE for 10-40 min. Geles were imaged in a gel documentation station using the Blue/Green LED technology (λ = 500 nm).

5.2.35 Gel extraction

Using gel electrophoresis, DNA was separated by size and the band of interested was cut out using a scalpel. innuPREP PCRpure Kit or the Wizard SV Gel and PCR Clean-Up System were used to extract the DNA from the agarose.
For the innuPREP PCRpure Kit, manufactures' instructions were followed and the DNA was eluted in 15-30 µl H2O.
The Wizard SV Gel and PCR Clean-Up System was used according to manufactures' protocol and DNA was eluted in 30-50 µl H2O. For long-term storage, DNA was stored at -20 °C.

5.2.36 MultiNA electrophoresis

This microchip electrophoresis system was used to run numerous samples in parallel. Electrophoresis was performed after manufacturers' instructions. Depending on the size of PCR products, the DNA-500 kit (25-500 bp) or the DNA-1000 kit (100-1,000 bp) was used. Prior to the gel electrophorese, PCR products had to be diluted by five-fold.

5.2.37 Bioanalyzer electrophoresis

Quality control of libraries, generated for next generation sequencing, was done using the 2100 Bioanalyzer system. Electrophoresis was performed using the High Sensitivity DNA kit according to manufacturers' protocol.

5.2.38 DNA restriction

For a restriction enzyme digest, 1-10 µl of DNA was combined with 0.5-1 µl of enzyme and 1x of the respective restriction enzyme buffer. Digest was incubated for at least 1 h at 37 °C.
Test digests, after plasmid preparations, were carried out with either 5 µl of plasmid preparation and 0.2 µl of restriction enzyme or 500 ng of plasmids and 0.5 µl of the restriction enzyme. Test digest were incubated for 30-40 min at 37 °C.

5.2.39 A-tailing of PCR products

To ligate PCR products into TA cloning vectors like the pGEM®-T Easy vector, an adenosine tail has to be added to the purified PCR product. PCR product was cleaned up using the innuPREP PCRpure Kit. The A-tailing reaction was set up as described in Table 5.38 and incubated for 25 min at 72 °C.

Table 5.38: Set up of A-tailing reaction.

Component	Volume
Cleaned up PCR product	7.25 µl
10x PolBuffer B	1 µl
2 mM dATP	1 µl
Taq Roboklon 5 U/µl	0.25 µl

Following manufacturers' instructions, the A-tailed PCR product was directly used for TA-cloning using the pGEM®-T Easy Vector System.

5.2.40 DNA ligation

Ligation reaction was performed in a PCR tube. A molar ratio of 1:4 Vector:Insert was used for the ligation. 2 µl Ligation High Ver.2 ligation mix was added to the vector and insert. H_2O was added to the reaction to reach a final volume of 6 µl. The reaction was mixed by pipetting and incubated for 30 min at 16 °C.

5.2.41 Transformation of chemically competent cells

In this thesis, two different cells (MachT1 and DH5α) were used for transformation.
For the transformation using MachT1 cells, 50 µl Mach1™ T1 Phage-resistant chemically competent *E. coli* cells were thawed on ice. 5 µl of DNA ligation was added to the cells and mixed by gentle steering with the pipette tip. A heat shock was performed in a thermal block at 42 °C for 45 sec, cells were subsequently placed on ice and incubated for 2

min. 300 µl of TB buffer was added to the cells, followed by a 45 min incubation at 37 °C and 200 rpm. Cells were plated on pre-warmed LB agar plates containing the respective selection antibiotic. For blue-white selection, 40 µl X-Gal (20 µg/ml) was spread on the pre-warmed LB plates, prior to cell plating.
For the transformation using DH5α cells, a 50 µl aliquot of cells was thawed on ice. Before the cells were thawed completely, 0.5-2 µl of DNA ligation was added to the cells and incubated for 5 min on ice. Heat shock was performed in a water bath at 42 °C for 30 sec. After the heat shock, cells were directly incubated for 2 min on ice. 300 µl of SOC was added to the cells and the cells were incubated for 20-30 min, 37 °C and 200 rpm (the incubation at 37 °C was neglected if the selection antibody was Ampicillin). Cells were spread on pre-warmed LB plates containing the respective selection antibiotic.
For both protocols, plates were incubated at 37 °C, overnight. Single colonies were picked and used for plasmid preparation.

5.2.42 Plasmid preparation

For small-scale plasmid preparation, bacteria from a single colony were inoculated in 3 ml LB medium containing the respective selection antibiotic. The cells were incubated overnight a 37 °C and 200 rpm. Cells were spun down for 1 min at 14,000 rpm and the supernatant was removed. The pellet was resuspended in 200 µl ice-cold P1 buffer. 200 µl of P2 buffer were added and the sample was mixed by inverting the tube 4-6x. 200 µl ice-cold P3 buffer was added to the sample, and again mixed by 4-6 inversions of the tube followed by a 15 min centrifugation step at 14,000 rpm and 10 °C. The supernatant was transferred into a new 1.5 ml tube and 500 µl Isopropanol was added and mixed by vigorously shaking. The sample was centrifuged for 15 min at 14,000 rpm and 10 °C. Supernatant was removed and the pellet was washed with 500 µl 70 % EtOH and a 5 min centrifugation step at 14,000 rpm and RT. The pellet was air-dried and resuspended in 40-50 µl H_2O, depending on the pellet size.
For plasmid preparation using the QIAprep Spin Miniprep Kit, a single colony was picked and inoculated in 2ml LB medium, containing the respective selection antibiotic. The bacteria culture was incubated at 37° C, 200 rpm, overnight. To harvest the cells, the overnight culture was centrifuged at 13,000 rpm for 1 min. The plasmid DNA purification was performed according to manufacturer's protocol. DNA was eluted in 50 µl TE buffer.For long-term storage, the purified plasmids were kept at -20 °C.

5.2.43 Preparation of sgRNAs

sgRNAs were designed using CCTop (Stemmer et al., 2015), and sgRNA templates were cloned as described in (Stemmer et al., 2015). To generate the sgRNA template for the *in vitro* transcription, 10 µg of template plasmid were digested with DraI, overnight at 37°C.

Fragments of the digest were separated by gel electrophoresis and the 300 bp band was extracted and purified using the innuPREP PCRpure Kit. DNA was eluted in 15 µl RNase-free H_2O. sgRNAs were transcribed using the MEGAscript™ T7 Transcription Kit, following manufacturer's instructions. 200 ng of template DNA were transcribed.
RNA was cleaned up using the RNeasy Mini Kit and following manufacturer's instructions. RNA was eluted in 25-30 µl RNase-free H_2O. Quality of sgRNA generation was controlled by running a test gel and concentration was determined using a micro-volume spectrophotometer. As working concentration, sgRNAs were diluted to 100-150 ng/µl. sgRNAs were stored at -80 °C.

5.2.44 Transcription of mRNA

Plasmids were linearized using EcoRV (*AC-GFP, mmCherry*) or AvaI (*α-bungarotoxin*) and transcription was performed using the mMESSAGE mMACHINE Sp6 Transcription Kit, following manufacturer's instructions.

5.2.45 cDNA preparation

To reverse transcribe RNA into cDNA the Super Script III Kit from Invitrogen was used. Assembly of the reaction was performed under RNase-free conditions, in a PCR tube, on ice. To reverse transcribe 300 ng - 2 µg of RNA, 1 µl of 50 mM OligodT20 Primer, 1 µl of annealing buffer were added to the RNA topped up to 8 µl with nuclease-free H_2O. The reaction was incubated for 5 min at 65 °C in a thermocycler and immediately placed on ice for at least 1 min. 10 µl 2x 1st Strand Reaction Mix and 2 µl Super Scripe III/RNase OUT Enzyme Mix were added to the reaction. The reaction was vortex and spun down, followed by an incubation for 50 min at 50 °C and a heat inactivation at 85 °C for 5 min. After the heat inactivation, the reaction was placed on ice. For long time storage, the cDNA was kept at -20°C.

6 Additional work

In this section I will present other work which is not directly related to the stated aim of this thesis. The project idea was brainstormed together with Thomas Thumberger. All experiments were performed and analyzed by me.

6.1 Phenocopying the *Da* mutant by manipulation of the somitic enhancer of *zic1/zic4* using an insulator element

As described previously, the *Da* mutant is an enhancer mutant (Moriyama et al., 2012; Ohtsuka et al., 2004). The somitic enhancer of *zic1/zic4* is disrupted by the insertion of a large transposon ("*Teratorn*", ca. 180kb (Inoue et al., 2017; Moriyama et al., 2012)) which is hypothesized to alter the transcriptional landscape. This results in the great reduction of the expression levels of *zic1/zic4* in the dorsal somites, and ultimately leading to the *Da* phenotype. We wondered if we could phenocopying the *Da* mutant by inserting a transcriptional terminator element at the transposon insertion site in Wt medaka. I used an transcriptional terminator derived from the ocean pout's (*Zoarces americanus*) antifreeze gene. This putative border element consists of a strong polyadenylation signal. In previous studies, this terminator had been used in genetic constructs to efficiently terminate transcription (Clark et al., 2011; Gibbs and Schmale, 2000). We were wondering if this strong terminator could act similar to an insulator, disrupting the chromosomal architecture and altering the transcriptional regulation of *zic1/zic4*. Furthermore we were curious if the regulatory activity of the somitic enhancer is disturbed by the enormous disruption due to the transposon insertion or because of the interference with an unknown regulatory motive, important for the enhancer's activity. To analysis this, I alter the genetic sequence by producing INDELs (insertions or deletions) using the CRISPR/Cas9 system.

6.1.1 Manipulation of the transposon insertion site can lead to altered *zic1* expression pattern in the dorsal somites

To manipulate the transposon insertion site, I performed targeted mutagenesis using the CRISPR/Cas9 system (Ansai and Kinoshita, 2014). I designed sgRNAs (with the help of Thomas Thumberger) just adjacent to the transposon insertion site (closest PAM to the

transposon insertion locus). The sgRNAs will guide the Cas9 protein to the target site, where the endonuclease introduces double strand breaks resulting in INDELs. To mimic transposon insertion, I co-injected the sgRNAs with Ocean Pout terminator (OPT) fragments, expecting the OPT to integrate at the transposon insertion site. I wanted to analyze whether sequence manipulation by INDELs or the insertion of an transcriptional terminator element are able to change the expression pattern of *zic1* in the dorsal somites. As a control experiment, I injected embryos with sgRNAs targeting the *oculocutaneous albinism 2* (*oca2*) locus, leading to a loss of pigmentation (Lischik et al., 2019) (Figure 6.1A, B, C). Alterations of *zic1* expression was analyzed by performing whole-mount *in situ* hybridization of stage 26 embryos after injection (Figure 6.1 A'-C").

All of the embryos injected with Cas9 mRNA and *oca2* sgRNAs showed no changes in *zic1* expression pattern (Figure 6.1A' + D). 45.5% of embryos injected with Cas9 mRNA and sgRNAs targeting *oca2* and the transposon insertion site (EnhD, short for "Enhancer D", the enhancer in which the transposon is inserted (Moriyama et al., 2012)) showed a change in *zic1* expression pattern (Figure 6.1B" + D) and even 57.1 % of embryos injected with Cas9 mRNA, sgRNAs against *oca2* locus, the transposon insertion locus and OPT fragment showed an altered *zic1* expression pattern (Figure 6.1C" + D). Alteration in expression pattern includes to various degrees loss of *zic1* expression in the dorsal somites (Figure 6.1B" + C", arrow heads), neural tube, neural tissues and the brain. Some embryos, showed severe mall formations including deformed heads, no head or no head and no tail (data not shown). These severe developmental mal formations occurred more often in embryos injected with sgRNAs targeting the transposon insertion site and the OPT fragment, compared to embryos only injected with sgRNAs against the transposon insertion locus (control embryos, injected with sgRNAs against *oca2* only, never showed mall formations). Embryos with mall formations were not included in the analysis in Figure 6.1.

Taken together, genetic manipulation of the somitic enhancer of *zic1/zic4* can lead to the loss of *zic1* expression in the dorsal somites.

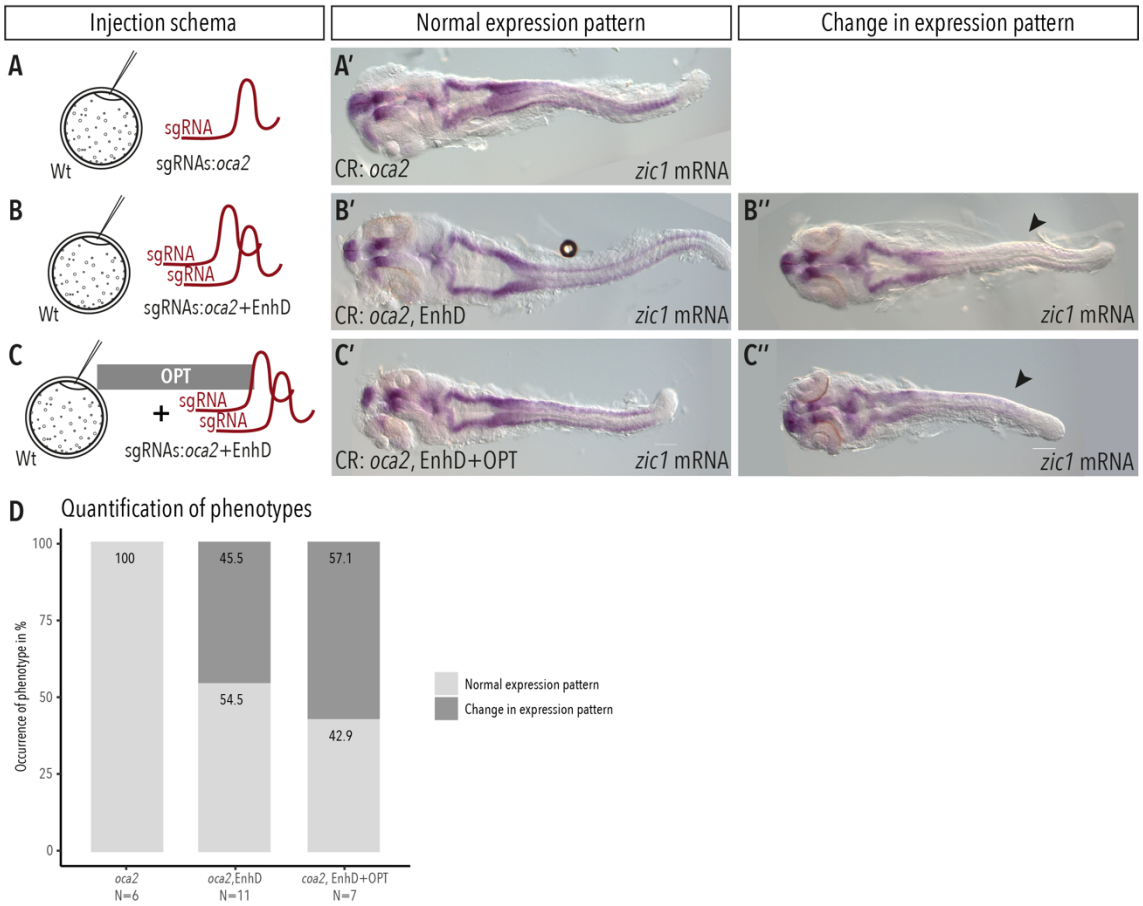

Figure 6.1: Manipulation of transposon insertion locus can lead to altered *zic1* expression pattern.
(A, B, C) Schematic representation of experimental approaches. (A) Control injection: sgRNAs targeting *oca2* are injected. (B) sgRNAs targeting *oca2* and the transposon insertion locus are injected (EnhD). (C) sgRNAs targeting *oca2*, the transposon insertion locus and ocean pout terminator fragments (OPT) are injected. (A'-D") Dorsal view of ISH against *zic1*. Manipulation of transposon insertion locus can lead to altered *zic1* expression pattern in stage 26 embryos. Arrow heads indicates loss of *zic1* expression in the dorsal somites. (A') Embryos injected with sgRNAs described in A. (B-B") Embryos injected with sgRNAs described in B. (C-C") Embryos injected with mix described in C. (D) Quantification of abnormal phenotypes after manipulation of transposon insertion locus. All embryos (N=6) injected with control mix (A) show normal *zic1* expression patter. 6 (54.5 %) of the embryos injected with mix B show normal *zic1* expression pattern, 5 embryos (45.5 %) show altered *zic1* expression pattern. Of the embryos injected with mix C, 3 embryos (42.9 %) showed normal *zic1* expression pattern, 4 embryos (57.1 %) show changes in *zic1* expression pattern. Scale bar = 100 µm.

6.1.2 Traits of the *Da* phenotype can be observed in the injected generation

To further analyze if INDELs or the insertion of the OPT fragment into the transposon insertion locus can phenocopy the *Da* mutant, I raised embryos injected with sgRNAs targeting the transposon insertion site as well as embryos injected with the sgRNAs plus the OPT fragment, to adult hood. Strikingly, one of the embryos injected with the sgRNAs and the OPT, showed traits of the *Da* mutant phenotype in adulthood (Figure 6.2C). In this fish, sparse silver pigments were observed on the dorsal site (Figure 6.2C, arrow head), which are in Wt only found on the belly (ventral side). Furthermore, the body and fin morphology of this fish looks like an intermediate between Wt medaka and the *Da* mutant, resembling the morphology of heterozygous *Da* mutants.
This observation further suggest that phenocopying of the *Da* phenotype might be possible by the manipulation the transposon insertion locus. What kind of manipulation and how the transcription is altered has to be further observed.

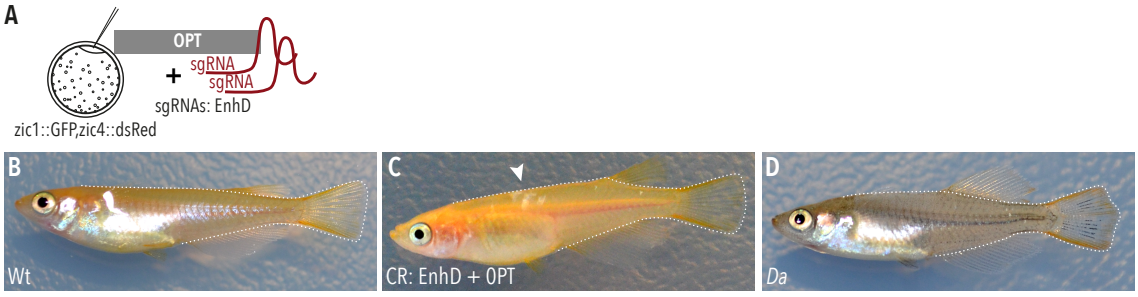

Figure 6.2: Traits of *Da* phenotype can be observed in the injected generation.
(A) Schematic representation of injection Mix. sgRNAs against the transposon insertion site (EnhD) and OPT fragments are injected. (B-D) Lateral view of adult medaka. Dotted lines outline body shapes. (B) Wt medaka. (C) Medaka injected with injection mix described in A. Arrow head points to silver pigments usually found on the belly, only. The body shape resembles the body shape of heterozygous *Da* mutants (n = 1). (D) *Da* mutant.

6.1.3 Transgenic lines containing a 35 bp or a 346 bp deletion around the transposon insertion site were not able to phenocopy the *Da* mutant

Previously described injections using sgRNAs adjacent the transposon insertion site (Figure 6.3A') generated two transgenic lines from two different founder fish. PCR analysis of genomic DNA from Wt medaka, homozygous and heterozygous crispant mutants showed an approximately 30 bp deletion in one line (Figure 6.3B) and an approximately 300 bp deletion in the other mutant line (Figure 6.3C). Transcriptional analysis revealed that the first line contains a 35 bp deletion, 9 bp upstream of the transposon insertion site, this line was named *EnhDΔ35bp* (Figure 6.3D). The second line contains a 346 pb deletion, 40 bp upstream of the transposon insertion locus. This line was named *EnhDΔ346bp* (Figure 6.3D).

Homozygous mutants of both lines did not show any trait of the *Da* mutant phenotype. This excludes that small/medium deletions in proximity of the transposon insertion site influence the regulatory activity of the somitic enhancer of *zic1/zic4*. It would be interesting to observe, if the expression level and pattern of *zic1/zic4* are altered in the created mutant lines.

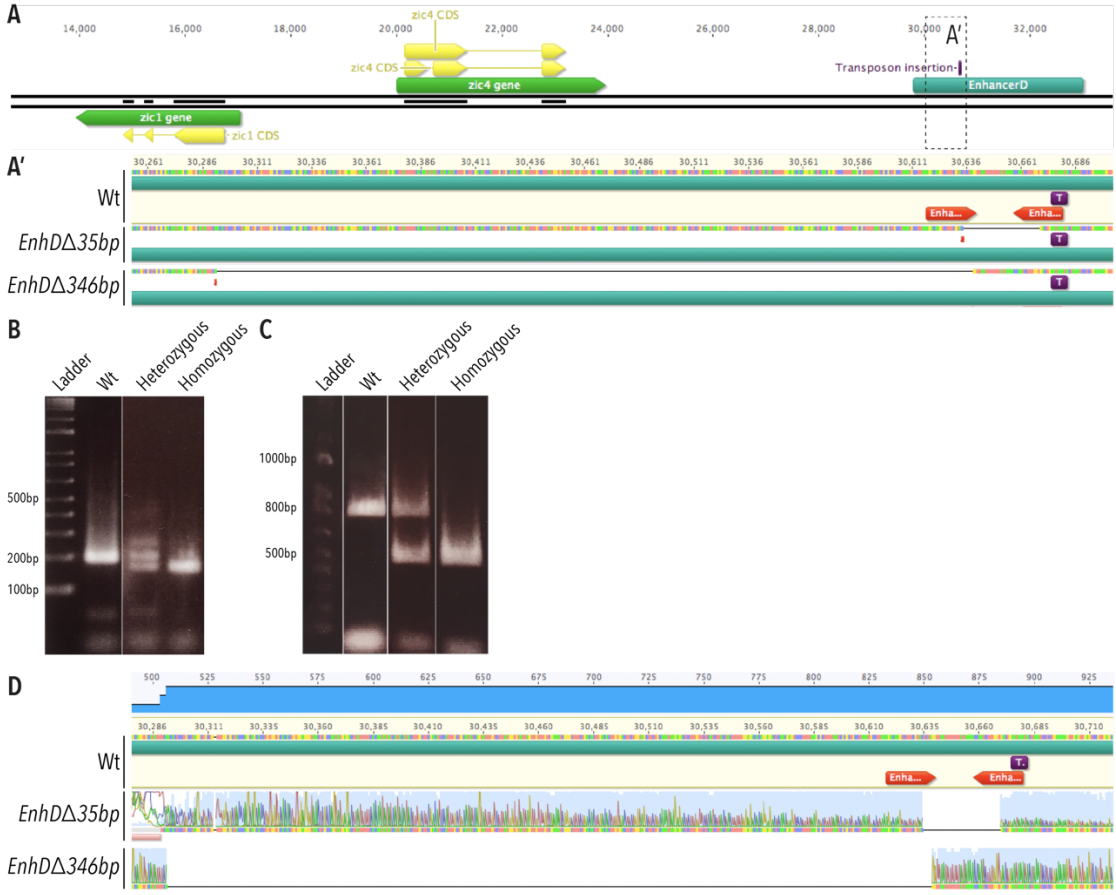

Figure 6.3: Manipulation of transposon insertion site by two sgRNAs flanking the locus, generated two transgenic line containing a 35bp deletion and a 346bp deletion.

(A) Genomic *zic1/zic4* locus in Wt fish. The transposon insertion site (purple) is downstream of *zic4* in a putative somite enhancer "Enhancer D" of *zic1/zic4.* (A') Zoom in at transposon insertion site. sgRNAs are indicated in red. Black lines show the 35bp and 346bp deletions, respectively. (B) Amplification of genomic DNA of Wt, *EnhDΔ35bp*$^{+/-}$ and *EnhDΔ35bp*$^{-/-}$ fish. *EnhDΔ35bp*$^{-/-}$ mutants show a deletion of around 30 bp in the Enhancer D mutant allele. (C) Genomic DNA amplification of Wt, *EnhDΔ346bp*$^{+/-}$ and *EnhDΔ346bp*$^{-/-}$ mutants. Homozygous EnhDΔ346bp mutants show approximal 300 bp deletion around the transposon insertion site. (D) Mutant alleles described in B and C were confirmed by sequencing.

6.1.4 Insertion of OPT fragments around the transposon insertion site creates *Da-like* mutants

Co-injections of the sgRNAs targeting the transposon insertion site with OPT fragments lead to the generation of mutant fish phenocopying the *Da* mutant. These mutants were named "*Da-like*" (Figure 6.4B). The *Da-like* fish show the same body and fin morphology

as well as the alteration in pigmentation (silver belly pigments found on the back side) as the *Da* mutant (Figure 6.4A-B). PCR amplification of gnomic DNA was used to confirm that at least one OPT element is inserted in the somitic enhancer of *zic1/zic4*. To amplify the Wt locus, primers were designed spanning the transposon insertion site, amplifying a 828bp fragment (Figure 6.4C). Since it is not possible to amplify the OPT, I used primers binding to the 5' and 3' end of the OPT and facing outwards. It was possible to amplify fragments using the OPT primers and the primers spanning the locus (Figure 6.4C'-C"). This verifies that at least one OPT fragment is inserted around the transposon insertion site. To investigate the number of OPT fragments inserted in this locus in the *Da-like* mutants, southern blots could be performed.

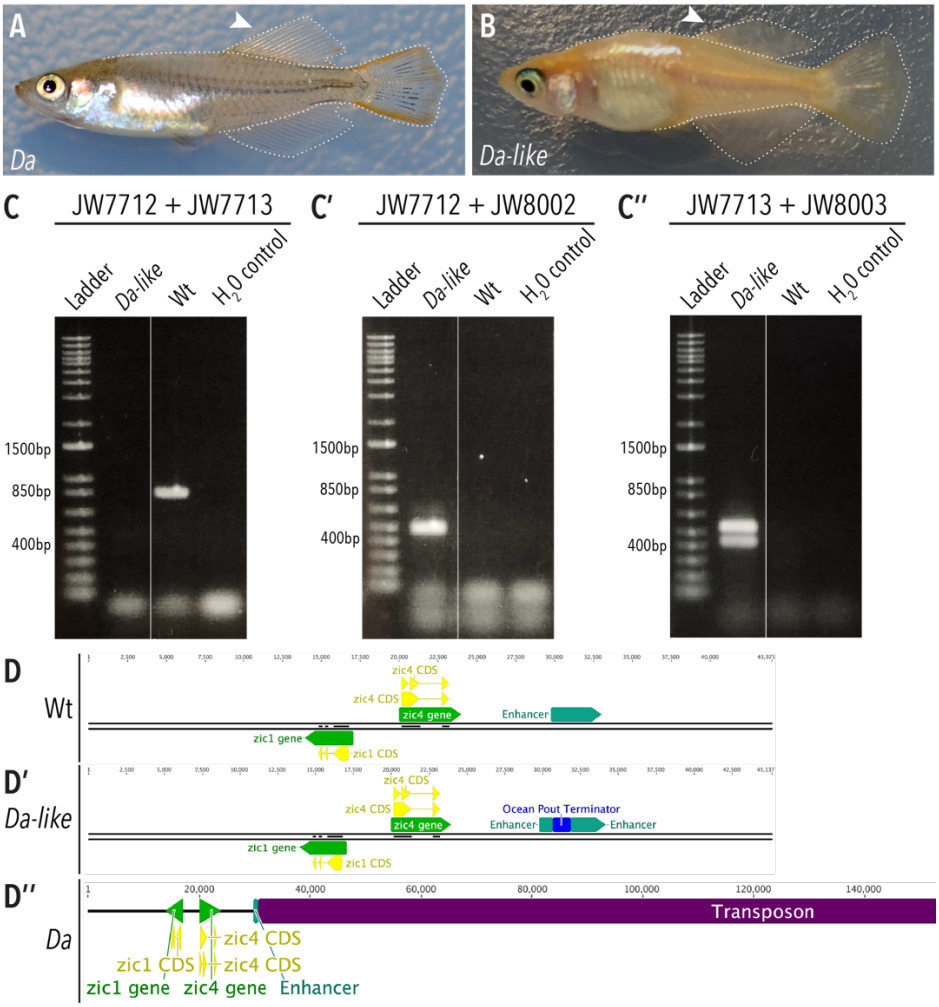

Figure 6.4: Insertion of OPT around the transposon insertion site generates *"Da-like"* mutants.
(A) Lateral view of adult *Da* mutant, arrow head points to the dorsal fin which has the shape of an anal fin. (B) Lateral view of adult *Da-like* mutant, arrow head points to dorsal fin which is shaped like an anal fin. The *Da-like* mutant phenocopys the *Da* mutant. (C-C") Amplification of genomic DNA of Wt and *Da-like* mutants.(C) An approximately 850 bp band, spanning the transposon insertion site, was amplified in Wt medaka. (C'-C") Primers binding to the 5' end (C') and 3' end (C") of the OPT amplified fragments of the endogenous locus and ends of the OPT, verifying the successful integration of OPT into the Enhancer D. (D-D") Schematic representation of the zic1/zic4 locus in Wt (D), *Da-like* mutant (D') and *Da* mutant (D"), Enhancer D is shown in turquoise ("Enhancer"). Scales: (D) 1-43,973 bp, (D') 1-45,137 bp, (D") 1-225768 bp.

It is intriguing that it is possible to phenocopy the *Da* mutant using an strong terminator of only 1,165 bp (in the case that only one OPT is inserted in the *Da-like* mutants) compared to the massive disruption of the enhancer caused by the transposon (ca. 180 kb) insertion in the *Da* mutant (Figure 6.4D'-D"). It would be interesting to investigate in which way the regulation of *zic1/zic4* transcription in the dorsal somites is altered in the *Da* mutant and the *Da-like* mutant. To observe this, chromosome conformation capture analysis can be performed. A small limitation might be that the *Da-like* mutant seem to not produce viable offspring (most embryos die during embryonic development), a way to overcome this could be by generating primary tissue culture from for example myofibers of *Da-like* adult fish.

Contributions

For the analysis of the ChIP-Seq in 2.1.3, Ryohei Nakamura assisted me by performing the motif analysis using the MEME-ChIP tool.
The hematoxylin staining on histological sections in 2.2.5 was performed by Atsuko Shimada.
The project focusing on phenocopying of the *Da* mutant in section 6.1 was done in collaboration with Thomas Thumberger. Experiments were performed and analyzed by me, however, conceptualization and discussion was a shared effort.

Acknowledgments

I was very fortunate to have two outstanding supervisors guiding me through my PhD.

Because this journey started in Germany, I would like to first thank you Jochen. When I first had this idea to do a Joint PhD between Heidelberg and Japan, you supported me from the start, helped me with the organization and probably most importantly, helped me finding the right collaborator in Japan. I am very grateful that you gave me the opportunity to do a Joint PhD in you lab. As a supervisor I deeply appreciate that you challenged me scientifically, and encouraged me when I needed it.

My deepest gratitude goes to Hiro, for being my supervisor in Japan. I am very honored that you gave me the opportunity to join your lab and that you were open for this collaboration. Thank you for giving me the freedom to work on many exciting projects and letting me follow my scientific curiosity. I learned so many things in your lab and I am truly grateful for your guidance and advice.

I would like to thank Lazaro for being part of my TAC committee, and the stimulating and helpful discussions, as well as for reaching out to me regularly when I was in Japan, thank you!
I would also like to thank my other TAC member Dr. Alexander Aulehla for great input and valuable feedback on my project.
I want to thank Prof. Annika Guse and Dr. Sergio Acebron for being part of my committee. I am very excited to have such a diverse and inspiring committee.

Additionally, I would like to thank Nakamura-san for his valuable advice and seemingly endless patience for teaching me how to analyze my sequencing results. I would like to thank Toru for all the interesting discussions and whiteboard sessions.
A big thanks goes to Atsuko Shimada, for sharing my excitement about new scientific findings and ideas to look into and for knowing the right things to say in moments when it got quite tough.

I would like to thank all my colleagues in Germany for providing a great working atmosphere. I am very happy that colleagues became friends and I want to especially mention Alicia, Alex and Clara for helping me out with writing my thesis in Japan. I am very much looking forward to having a coffee with you guys again soon.
I would like to thank my colleagues in Japan for taking me in and making me feel home quickly. A special thank goes to Flore, who introduced me to everybody and everything. My experience here in Tokyo would not be the same without you!

I would like to thank Karo and Mia, without you, I would not have come so far! Thank you for being there for me, no matter what.

Last but not least, I would like to thank my family for their boundless support, for encouraging me and always believing in me.

References

Abe, K., Shimada, A., Tayama, S., Nishikawa, H., Kaneko, T., Tsuda, S., Karaiwa, A., Matsui, T., Ishitani, T., and Takeda, H. (2019). Horizontal Boundary Cells, a Special Group of Somitic Cells, Play Crucial Roles in the Formation of Dorsoventral Compartments in Teleost Somite. CellReports *27*, 928--939.e4.

Ahmed, M.U., Maurya, A.K., Cheng, L., Jorge, E.C., Schubert, F.R., Maire, P., Basson, M.A., Ingham, P.W., and Dietrich, S. (2017). Engrailed controls epaxial-hypaxial muscle innervation and the establishment of vertebrate three-dimensional mobility. Dev. Biol.

Amthor, H., Christ, B., and Patel, K. (1999). A molecular mechanism enabling continuous embryonic muscle growth - A balance between proliferation and differentiation. Development.

Ansai, S., and Kinoshita, M. (2014). Targeted mutagenesis using CRISPR/Cas system in medaka. Biol. Open *3*, 362–371.

Aoyama, H., and Asamoto, K. (1988). Determination of somite cells: Independence of cell differentiation and morphogenesis. Development.

Aruga, J., Mizugishi, K., Koseki, H., Imai, K., Balling, R., Noda, T., and Mikoshiba, K. (1999). Zic1 regulates the patterning of vertebral arches in cooperation with Gli3. Mech. Dev. *89*, 141–150.

Aruga, J., Kamiya, A., Takahashi, H., Fujimi, T.J., Shimizu, Y., Ohkawa, K., Yazawa, S., Umesono, Y., Noguchi, H., Shimizu, T., et al. (2006). A wide-range phylogenetic analysis of Zic proteins: Implications for correlations between protein structure conservation and body plan complexity. Genomics *87*, 783–792.

Atit, R., Sgaier, S.K., Mohamed, O.A., Taketo, M.M., Dufort, D., Joyner, A.L., Niswander, L., and Conlon, R.A. (2006). β-catenin activation is necessary and sufficient to specify the dorsal dermal fate in the mouse. Dev. Biol.

Bahri, S., Wang, S., Conder, R., Choy, J., Vlachos, S., Dong, K., Merino, C., Sigrist, S., Molnar, C., Yang, X., et al. (2010). The leading edge during dorsal closure as a model for epithelial plasticity: Pak is required for recruitment of the Scribble complex and septate junction formation. Development *137*, 2023–2032.

Bajoghli, B., Aghaallaei, N., Heimbucher, T., and Czerny, T. (2004). An artificial promoter construct for heat-inducible misexpression during fish embryogenesis. Dev. Biol. *271*, 416–430.

Barresi, M.J.F., D'Angelo, J.A., Hernández, L.P., and Devoto, S.H. (2001). Distinct mechanisms regulate slow-muscle development. Curr. Biol.

Behrens, J., Von Kries, J.P., Kühl, M., Bruhn, L., Wedlich, D., Grosschedl, R., and Birchmeier, W. (1996). Functional interaction of β-catenin with the transcription factor LEF- 1. Nature.

Benedyk, M.J., Mullen, J.R., and DiNardo, S. (1994). Odd-paired: A zinc finger pair-rule protein required for the timely activation of engrailed and wingless in Drosophila embryos.

Genes Dev.

Bilić, J., Huang, Y.L., Davidson, G., Zimmermann, T., Cruciat, C.M., Bienz, M., and Niehrs, C. (2007). Wnt induces LRP6 signalosomes and promotes dishevelled-dependent LRP6 phosphorylation. Science (80-.).

Biressi, S., Molinaro, M., and Cossu, G. (2007). Cellular heterogeneity during vertebrate skeletal muscle development. Dev. Biol.

Blank, M.C., Grinberg, I., Aryee, E., Laliberte, C., Chizhikov, V. V., Mark Henkelman, R., and Millen, K.J. (2011). Multiple developmental programs are altered by loss of Zic1 and Zic4 to cause Dandy-Walker malformation cerebellar pathogenesis. Development.

Blitzer, J.T., and Nusse, R. (2006). A critical role for endocytosis in Wnt signaling. BMC Cell Biol.

Borycki, A.G., and Emerson, C.P. (1999). Multiple Tissue Interactions and Signal Transduction Pathways Control Somite Myogenesis. Curr. Top. Dev. Biol.

Bottomly, D., Kyler, S.L., McWeeney, S.K., and Yochum, G.S. (2010). Identification of β-catenin binding regions in colon cancer cells using ChIP-Seq. Nucleic Acids Res. *38*, 5735–5745.

Brand-Saberi, B., Müller, T.S., Wilting, J., Christ, B., and Birchmeier, C. (1996). Scatter factor/hepatocyte growth factor (SF/HGF) induces emigration of myogenic cells at interlimb level in vivo. Dev. Biol. *179*, 303–308.

Brunelli, S., Relaix, F., Baesso, S., Buckingham, M., and Cossu, G. (2007). Beta catenin-independent activation of MyoD in presomitic mesoderm requires PKC and depends on Pax3 transcriptional activity. Dev. Biol. *304*, 604–614.

Brunt, L., and Scholpp, S. (2018). The function of endocytosis in Wnt signaling. Cell. Mol. Life Sci. *75*, 785–795.

Buckingham, M. (2001). Skeletal muscle formation in vertebrates. Curr. Opin. Genet. Dev.

Bussmann, J., and Raz, E. (2015). Chemokine-guided cell migration and motility in zebrafish development. EMBO J. *34*, 1309–1318.

Butler, M.T., and Wallingford, J.B. (2017). Planar cell polarity in development and disease. Nat. Publ. Gr. *18*, 375–388.

De Calisto, J., Araya, C., Marchant, L., Riaz, C.F., and Mayor, R. (2005). Essential role of non-canonical Wnt signalling in neural crest migration. Development *132*, 2587–2597.

Carlson, B.M. (2015). Establishment of Basic Embryonic Body Plan. In Reference Module in Biomedical Sciences, p.

Centanin, L., Ander, J.-J., Hoeckendorf, B., Lust, K., Kellner, T., Kraemer, I., Urbany, C., Hasel, E., Harris, W. a, Simons, B.D., et al. (2014). Exclusive multipotency and preferential asymmetric divisions in post-embryonic neural stem cells of the fish retina. Development *141*, 3472–3482.

Cheng, L., Alvares, L.E., Ahmed, M.U., El-Hanfy, A.S., and Dietrich, S. (2004). The epaxial-hypaxial subdivision of the avian somite. Dev. Biol.

Cinnamon, Y., Ben-Yair, R., and Kalcheim, C. (2006). Differential effects of N-cadherin-mediated adhesion on the development of myotomal waves. Development *133*, 1101–1112.

Ciruna, B., and Rossant, J. (2001). Mesoderm Cell Fate Specification and Morphogenetic Movement at the Primitive Streak. Dev Cell.

Clark, K.J., Balciunas, D., Pogoda, H.-M., Ding, Y., Westcot, S.E., Bedell, V.M., Greenwood, T.M., Urban, M.D., Skuster, K.J., Petzold, A.M., et al. (2011). In vivo protein trapping produces a functional expression codex of the vertebrate proteome. Nat. Methods *8*, 506–512.

Clifton, G. (2002). Functional Anatomy of the Vertebrates: An evolutionary perspective, 3. Biomechanics.

Cossu, G., Tajbakhsh, S., and Buckingham, M. (1996). How is myogenesis initiatedinthe embryo? 1–6.

Coumailleau, P., Penrad-Mobayed, M., Lecomte, C., Bollérot, K., Simon, F., Poellinger, L., and Angelier, N. (2000). Characterization and developmental expression of xSim, a Xenopus bHLH/PAS gene related to the Drosophila neurogenic master gene single-minded. Mech. Dev. *99*, 163–166.

Delfini, M.C., De La Celle, M., Gros, J., Serralbo, O., Marics, I., Seux, M., Scaal, M., and Marcelle, C. (2009). The timing of emergence of muscle progenitors is controlled by an FGF/ERK/SNAIL1 pathway. Dev. Biol.

Devoto, S.H., Melançon, E., Eisen, J.S., and Westerfield, M. (1996). Identification of separate slow and fast muscle precursor cells in vivo, prior to somite formation. Development.

Devoto, S.H., Stoiber, W., Hammond, C.L., Steinbacher, P., Haslett, J.R., Barresi, M.J.F., Patterson, S.E., Adiarte, E.G., and Hughes, S.M. (2006). Generality of vertebrate developmental patterns: Evidence for a dermomyotome in fish. Evol. Dev.

Dietrich, S., Schubert, F.R., and Lumsden, A. (1997). Control of dorsoventral pattern in the chick paraxial mesoderm. Development.

Djiane, A., Riou, J.F., Umbhauer, M., Boucaut, J.C., and Shi, D.L. (2000). Role of frizzled 7 in the regulation of convergent extension movements during gastrulation in Xenopus laevis. Development.

Dockter, J., and Ordahl, C.P. (2000). Dorsoventral axis determination in the somite: A re-examination. Development.

Dockter, J.L., and Ordahl, C.P. (1998). Determination of sclerotome to the cartilage fate. Development.

Doenz, G., Dorn, S., Aghaallaei, N., Bajoghli, B., Riegel, E., Aigner, M., Bock, H., Werner, B., Lindhorst, T., and Czerny, T. (2018). The function of tcf3 in medaka embryos: efficient knockdown with pePNAs. BMC Biotechnol. *18*, 1–14.

Donà, E., Barry, J.D., Valentin, G., Quirin, C., Khmelinskii, A., Kunze, A., Durdu, S., Newton, L.R., Fernandez-Minan, A., Huber, W., et al. (2013). Directional tissue migration through a self-generated chemokine gradient. Nature.

Driever, W., Solnica-Krezel, L., Schier, A.F., Neuhauss, S.C.F., Malicki, J., Stemple, D.L., Stainier, D.Y.R., Zwartkruis, F., Abdelilah, S., Rangini, Z., et al. (1996). A genetic screen for mutations affecting embryogenesis in zebrafish. Development.

Du, S.J., Purcell, S.M., Christian, J.L., McGrew, L.L., and Moon, R.T. (1995). Identification of distinct classes and functional domains of Wnts through expression of wild-

type and chimeric proteins in Xenopus embryos. Mol. Cell. Biol.

Elsen, G.E., Choi, L.Y., Millen, K.J., Grinblat, Y., and Prince, V.E. (2008). Zic1 and Zic4 regulate zebrafish roof plate specification and hindbrain ventricle morphogenesis. Dev. Biol. *314*, 376–392.

Feng, X., Adiarte, E.G., and Devoto, S.H. (2006). Hedgehog acts directly on the zebrafish dermomyotome to promote myogenic differentiation. Dev. Biol.

Fernández-Miñán, A., Bessa, J., Tena, J.J., and Gómez-Skarmeta, J.L. (2016). Assay for transposase-accessible chromatin and circularized chromosome conformation capture, two methods to explore the regulatory landscapes of genes in zebrafish. Methods Cell Biol.

Fetcho, J.R. (1987). A review of the organization and evolution of motoneurons innervating the axial musculature of vertebrates. Brain Res. Rev.

Fujimi, T.J., Mikoshiba, K., and Aruga, J. (2006). Xenopus Zic4: Conservation and diversification of expression profiles and protein function among the Xenopus Zicfamily. Dev. Dyn. *235*, 3379–3386.

Fukamachi, S., Shimada, A., and Shima, A. (2001). Mutations in the gene encoding B, a novel transporter protein, reduce melanin content in medaka. Nat. Genet.

Fukamachi, S., Asakawa, S., Wakamatsu, Y., Shimizu, N., Mitani, H., and Shima, A. (2004). Conserved function of medaka pink-eyed dilution in melanin synthesis and its divergent transcriptional regulation in gonads among vertebrates. Genetics.

Furutani-Seiki, M., Sasado, T., Morinaga, C., Suwa, H., Niwa, K., Yoda, H., Deguchi, T., Hirose, Y., Yasuoka, A., Henrich, T., et al. (2004). A systematic genome-wide screen for mutations affecting organogenesis in Medaka, Oryzias latipes. Mech. Dev.

Galli, L.M., Willert, K., Nusse, R., Yablonka-Reuveni, Z., Nohno, T., Denetclaw, W., and Burrus, L.W. (2004). A proliferative role for Wnt-3a in chick somites. Dev. Biol. *269*, 489–504.

Gammons, M. V., Renko, M., Johnson, C.M., Rutherford, T.J., and Bienz, M. (2016). Wnt Signalosome Assembly by DEP Domain Swapping of Dishevelled. Mol. Cell.

Ganassi, M., Badodi, S., Ortuste Quiroga, H.P., Zammit, P.S., Hinits, Y., and Hughes, S.M. (2018). Myogenin promotes myocyte fusion to balance fibre number and size. Nat. Commun. *9*, 17–19.

Garriock, R.J., and Krieg, P.A. (2007). Wnt11-R signaling regulates a calcium sensitive EMT event essential for dorsal fin development of Xenopus. Dev. Biol. *304*, 127–140.

Geetha-Loganathan, P. (2006). Regulation of ectodermal Wnt6 expression by the neural tube is transduced by dermomyotomal Wnt11: a mechanism of dermomyotomal lip sustainment. Development *133*, 2897–2904.

Gerhart, J., Elder, J., Neely, C., Schure, J., Kvist, T., Knudsen, K., and George-Weinstein, M. (2006). MyoD-positive epiblast cells regulate skeletal muscle differentiation in the embryo. J. Cell Biol.

Gerhart, J., Scheinfeld, V.L., Milito, T., Pfautz, J., Neely, C., Fisher-Vance, D., Sutter, K., Crawford, M., Knudsen, K., and George-Weinstein, M. (2011). Myo/Nog cell regulation of bone morphogenetic protein signaling in the blastocyst is essential for normal morphogenesis and striated muscle lineage specification. Dev. Biol. *359*, 12–25.

Gerlach, J.P., Jordens, I., Tauriello, D.V.F., Land-Kuper, I. van t., Bugter, J.M., Noordstra, I., van der Kooij, J., Low, T.Y., Pimentel-Muiños, F.X., Xanthakis, D., et al. (2018). TMEM59 potentiates Wnt signaling by promoting signalosome formation. Proc. Natl. Acad. Sci. U. S. A.

Gibbs, P.D.L., and Schmale, M.C. (2000). GFP as a Genetic Marker Scorable Throughout the Life Cycle of Transgenic Zebra Fish. Mar. Biotechnol. 1–19.

Gilbert, S.F., and Barresi, M.J.F. (2017). Developmental Biology, 11th Edition 2016.

Glass, B.P., and Goodrich, E.S. (1960). Studies on the Structure and Development of Vertebrates. J. Mammal.

Goto, H., Tomono, Y., Ajiro, K., Kosako, H., Fujita, M., Sakurai, M., Okawa, K., Iwamatsu, A., Okigaki, T., Takahashi, T., et al. (1999). Identification of a Novel Phosphorylation Site on Histone H3 Coupled with Mitotic Chromosome Condensation*. J. Biol. Chem. 1–8.

Goulding, M., Lumsden, A., and Paquette, A.J. (1994). Regulation of Pax-3 expression in the dermomyotome and its role in muscle development. Development.

Grabher, C., and Wittbrodt, J. (2007). Meganuclease and transposon mediated transgenesis in medaka. Genome Biol.

Gros, J., Manceau, M., Thomé, V., and Marcelle, C. (2005). A common somitic origin for embryonic muscle progenitors and satellite cells. Nature.

Gros, J., Serralbo, O., and Marcelle, C. (2008). WNT11 acts as a directional cue to organize the elongation of early muscle fibres. Nature *457*, 589–593.

Groves, J.A., Hammond, C.L., and Hughes, S.M. (2005). Fgf8 drives myogenic progression of a novel lateral fast muscle fibre population in zebrafish. Development.

Hagemann, A.I.H., Kurz, J., Kauffeld, S., Chen, Q., Reeves, P.M., Weber, S., Schindler, S., Davidson, G., Kirchhausen, T., and Scholpp, S. (2014). Correction to In vivo analysis of formation and endocytosis of the Wnt/β-Catenin signaling complex in zebrafish embryos [J. Cell Sci. 127, (2014) 3970-3982]. J. Cell Sci. *127*, 5331.

Hamade, A., Deries, M., Begemann, G., Bally-Cuif, L., Genêt, C., Sabatier, F., Bonnieu, A., and Cousin, X. (2006). Retinoic acid activates myogenesis in vivo through Fgf8 signalling. Dev. Biol.

Hammond, C.L., Hinits, Y., Osborn, D.P.S., Minchin, J.E.N., Tettamanti, G., and Hughes, S.M. (2007). Signals and myogenic regulatory factors restrict pax3 and pax7 expression to dermomyotome-like tissue in zebrafish. Dev. Biol.

Hardy, K.M., Garriock, R.J., Yatskievych, T.A., Susan, L., Agostino, D., Antin, P.B., and Krieg, P.A. (2008). Non-canonical Wnt signaling through Wnt5a/b and a novel Wnt11 gene, Wnt11b, regulates cell migration during avian gastrulation. Dev. Biol. *320*, 391–401.

Hayes, P., and Solon, J. (2017). Drosophila dorsal closure: An orchestra of forces to zip shut the embryo. Mech. Dev. *144*, 2–10.

Heasman, S.J., and Ridley, A.J. (2008). Mammalian Rho GTPases: New insights into their functions from in vivo studies. Nat. Rev. Mol. Cell Biol.

Heisenberg, C.-P., Tada, M., Rauch, G.-J., Saude, L., Concha, M.L., Geisler, R., Stemple, D.L., Smith, J.C., and Wilson, S.W. (2000). Silberblick/Wnt11 mediates convergent

extension movements during zebrafsh gastrulation . Nature 1–6.

Hollway, G.E., Bryson-Richardson, R.J., Berger, S., Cole, N.J., Hall, T.E., and Currie, P.D. (2007). Whole-Somite Rotation Generates Muscle Progenitor Cell Compartments in the Developing Zebrafish Embryo. Dev. Cell *12*, 207–219.

Holstein, T.W. (2012). The evolution of the wnt pathway. Cold Spring Harb. Perspect. Biol.

Houtmeyers, R., Souopgui, J., Tejpar, S., and Arkell, R. (2013). The ZIC gene family encodes multi-functional proteins essential for patterning and morphogenesis. Cell. Mol. Life Sci. *70*, 3791–3811.

Hu, B., Gao, Y., Davies, L., Woo, S., Topczewski, J., Jessen, J.R., and Lin, F. (2018). Glypican 4 and Mmp14 interact in regulating the migration of anterior endodermal cells by limiting extracellular matrix deposition. Dev. *145*.

Huber, O., Korn, R., McLaughlin, J., Ohsugi, M., Herrmann, B.G., and Kemler, R. (1996). Nuclear localization of β-catenin by interaction with transcription factor LEF-1. Mech. Dev.

Hutcheson, D.A., Zhao, J., Merrell, A., Haldar, M., and Kardon, G. (2009). Embryonic and fetal limb myogenic cells are derived from developmentally distinct progenitors and have different requirements for beta-catenin. Genes Dev. *23*, 997–1013.

Iida, A., Inagaki, H., Suzuki, M., Wakamatsu, Y., Hori, H., and Koga, A. (2004). The Tyrosinase Gene of the ib Albino Mutant of the Medaka Fish Carries a Transposable Element Insertion in the Promoter Region. Pigment Cell Res.

Ikeda, S., Kishida, S., Yamamoto, H., Murai, H., Koyama, S., and Kikuchi, A. (1998). Axin, a negative regulator of the Wnt signaling pathway, forms a complex with GSK-3β and. EMBO J. *17*, 1371–1384.

Ikeya, M., and Takada, S. (1998). Wnt signaling from the dorsal neural tube is required for the formation of the medial dermomyotome. 1–8.

Innocenti, M. (2018). New insights into the formation and the function of lamellipodia and ruffles in mesenchymal cell migration. 1–17.

Inohaya, K., Takano, Y., and Kudo, A. (2010). Production of Wnt4b by floor plate cells is essential for the segmental patterning of the vertebral column in medaka. Development.

Inoue, Y., Saga, T., Aikawa, T., Kumagai, M., Shimada, A., Kawaguchi, Y., Naruse, K., Morishita, S., Koga, A., and Takeda, H. (2017). Complete fusion of a transposon and herpesvirus created the Teratorn mobile element in medaka fish. Nat. Commun. *8*, 1–14.

Insall, R., and Andrew, N. (2007). Chemotaxis in Dictyostelium: how to walk straight using parallel pathways. Curr. Opin. Microbiol.

Isabel Olivera-Martinez, I., Missier, S., Fraboulet, S., Thélu, J., and DhouaillyDanielle (2002). Differential regulation of the chick dorsal thoracic dermal progenitors from the medial dermomyotome. Development 1–10.

Ishikawa, Y. (1990). Development of caudal structures of a morphogenetic mutant (Da) in the teleost fish, medaka (Oryzias latipes). J. Morphol.

Ishikawa, Y., and et al (1999). Introduction of mutations by ENU in the medaka germline. Fish Biol. J. Medaka *10*, 27–29.

Ishikawa, T., Ansai, S., Kinoshita, M., and Mori, K. (2018). A Collection of Transgenic

Medaka Strains for Efficient Site-Directed Transgenesis Mediated by phiC31 Integrase. G3: Genes|Genomes|Genetics *8*, 2585–2593.

Iwamatsu, T. (2004). Stages of normal development in the medaka Oryzias latipes. Mech. Dev.

Jackson, H.E., and Ingham, P.W. (2013). Control of muscle fibre-type diversity during embryonic development: The zebrafish paradigm. Mech. Dev.

Jho, E., Zhang, T., Domon, C., Joo, C.-K., Freund, J.-N., and Costantini, F. (2002). Wnt/β-Catenin/Tcf Signaling Induces the Transcription of Axin2, a Negative Regulator of the Signaling Pathway. Mol. Cell. Biol.

Johnson, R.L., Laufer, E., Riddle, R.D., and Tabin, C. (1994). Ectopic expression of Sonic hedgehog alters dorsal-ventral patterning of somites. Cell.

Jussila, M., and Ciruna, B. (2017). Zebrafish models of non-canonical Wnt/planar cell polarity signalling: fishing for valuable insight into vertebrate polarized cell behavior. Wiley Interdiscip. Rev. Dev. Biol. *6*, e267--13.

Kahane, N., Ribes, V., Kicheva, A., Briscoe, J., and Kalcheim, C. (2013). The transition from differentiation to growth during dermomyotome-derived myogenesis depends on temporally restricted hedgehog signaling. Dev.

Kasahara, M., Naruse, K., Sasaki, S., Nakatani, Y., Qu, W., Ahsan, B., Yamada, T., Nagayasu, Y., Doi, K., Kasai, Y., et al. (2007). The medaka draft genome and insights into vertebrate genome evolution. Nature *447*, 714–719.

Kato, N., and Aoyama, H. (1998). Dermomyotomal origin of the ribs as revealed by extirpation and transplantation experiments in chick and quail embryos. Development.

Kawanishi, T., Kaneko, T., Moriyama, Y., Kinoshita, M., Yokoi, H., Suzuki, T., Shimada, A., and Takeda, H. (2013). Modular development of the teleost trunk along the dorsoventral axis and zic1/zic4 as selector genes in the dorsal module. Development *140*, 1486–1496.

Kearse, M., Moir, R., Wilson, A., Stones-Havas, S., Cheung, M., Sturrock, S., Buxton, S., Cooper, A., Markowitz, S., Duran, C., et al. (2012). Geneious Basic: An integrated and extendable desktop software platform for the organization and analysis of sequence data. Bioinformatics *28*, 1647–1649.

Keenan, S.R., and Currie, P.D. (2019). The Developmental Phases of Zebrafish Myogenesis. J. Dev. Biol. *7*, 12–21.

Kelsh, R.N., Inoue, C., Momoi, A., Kondoh, H., Furutani-Seiki, M., Ozato, K., and Wakamatsu, Y. (2004). The Tomita collection of medaka pigmentation mutants as a resource for understanding neural crest cell development. Mech. Dev.

Kishimoto, Y., Lee, K.H., Zon, L., Hammerschmidt, M., and Schulte-Merker, S. (1997). The molecular nature of zebrafish swirl: BMP2 function is essential during early dorsoventral patterning. Development.

Koga, A., and Hiroshi, H. (1997). Albinism Due to Transposable Element Insertion in Fish. Pigment Cell Res.

Koga, A., Inagaki, H., Bessho, Y., and Hori, H. (1995). Insertion of a novel transposable element in the tyrosinase gene is responsible for an albino mutation in the medaka fish, Oryzias latipes. MGG Mol. Gen. Genet.

Kondo, S., Kuwahara, Y., Kondo, M., Naruse, K., Mitani, H., Wakamatsu, Y., Ozato, K., Asakawa, S., Shimizu, N., and Shima, A. (2001). The medaka rs-3 locus required for scale development encodes ectodysplasin-A receptor. Curr. Biol.

Konigsberg, I.R. (1963). Clonal analysis of myogenesis. Science (80-.).

Kraft, B., Berger, C.D., Wallkamm, V., Steinbeisser, H., and Wedlich, D. (2012). Wnt-11 and Fz7 reduce cell adhesion in convergent extension by sequestration of PAPC and C-cadherin. J. Cell Biol.

Kühl, M., Geis, K., Sheldahl, L.C., Pukrop, T., Moon, R.T., and Wedlich, D. (2001). Antagonistic regulation of convergent extension movements in Xenopus by Wnt/β-catenin and Wnt/Ca2+ signaling. Mech. Dev.

Kunick, C., Lauenroth, K., Leost, M., Meijer, L., and Lemcke, T. (2004). 1-Azakenpaullone is a selective inhibitor of glycogen synthase kinase-3β. Bioorg. Med. Chem. Lett. *14*, 413–416.

Lamouille, S., Xu, J., and Derynck, R. (2014). Molecular mechanisms of epithelial-mesenchymal transition. Nat. Rev. Mol. Cell Biol.

Lee, C.S., Buttitta, L.A., May, N.R., Kispert, A., and Fan, C.M. (2000). SHH-N upregulates Sfrp2 to mediate its competitive interaction with WNT1 and WNT4 in the somitic mesoderm. Development.

Lee, C.S., Buttitta, L., and Fan, C.M. (2001). Evidence that the WNT-inducible growth arrest-specific gene 1 encodes an antagonist of sonic hedgehog signaling in the somite. Proc. Natl. Acad. Sci. U. S. A.

Leithner, A., Eichner, A., Müller, J., Reversat, A., Brown, M., Schwarz, J., Merrin, J., De Gorter, D.J.J., Schur, F., Bayerl, J., et al. (2016). Diversified actin protrusions promote environmental exploration but are dispensable for locomotion of leukocytes. Nat. Cell Biol.

Li, H., and Durbin, R. (2009). Fast and accurate short read alignment with Burrows-Wheeler transform. Bioinformatics *25*, 1754–1760.

Li, H., Handsaker, B., Wysoker, A., Fennell, T., Ruan, J., Homer, N., Marth, G., Abecasis, G., and Durbin, R. (2009). The Sequence Alignment/Map format and SAMtools. Bioinformatics *25*, 2078–2079.

Lindeman, L.C., Vogt-Kielland, L.T., Aleström, P., and Collas, P. (2009). Fish'n ChIPs: Chromatin immunoprecipitation in the Zebrafish embryo. Methods Mol. Biol.

Linker, C. (2005). Beta-Catenin-dependent Wnt signalling controls the epithelial organisation of somites through the activation of paraxis. Development *132*, 3895–3905.

Lischik, C.Q., Adelmann, L., and Wittbrodt, J. (2019). Enhanced in vivo-imaging in medaka by optimized anaesthesia, fluorescent protein selection and removal of pigmentation. PLoS One *14*, e0212956--19.

Loosli, F., Winkler, S., Burgtorf, C., Wurmbach, E., Ansorge, W., Henrich, T., Grabher, C., Arendt, D., Carl, M., Krone, A., et al. (2001). Medaka eyeless is the key factor linking retinal determination and eye growth. Development.

Ma, W., Noble, W.S., and Bailey, T.L. (2014). Motif-based analysis of large nucleotide data sets using MEME-ChIP. Nat. Protoc. *9*, 1428–1450.

MacDonald, B.T., Tamai, K., and He, X. (2009). Wnt/$β$-Catenin Signaling: Components, Mechanisms, and Diseases. Dev. Cell *17*, 9–26.

Marcelle, C., Stark, M.R., and Bronner-fraser, M. (1997). Coordinate actions of BMPs , Wnts , Shh and Noggin mediate patterning of the dorsal somite. *3963*, 3955–3963.

Marchal, L., Luxardi, G., Thome´, V., and Kodjabachian, L. (2009). BMP inhibition initiates neural induction via FGF signaling and Zic genes. PNAS *106*, 17437–17442.

Matthews, H.K., Broders-Bondon, F., Thiery, J.P., and Mayor, R. (2008a). Wnt11ris required for cranial neural crest migration. Dev. Dyn. *237*, 3404–3409.

Matthews, H.K., Marchant, L., Carmona-Fontaine, C., Kuriyama, S., Larraín, J., Holt, M.R., Parsons, M., and Mayor, R. (2008b). Directional migration of neural crest cells in vivo is regulated by Syndecan-4/Rac1 and non-canonical Wnt signaling/RhoA. Development.

Maurya, A.K., Tan, H., Souren, M., Wang, X., Wittbrodt, J., and Ingham, P.W. (2011). Integration of Hedgehog and BMP signalling by the engrailed2a gene in the zebrafish myotome. Development.

McMahon, J.A., Takada, S., Zimmerman, L.B., Fan, C.M., Harland, R.M., and McMahon, A.P. (1998). Noggin-mediated antagonism of BMP signaling is required for growth and patterning of the neural tube and somite. Genes Dev.

Mejillano, M.R., Kojima, S.I., Applewhite, D.A., Gertler, F.B., Svitkina, T.M., and Borisy, G.G. (2004). Lamellipodial versus filopodial mode of the actin nanomachinery: Pivotal role of the filament barbed end. Cell.

Mendieta-Serrano, M.A., Schnabel, D., Lomel\'\i, H., and Salas-Vidal, E. (2013). Cell Proliferation Patterns in Early Zebrafish Development. Anat. Rec. *296*, 759–773.

Merzdorf, C.S., and Sive, H.L. (2006). The zic1 gene is an activator of Wnt signaling. Int. J. Dev. Biol. *50*, 611–617.

Meyers, J.R., Hu, L., Moses, A., Kaboli, K., Papandrea, A., and Raymond, P.A. (2012). beta-catenin/Wnt signaling controls progenitor fate in the developing and regenerating zebrafish retina. Neural Dev *7*, 30.

Mintz, B., and Baker, W.W. (1967). Normal mammalian muscle differentiation and gene control of isocitrate dehydrogenase synthesis. Proc. Natl. Acad. Sci. U. S. A.

Molenaar, M., Van De Wetering, M., Oosterwegel, M., Peterson-Maduro, J., Godsave, S., Korinek, V., Roose, J., Destrée, O., and Clevers, H. (1996). XTcf-3 transcription factor mediates β-catenin-induced axis formation in xenopus embryos. Cell.

Morgan, M., Anders, S., Lawrence, M., Aboyoun, P., Pages, H., and Gentleman, R. (2009). ShortRead: a bioconductor package for input, quality assessment and exploration of high-throughput sequence data. Bioinformatics *25*, 2607–2608.

Moriyama, Y., Kawanishi, T., Nakamura, R., Tsukahara, T., Sumiyama, K., Suster, M.L., Kawakami, K., Toyoda, A., Fujiyama, A., Yasuoka, Y., et al. (2012). The Medaka zic1/zic4 Mutant Provides Molecular Insights into Teleost Caudal Fin Evolution. Curr. Biol. *22*, 1–7.

Morosan-Puopolo, G., Balakrishnan-Renuka, A., Yusuf, F., Chen, J., Dai, F., Zoidl, G., Lüdtke, T.H.W., Kispert, A., Theiss, C., Abdelsabour-Khalaf, M., et al. (2014). Wnt11 Is

Required for Oriented Migration of Dermogenic Progenitor Cells from the Dorsomedial Lip of the Avian Dermomyotome. PLoS One *9*, e92679--16.

Münsterberg, A.E., Kitajewski, J., Bumcrot, D.A., McMahon, A.P., and Lassar, A.B. (1995). Combinatorial signaling by Sonic hedgehog and Wnt family members induces myogenic bHLH gene expression in the somite. Genes Dev.

Nachman, G. (2019). iTerm2.

Nakamura, R., Tsukahara, T., Qu, W., Ichikawa, K., Otsuka, T., Ogoshi, K., Saito, T.L., Matsushima, K., Sugano, S., Hashimoto, S., et al. (2014). Large hypomethylated domains serve as strong repressive machinery for key developmental genes in vertebrates. Development *141*, 2568–2580.

Nakamura, Y., de Paiva Alves, E., Veenstra, G.J.C., and Hoppler, S. (2016). Tissue- and stage-specific Wnt target gene expression is controlled subsequent to $β$-catenin recruitment to cis-regulatory modules. Development 1–35.

Nakata, K., Nagai, T., Aruga, J., and Mikoshiba, K. (1998). Xenopus Zic family and its role in neural and neural crest development. Mech. Dev.

Naruse, K., Tanaka, M., and Takeda, H. (2011). Medaka - A Model for Organogenesis, Human Disease, and Evolution.

Nguyen-Chi, M.E., Bryson-Richardson, R., Sonntag, C., Hall, T.E., Gibson, A., Sztal, T., Chua, W., Schilling, T.F., and Currie, P.D. (2012). Morphogenesis and Cell Fate Determination within the Adaxial Cell Equivalence Group of the Zebrafish Myotome. PLoS Genet.

Nikolopoulou, E., Galea, G.L., Rolo, A., Greene, N.D.E., and Copp, A.J. (2017). Neural tube closure: cellular, molecular and biomechanical mechanisms. Development *144*, 552–566.

Nomiyama, H., Osada, N., and Yoshie, O. (2013). Systematic classification of vertebrate chemokines based on conserved synteny and evolutionary history. Genes to Cells.

Norden, C., and Lecaudey, V. (2019). Collective cell migration: general themes and new paradigms. Curr. Opin. Genet. Dev.

Ohkawara, B., Glinka, A., and Niehrs, C. (2011). Rspo3 Binds Syndecan 4 and Induces Wnt/PCP Signaling via Clathrin-Mediated Endocytosis to Promote Morphogenesis. Dev. Cell *20*, 303–314.

Ohtsuka, M., Kikuchi, N., Yokoi, H., Kinoshita, M., Wakamatsu, Y., Ozato, K., Takeda, H., Inoko, H., and Kimura, M. (2004). Possible roles of zic1 and zic4, identified within the medaka Double anal fin (Da) locus, in dorsoventral patterning of the trunk-tail region (related to phenotypes of the Da mutant). Mech. Dev. *121*, 873–882.

Olivera-Martinez, I., Thelu, J., and Dhouailly, D. (2004). Molecular mechanisms controlling dorsal dermis generation from the somitic dermomyotome. Int. J. Dev. Biol. *48*, 93–101.

Ordahl, C.P., and Le Douarin, N.M. (1992). Two myogenic lineages within the developing somite. Development.

Ordahl, C.P., Berdougo, E., Venters, S.J., and Denetclaw, W.F. (2001). The dermomyotome dorsomedial lip drives growth and morphogenesis of both the primary

myotome and dermomyotome epithelium. 1–14.

Otto, A., Schmidt, C., and Patel, K. (2006). Pax3 and Pax7 expression and regulation in the avian embryo. Anat. Embryol. (Berl). *211*, 293–310.

Ouko, L., Ziegler, T.R., Gu, L.H., Eisenberg, L.M., and Yang, V.W. (2004). Wnt11 Signaling Promotes Proliferation, Transformation, and Migration of IEC6 Intestinal Epithelial Cells. J. Biol. Chem. *279*, 26707–26715.

Parr, B.A., Shea, M.J., Vassileva, G., and McMahon, A.P. (1993). Mouse Wnt genes exhibit discrete domains of expression in the early embryonic CNS and limb buds. Development.

Pickering, K., Alves-Silva, J., Goberdhan, D., and Millard, T.H. (2013). Par3/Bazooka and phosphoinositides regulate actin protrusion formation during Drosophila dorsal closure and wound healing. Dev. *140*, 800–809.

Plouhinec, J.L., Roche, D.D., Pegoraro, C., Figueiredo, A.L., Maczkowiak, F., Brunet, L.J., Milet, C., Vert, J.P., Pollet, N., Harland, R.M., et al. (2014). Pax3 and Zic1 trigger the early neural crest gene regulatory network by the direct activation of multiple key neural crest specifiers. Dev. Biol. *386*.

Pourquié, O., Coltey, M., Teillet, M.A., Ordahl, C., and Le Douarin, N.M. (1993). Control of dorsoventral patterning of somitic derivatives by notochord and floor plate. Proc. Natl. Acad. Sci. U. S. A.

Pourquié, O., Fan, C.M., Coltey, M., Hirsinger, E., Watanabe, Y., Bréant, C., Francis-West, P., Brickell, P., Tessier-Lavigne, M., and Le Douarin, N.M. (1996). Lateral and axial signals involved in avian somite patterning: A role for BMP4. Cell.

van Raamsdonk, W., van't Veer, L., Veeken, K., Heyting, C., and Pool, C.W. (1982). Differentiation of muscle fiber types in the teleost Brachydanio rerio, the zebrafish - Posthatching development. Anat. Embryol. (Berl).

Reifers, F., Böhli, H., Walsh, E.C., Crossley, P.H., Stainier, D.Y.R., and Brand, M. (1998). Fgf8 is mutated in zebrafish acerebellar (ace) mutants and is required for maintenance of midbrain-hindbrain boundary development and somitogenesis. Development.

Reshef, R., Maroto, M., and Lassar, A.B. (1998). Regulation of dorsal somitic cell fates: BMPs and Noggin control the timing and pattern of myogenic regulator expression. Genes Dev.

Richardson, B.E., Nowak, S.J., and Baylies, M.K. (2008). Myoblast fusion in fly and vertebrates: New genes, new processes and new perspectives. Traffic.

Ridley, A.J. (2011). Life at the leading edge. Cell.

Rohr, K.B., Schulte-Merker, S., and Tautz, D. (1999). Zebrafish zic1 expression in brain and somites is affected by BMP and hedgehog signalling. Mech. Dev. *85*, 147–159.

Rolo, A., Savery, D., Escuin, S., de Castro, S.C., Armer, H.E.J., Munro, P.M.G., Molè, M.A., Greene, N.D.E., and Copp, A.J. (2016). Regulation of cell protrusions by small GTPases during fusion of the neural folds. Elife *5*, 1–24.

Rossi, G., and Messina, G. (2014). Comparative myogenesis in teleosts and mammals. Cell. Mol. Life Sci. *71*, 3081–3099.

Rothschild, S.C., Lahvic, J., Francescatto, L., McLeod, J.J.A., Burgess, S.M., and Tombes,

R.M. (2013). CaMK-II activation is essential for zebrafish inner ear development and acts through Delta-Notch signaling. Dev. Biol.

RStudio Team (2020). RStudio: Integrated Development for R. RStudio. PBC, Boston.

Sakanaka, C., Weiss, J.B., and Williams, L.T. (1998). Bridging of β-catenin and glycogen synthase kinase-3β by Axin and inhibition of β-catenin-mediated transcription. Proc. Natl. Acad. Sci. U. S. A. *95*, 3020–3023.

Sato, T. (2005). Neural crest determination by co-activation of Pax3 and Zic1 genes in Xenopus ectoderm. Development *132*, 2355–2363.

Schilling, N. (2011). Evolution of the axial system in craniates: Morphology and function of the perivertebral musculature. Front. Zool.

Schindelin, J., Arganda-Carreras, I., Frise, E., Kaynig, V., Longair, M., Pietzsch, T., Preibisch, S., Rueden, C., Saalfeld, S., Schmid, B., et al. (2012). \textbf{Fiji: an open-source platform for biological-image analysis } . Nat. Methods *9*, 676–682.

Schmidt, C., Stoeckelhuber, M., McKinnell, I., Putz, R., Christ, B., and Patel, K. (2004). Wnt 6 regulates the epithelialisation process of the segmental plate mesoderm leading to somite formation. Dev. Biol.

Sefton, E.M., and Kardon, G. (2019). Connecting muscle development, birth defects, and evolution: An essential role for muscle connective tissue. In Current Topics in Developmental Biology, p.

Serralbo, O., and Marcelle, C. (2014). Migrating cells mediate long-range WNT signaling. Development *141*, 2057–2063.

Shimizu, N., Kawakami, K., and Ishitani, T. (2012). Visualization and exploration of Tcf/Lef function using a highly responsive Wnt/$β$-catenin signaling-reporter transgenic zebrafish. Dev. Biol. *370*, 71–85.

Sieiro, D., Rios, A.C., Hirst, C.E., and Marcelle, C. (2016). Cytoplasmic NOTCH and membrane- derived beta-catenin link cell fate choice to epitherlial-mesechymal transition during myogenesis. Elife 1–21.

Stamos, J.L., and Weis, W.I. (2013). The β-catenin destruction complex. Cold Spring Harb. Perspect. Biol.

Steinbacher, P., Haslett, J.R., Obermayer, A., Marschallinger, J., Bauer, H.C., Sänger, A.M., and Stoiber, W. (2007). MyoD and Myogenin expression during myogenic phases in brown trout: A precocious onset of mosaic hyperplasia is a prerequisite for fast somatic growth. Dev. Dyn.

Stellabotte, F., and Devoto, S.H. (2007). The teleost dermomyotome. Dev. Dyn. *236*, 2432–2443.

Stellabotte, F., Dobbs-McAuliffe, B., Fernández, D.A., Feng, X., and Devoto, S.H. (2007). Dynamic somite cell rearrangements lead to distinct waves of myotome growth. Development.

Stemmer, M., Thumberger, T., del Sol Keyer, M., Wittbrodt, J., and Mateo, J.L. (2015). CCTop: An Intuitive, Flexible and Reliable CRISPR/Cas9 Target Prediction Tool. PLoS One *10*, e0124633--11.

Sun Rhodes, L.S., and Merzdorf, C.S. (2006). The zic1 gene is expressed in chick somites but not in migratory neural crest.

Tajbakhsh, S., Borello, U., Vivarelli, E., Kelly, R., Papkoff, J., Duprez, D., Buckingham, M., and Cossu, G. (1998). Differential activation of Myf5 and MyoD by different Wnts in explants of mouse paraxial mesoderm and the later activation of myogenesis in the absence of Myf5. Development.

Talbot, J., and Maves, L. (2016). Skeletal muscle fiber type: using insights from muscle developmental biology to dissect targets for susceptibility and resistance to muscle disease. Wiley Interdiscip. Rev. Dev. Biol.

Tallafuss, A., Gibson, D., Morcos, P., Li, Y., Seredick, S., Eisen, J., and Washbourne, P. (2012). Turning gene function ON and OFF using sense and antisense photo-morpholinos in zebrafish. Development *139*, 1691–1699.

Tamiya, G., Wakamatsu, Y., and Ozato, K. (1997). An embryological study of ventralization of dorsal structures in the tail of medaka (Oryzias latipes) Da mutants. 1–8.

Theveneau, E., and Mayor, R. (2012). Neural crest delamination and migration: From epithelium-to-mesenchyme transition to collective cell migration. Dev. Biol. *366*, 34–54.

Thiery, J.P., Acloque, H., Huang, R.Y.J., and Nieto, M.A. (2009). Epithelial-Mesenchymal Transitions in Development and Disease. Cell.

Tomida, H. (1992). The lists of the mutants and strains of the medaka, common gambusia, silver crucian carp, goldfish and golden venus fish maintained in the Laboratory of Freshwater Fish Stocks, Nagoya University. Fish Biol. J. Medaka *4*.

Touma, M., Kang, X., Gao, F., Zhao, Y., Cass, A.A., Biniwale, R., Xiao, X., Eghbali, M., Coppola, G., Reemtsen, B., et al. (2017). Wnt11 regulates cardiac chamber development and disease during perinatal maturation. JCI Insight *2*, H1--19.

Toyama, K. (1916). On some Mendelian characters (in Japanese). Rep. Jap. Breed. Soc.

Tseng, Y.H., Kokkotou, E., Schulz, T.J., Huang, T.L., Winnay, J.N., Taniguchi, C.M., Tran, T.T., Suzuki, R., Espinoza, D.O., Yamamoto, Y., et al. (2008). New role of bone morphogenetic protein 7 in brown adipogenesis and energy expenditure. Nature.

Tweedy, L., and Insall, R.H. (2020). Self-Generated Gradients Yield Exceptionally Robust Steering Cues. Front. Cell Dev. Biol. *8*, 1–10.

Tweedy, L., Susanto, O., and Insall, R.H. (2016). Self-generated chemotactic gradients - cells steering themselves. Curr. Opin. Cell Biol.

Tweedy, L., Thomason, P.A., Paschke, P.I., Martin, K., Machesky, L.M., Zagnoni, M., and Insall, R.H. (2020). Seeing around corners: Cells solve mazes and respond at a distance using attractant breakdown. Science (80-.).

Ulrich, F., Concha, M.L., Heid, P.J., Voss, E., Witzel, S., Roehl, H., Tada, M., Wilson, S.W., Adams, R.J., Soll, D.R., et al. (2003). Slb/Wnt11 controls hypoblast cell migration and morphogenesis at the onset of zebrafish gastrulation. Development *130*, 5375–5384.

University of Utah (2020). FluoRender.

Urasaki, A., Morvan, G., and Kawakami, K. (2006). Functional dissection of the Tol2 transposable element identified the minimal cis-sequence and a highly repetitive sequence in

the subterminal region essential for transposition. Genetics.

Valouev, A., Johnson, D.S., Sundquist, A., Medina, C., Anton, E., Batzoglou, S., Myers, R.M., and Sidow, A. (2008). Genome-wide analysis of transcription factor binding sites based on ChIP-Seq data. Nat. Methods *5*, 829–834.

Venkiteswaran, G., Lewellis, S.W., Wang, J., Reynolds, E., Nicholson, C., and Knaut, H. (2013). Generation and dynamics of an endogenous, self-generated signaling gradient across a migrating tissue. Cell.

Wang, Q., Symes, A.J., Kane, C.A., Freeman, A., Nariculam, J., Munson, P., Thrasivoulou, C., Masters, J.R.W., and Ahmed, A. (2010). A novel role for Wnt/Ca2+ signaling in actin cytoskeleton remodeling and cell motility in prostate cancer. PLoS One *5*.

Wickham, H. (2009). ggplot2 (New York, NY: Springer New York).

Wiese, K.E., Nusse, R., and van Amerongen, R. (2018). Wnt signalling: conquering complexity. Development *145*, dev165902--9.

Willert, K., Brown, J.D., Danenberg, E., Duncan, A.W., Weissman, I.L., Reya, T., Yates, J.R., and Nusse, R. (2003). Wnt proteins are lipid-modified and can act as stem cell growth factors. Nature.

Williams, B.A., and Ordahl, C.P. (1997). Emergence of determined myotome precursor cells in the somite. Development.

WinPython distribution of Python (2019). Python 3.8.

Wittbrodt, J., Shima, A., and Schartl, M. (2002). Medaka - A model organism from the Far East. Nat. Rev. Genet.

Witzel, S., Zimyanin, V., Carreira-Barbosa, F., Tada, M., and Heisenberg, C.P. (2006). Wnt11 controls cell contact persistence by local accumulation of Frizzled 7 at the plasma membrane. J. Cell Biol.

Wolda, S.L., Moody, C.J., and Moon, R.T. (1993). Overlapping expression of Xwnt-3A and Xwnt-1 in neural tissue of Xenopus laevis embryos. Dev. Biol.

Wolff, C., Roy, S., and Ingham, P.W. (2003). Multiple muscle cell identities induced by distinct levels and timing of Hedgehog activity in the zebrafish embryo. Curr. Biol.

Wood, W., Jacinto, A., Grose, R., Woolner, S., Gale, J., Wilson, C., and Martin, P. (2002). Wound healing recapitulates morphogenesis in Drosophila embryos. Nat. Cell Biol. *4*, 1–7.

Wu, G.Y., and Cline, H.T. (1998). Stabilization of dendritic arbor structure in vivo by CaMKII. Science (80-.).

Yamamoto, T. (1975). Medaka (killifish) : biology and strains (Tokyo: Distributed by Keigaku Pub. Co.).

Yin, J., Lee, R., Ono, Y., Ingham, P.W., and Saunders, T.E. (2018). Spatiotemporal Coordination of FGF and Shh Signaling Underlies the Specification of Myoblasts in the Zebrafish Embryo. Dev. Cell.

Zhang, Y., Liu, T., Meyer, C.A., Eeckhoute, J., Johnson, D.S., Bernstein, B.E., Nussbaum, C., Myers, R.M., Brown, M., Li, W., et al. (2008). Model-based analysis of ChIP-Seq (MACS). Genome Biol.

Zhou, Y., Zhang, Y., and Zhu, D. (2018). Myostatin promotes the epithelial-to-

mesenchymal transition of the dermomyotome during somitogenesis. Dev. Dyn. *247*, 1241–1252.

Zigmond, S.H. (1977). Ability of polymorphonuclear leukocytes to orient in gradients of chemotactic factors. J. Cell Biol.

(1999). Zic1 regulates the patterning of vertebral arches in cooperation with Gli3. 1–10.

Declaration

Herewith I declare that I prepared the PhD Thesis "Molecular and cellular mechanisms of myotome dorsalization in the medaka embryo" on my own and with no other sources and aids than quoted.

Heidelberg, 2021

List of Figures

List of Videos

List of Tables